Controls of the phosphate sorption and desorption kinetics of organic matter-goethite associations

vorgelegt von
Diplom Geograph
Christian Mikutta

von der Fakultät VI
der Technischen Universität Berlin
zur Erlangung des Grades

Doktor der Naturwissenschaften
-Dr. rer. nat.-

genehmigte Dissertation

Promotionsausschuss:
Vorsitzender: Prof. Dr. B.-M. Wilke
Berichter: Prof. Dr. M. Kaupenjohann
Berichter: Privatdozent Dr. M. Kleber
Berichter: Dr. K. Kaiser
Tag der wissenschaftlichen Aussprache: 13. April 2006

Berlin 2006
D 83

Der Ball ist rund.

Ein Spiel geht 90 Minuten.

Das nächste Spiel ist immer das Schwerste.

(Josef ‚Sepp' Herberger, Deutscher Philosoph)

Table of contents

List of Figures

List of Tables

Summary

Phosphorus deficiency is a limiting factor for the growth of plants in acidic soils due to the strong sorption of phosphate to sesquioxides. For this reason, plants exude an array of organic compounds into the rhizosphere. Many studies document an increase in bioavailability of phosphate because of exudation of anions of polycarboxylic low-molecular-weight organic acids (LMWOA). In addition, plants exude macromolecular organic matter such as polysaccharides of mucilage. However, the effect of mucilage on the bioavailability of phosphate is poorly understood.

The sorption of phosphate to Fe oxides usually comprises a fast and a slow reaction. For goethite (α-FeOOH) the fast reaction is due to the adsorption of phosphate to external goethite surfaces, while the slow reaction is caused by the diffusion of phosphate into micro- (Ø <2 nm) and mesopores (Ø 2-50 nm) of the adsorbent. The main objective of this thesis was to test, whether organic root exudates clog pores of Fe oxides and thus inhibit the pore diffusion of phosphate.

Polygalacturonate (PGA) is commonly used as a model substance for plant-derived mucilage. This approach is questionable in case properties of macromolecular root exudates collected *in situ* differ from those of PGA. Therefore, another objective was to compare porosities and phosphate desorption kinetics of Fe oxides that were equilibrated with PGA and non-axenically collected macromolecular root exudates of maize plants.

Swelling of organic coatings may change their surface coverage, and hence the accessibility of mineral surfaces to phosphate. Therefore, another objective of this thesis was to investigate the influence of hydration of PGA coatings on the phosphate sorption kinetics of sesquioxides.

To address these objectives, goethites (α-FeOOH) were equilibrated with high- and low-molecular-weight organic matter and subsequently analyzed for their porosity by gas adsorption (N_2 and CO_2). Polygalacturonate, soil-derived dissolved organic matter (DOM) and mucigel (MU) of maize plants (*Zea mays* L.) were used as high-molecular-weight organic sorbates, while citrate and galacturonate (GA) were used as low-molecular-weight sorbates. Phosphate sorption and desorption experiments were conducted in batch at pH 5 for up to three weeks. The influence of hydration of PGA coatings on the phosphate sorption kinetics was investigated by batch experiments after PGA-coated alumina (Al_2O_3) had been equilibrated in water for two and 170 hours, respectively. Additionally, samples were examined by ^{1}H-NMR relaxometry and differential scanning calorimetry (DSC).

All organic substances decreased the volume of goethite pores <5 nm. Despite a reduced porosity, the slow phosphate sorption to PGA-coated goethites was not related to their micro- and mesopore volumes. Instead, the phosphate sorption was related to the PGA desorption, indicating that the gradual desorption of PGA by phosphate and/or the diffusion of phosphate through PGA coatings kinetically control the rate of the slow phosphate sorption.

Citrate inhibited the slow phosphate sorption to pure goethite and goethite that had been equilibrated with DOM. This observation was ascribed to both the clogging of micropores by citrate and the citrate-induced dissolution of the adsorbents.

Desorption experiments with goethite treated with GA, PGA and MU revealed that goethite pores became less accessible to phosphate after PGA addition only. Results of desorption experiments with GA and PGA suggest that organic sorbates enforce the fixation of phosphate in <5-nm pores of goethite. Polygalacturonate and MU affected contrarily the phosphate desorption kinetics of goethite, presumably because the MU contained significant amounts of phosphate and mineral matter and a low amount of uronic acids.

The hydration of PGA-coated alumina for 170 hours increased the amount of phosphate that was rapidly sorbed to external mineral surfaces compared with a hydration time of only two hours. This result was ascribed to a restructuring of PGA upon hydration, which enhanced the accessibility of external mineral surfaces to phosphate.

In conclusion, the clogging of goethite pores by PGA is not relevant for the phosphate sorption kinetics of PGA-coated goethites. Contrary, anions of LMWOAs clog micropores of goethite and thus inhibit the micropore diffusion of phosphate. Because PGA may differ in its chemical composition from high-molecular-weight root exudates collected *in situ* (mucigel), predictions on the phosphate dynamics in the rhizosphere based on batch experiments with PGA are rendered more difficult. The permeability of anionic polyelectrolyte coatings has been identified as a further control of the accessibility of mineral surfaces to nutrients or contaminants in the rhizosphere.

Zusammenfassung

Mangelnde P-Versorgung limitiert das Pflanzenwachstum auf sauren Standorten auf Grund der starken Bindung von Phosphat an Sesquioxide. Viele Untersuchungen dokumentieren eine P-Mobilisierung durch wurzel-exsudierte Anionen niedermolekularer Polycarbonsäuren (LMWOA). Daneben exsudieren Pflanzen Polysacharide als einen Hauptbestandteil der Mucilage. Deren Einfluss auf die Bioverfügbarkeit von Phosphat ist jedoch weitestgehend unverstanden.

Die Sorption von Phosphat an Fe-Oxide teilt sich gewöhnlich in eine schnelle und eine langsame Reaktion. Für Goethit (α-FeOOH) besteht die schnelle Reaktion in der Adsorption des Phosphats an äußere Oberflächen, wohingegen die langsame Reaktion durch die Diffusion von Phosphat in Mikro- (Ø <2 nm) und Mesoporen (Ø 2-50 nm) des Adsorbenten hervorgerufen wird. Bislang ist unbekannt, ob mineral-assoziierte Wurzelexsudate die Zugänglichkeit von Mineralporen für Phosphat einschränken. Das Hauptziel dieser Arbeit war es daher zu untersuchen, ob organische Wurzelexsudate die Poren von Fe-Oxiden verschließen und damit die Porendiffusion von Phosphat unterbinden.

Die Verwendung von Polygalakturonat (PGA) als Modellsubstanz für pflanzenbürtige Mucilage ist nicht gerechtfertigt, wenn sich die Eigenschaften *in situ* gewonnener makromolekularer Wurzelesxudate von denen der PGA unterscheiden. Daher sollte die Porosität sowie die Kinetik der Phosphatdesorption von Fe-Oxiden verglichen werden, welche mit PGA und hochmolekularen, nicht keimfrei gewonnenen Wurzelexsudaten von Maispflanzen equilibriert wurden.

Weil die Quellung organischer Beläge die Zugänglichkeit von Mineraloberflächen für Phosphat verändern könnte, sollte darüber hinaus der Einfluss der Befeuchtung von PGA-Belägen auf die Phosphatsorptionskinetik von Sesquioxiden ermittelt werden.

Zur Bearbeitung genannter Fragestellungen wurden Goethite (α-FeOOH) mit hoch- und niedermolekularer organischer Substanz equilibriert. Anschließend wurden ihre Porositäten mittels Gasadsorption bestimmt (N_2 und CO_2). Polygalakturonat, bodenbürtige gelöste organische Substanz (DOM) und Mucigel (MU) von Maispflanzen (*Zea mays* L.) wurden als hochmolekulare, Citrat und Galakturonat (GA) als niedermolekulare Sorbate verwendet. Phosphatsorptions- und desorptionsexperimente wurden im Batchversuch bei pH 5 über einen Zeitraum von bis zu drei Wochen durchgeführt.

Der Einfuß der Befeuchtung von PGA-Belägen auf die Sorptionskinetik von Phosphat wurde mit Batchexperimenten untersucht, nachdem PGA-belegtes Al-Oxid (Al_2O_3) für zwei bzw. 170 Stunden in Wasser bei pH 5 equilibriert wurde. Zusätzlich wurden die Pro-

ben mittels ^{1}H-NMR Relaxometrie und Differentieller Scanning Kalorimetrie (DSC) charakterisiert.

Alle organischen Substanzen reduzierten das <5-nm Porenvolumen von Goethit. Trotz verringerter Porosität wies die langsame Sorption von Phosphat an PGA-belegte Goethite keine Beziehung zu deren Mikro- und Mesoporenvolumen auf. Die Phosphatsorption war mit der PGA-Desorption korreliert, was zeigt, dass die schrittweise Desorption von PGA und/oder die Diffusion von Phosphat durch die organische Beläge die Rate der langsamen Phosphatsorption kinetisch kontrollieren.

Citrat verhinderte die langsame Phosphatsorption an reinem Goethit und Goethit, welcher mit DOM equilibriert wurde. Diese Beobachtung wurde auf einen Mikroporenverschluss durch Citrat sowie die citrat-induzierte Auflösung der Adsorbenten zurückgeführt.

Desorptionsexperimente mit GA-, PGA- und MU-behandeltem Goethit zeigten, dass nur nach PGA-Sorption Goethitporen für Phosphat weniger zugänglich waren. Ergebnisse aus Versuchen mit GA und PGA deuten darauf hin, dass organische Sorbate die Festlegung von Phosphat in <5-nm Goethitporen verstärken. Polygalakturonat und MU beeinflussten die Kinetik der Phosphatdesorption gegensätzlich, vermutlich auf Grund des im MU enthaltenen Phosphats und mineralischer Substanz sowie seines geringen Gehaltes an Uronsäuren.

Die Befeuchtung von PGA-belegtem Al-Oxid in Wasser für 170 Stunden erhöhte die Menge des schnell sorbierten Phosphats gegenüber einer Befeuchtungszeit von nur zwei Stunden. Dieses Ergebnis wurde auf die Umstrukturierung der PGA-Moleküle auf der Al-Oxidoberfläche infolge Befeuchtung zurückgeführt.

Aus den Ergebnissen lässt sich schlussfolgern, dass der Verschluss von Goethitporen durch PGA nicht relevant ist für die Phosphatsorptionskinetik von PGA-belegtem Goethit. Im Gegensatz dazu verschließen Anionen der LMWOAs Mikroporen von Goethit und unterbinden damit die Mikroporendiffusion von Phosphat. Da PGA in ihrer Zusammensetzung stark von *in situ* gesammelten makromolekularen Wurzelexudaten (Mucigel) abweichen kann, sind Aussagen über die Phosphatdynamik in der Rhizosphäre über Batchxperimente mit PGA erschwert. Die Permeabilität anionischer Polyelektrolytbeläge wurde als weitere Steuergröße für die Zugänglichkeit von Mineraloberflächen für Nähr- oder Schadstoffe in der Rhizosphäre identifiziert.

1. General Introduction

1.1 The slow sorption of phosphate by Fe oxides

The sorption of phosphate to Fe oxides usually comprises a fast and a slow reaction (Kuo and Lotse, 1974; Barrow et al., 1981; Torrent et al., 1990, 1992; Strauss et al., 1997). The slow sorption reaction of goethite with phosphate can last for weeks (Strauss et al., 1997). Rate-limiting for the initial fast reaction of goethite (α-FeOOH) is the ligand-exchange between singly coordinated hydroxyls of external, readily accessible surfaces, i.e., primarily of (101) surfaces (Cornell and Schwertmann, 2003). The slow phosphate sorption has been ascribed to the diffusion of phosphate into intraparticle micro- and mesopores of the adsorbent (Barrow et al., 1993; Strauss et al., 1997) or into pores of aggregates (interparticle pores, Anderson et al., 1985; Willet et al., 1988). The extent of the slow phosphate sorption or desorption reaction of Fe oxides depends on the micro- and mesoporosity, the shape of pores, and hence on the crystallinity of the oxide (Madrid and Arambarri, 1985; Cabrera et al., 1981; Torrent et al., 1990, 1992; Strauss et al., 1997). Following IUPAC (Rouquerol et al., 1994), micro- and mesopores are defined here as pores having a size of <2 nm and 2-50 nm, respectively. Intraparticle pores of goethite are located at domain boundaries (<50-nm pores between subcrystals), or are randomly distributed over the whole goethite surface (<1-nm pores; Fischer et al., 1996; Prélot et al., 2003). Fischer et al. (1996) argued that the diffusion of phosphate into interdomain pores is not limited when pores are ~20-30 nm wide, but becomes limited with increasing penetration depth of phosphate as pores get narrower unless they finally reach molecular dimensions.

The theory of pore diffusion of oxyanions is not only confined to Fe oxides and phosphate: The diffusion of phosphate into micropores of Al-based drinking-water treatment residuals (WTR) has been reported by Makris et al. (2004). Likewise, Shin et al. (2004) discussed the differences in the phosphate sorption kinetics between Al-impregnated mesoporous silica and activated alumina in terms of pore structure. Fuller et al. (1993) showed that the adsorption of As(V) to ferrihydrite is limited by diffusion of As(V) to sorption sites located in pores of ferrihydrite aggregates.

1.2 Increase in phosphate bioavailability by organic root exudates in the rhizosphere

The rhizosphere is defined as a zone surrounding plant roots, which is modified by root activity (Ryan et al., 2001). Phosphate concentrations in the soil solution are usually less than 20 µM (Barber, 1974). Phosphorus requirements of plants depend on plant species and may range from <0.1 to 60 µM (Asher and Loneragan, 1967; Breeze et al., 1984). Sev-

eral studies showed that a zone of P depletion exists normal to the root of various plant species (Brewster et al., 1976; Temple-Smith and Menary, 1977; Hendriks et al., 1981). The size of this P depletion zone ranges from 1 to 5 mm (Ryan et al., 2001, Fig. 2 therein). One strategy by which plants directly or indirectly facilitate the procurement of phosphate in the rhizosphere is the root exudation of organic compounds (Hinsinger, 2001; Dakora and Phillips, 2002). The processes triggered by plants in response to P-deficiency are highly context-dependent and may vary considerably among plant species, plant nutritional status, and ambient soil conditions (Hinsinger, 2001). Organic root exudates that increase the bioavailability of phosphate include enzymes (phosphatase), siderophores, and anions of low-molecular-weight organic acids (LMWOA) other than those belonging to the siderophores (Hinsinger, 2001; Dakora and Phillips, 2002).

Phosphatases are enzymes capable of hydrolyzing and mobilizing inorganic P from organic phosphate esters (Duff et al., 1994). Low phosphate solution concentrations induce the production of extracellular and intracellullar acid phosphatases, and an increase in the proportion of acid phosphatases in root exudates (Goldstein et al., 1988; Lee, 1988; Dinkelaker and Marschner, 1992). The positive effect of increased acid phosphatase secretion on phosphate nutrition has been evidenced for lupin plants (Tadano and Sakai, 1991).

Phytosiderophores are organic low-molecular-weight compounds of the mugineic acid family that form strong 1:1 complexes with Fe(III). Exudation of siderophores by plants has been only observed in the class of monocotyledons for the family of Gramineae (grasses) (Reichard, 2005). The dissolution of phosphate-loaded Fe oxides by phytosiderophores may increase phosphate solution concentrations in the soil rhizosphere, but direct evidences are still lacking (Hinsinger, 2001).

The role of LMWOA anions in the acquisition of phosphate has been most intensively studied. From an extensive literature survey, Guppy et al. (2005) conclude that the sorption competition between LMWOA anions and phosphate is only likely to be of ecological relevance in the rhizosphere, where the concentrations are high compared with concentrations of LMWOA anions of <10 µM typically encountered in soil solution (Guppy et al., 2005). The exudation of LMWOA anions by plants has been consistently shown to increase in response to P deficiency. This has been observed for plant species such as oilseed rape, white lupin, and alfalfa (Hinsinger, 2001 and ref. therein). Among exuded LMWOA anions citrate and malate have been shown in these studies to be the major contributors in the plant's response to P starvation. A special adaptation to low P status in soils is the development of proteoid roots of white lupin that exhibit a higher rate of citrate exudation

than other root compartments, and where the efflux of citrate increases at low phosphate solution concentration (Keerthisinghe et al., 1998; Neumann and Römheld, 1999). The increase in bioavailability of phosphate after exudation of LMWOA anions has been attributed to sorption competition between LMWOA anions and phosphate, the complexation of polyvalent metals that would otherwise immobilize phosphate, the decrease in surface charge of variable charge colloids, and/or the formation of soluble LMWOA-metal-phosphate complexes (Gardner et al., 1983; Jones et al., 1996; Kirk, 1999; Geelhoed et al., 1999; Guppy et al., 2005).

In addition to low-molecular-weight organic compounds, plants exude high-molecular-weight organic substances like components of mucilages that may contribute to P nutrition of plants. Mucilages are pectin-like high-molecular-weight root exudates of many plant species such as wheat, maize, rice, pea and cowpea (Knee et al., 2001). They are primarily secreted by root cap cells (Paull and Jones, 1975; Rougier, 1981) and comprise about 90-95% polymerized sugars with about 20-35% of uronic acids (Cortez and Billes, 1982; Morel et al., 1986). Gaume et al. (2000) and Grimal et al. (2001) showed that maize mucilage decreases the sorption of phosphate to Fe oxides. Sorption competition, microaggregation of Fe oxide particles, and the decrease in surface charge of the adsorbent by mucilage were invoked by these authors to explain their experimental results.

1.3 Research objectives

In soils, mineral surfaces are partly covered with organic matter (Mayer and Xing, 2001; Amelung et al., 2002; Gerin et al., 2003; Mayer et al., 2004). Organic coatings on mineral surfaces might be especially relevant in the rhizosphere, where the input of organic C as so-called rhizodeposition is large. Evaluating 43 tracer studies, Nguyen (2003) calculated that on average 17% of the net C fixed by photosynthesis is lost by roots, which corresponds to 50% of C exported by shoots to belowground. Hütsch et al. (2002) reported a value of 20% of photosynthetically fixed C that is released into the soil during vegetation period. Therefore, organic coatings on mineral surfaces are highly probable adjacent to plant roots, especially root caps.

The incorporation of organic matter into mineral pores has been shown by various researchers (Kaiser and Guggenberger, 2003; Lang and Kaupenjohann, 2003; Mayer et al., 2004; Mikutta et al., 2004; Zimmerman et al., 2004a, b). The clogging of mineral pores by root exudates may decrease the accessibility of mineral pores to phosphate, and hence increase its bioavailability. Especially mucilages have been implicated to strongly bind soil

particles together, thus coating mineral surfaces at the soil-root interface (Vermeer and McCully, 1982; Watt et al., 1993). Gaume et al. (2000) discussed the decreased phosphate sorption to mucilage-treated ferrihydrite in terms of a reduced accessibility of interparticle pores to phosphate due to microaggregation of ferrihydrite particles by mucilage. More recently, Lang and Kaupenjohann (2003) demonstrated that sorption of dissolved organic matter to goethites decreased the accessibility of intraparticle pores to molybdate. Apart from these studies, no reports are available on the clogging of Fe and Al oxide pores by organic matter and its effect on the immobilization kinetics of oxyanions. The proposed pore clogging mechanism might be of relevance in the rhizosphere under acid conditions as phosphate would otherwise be strongly immobilized in pores of sesquioxides.

Therefore, the main objective of this thesis was to elucidate whether the clogging of pores of Fe oxides by root exudates is a potential mechanism by which plants increase the bioavailability of phosphate in the rhizosphere. I hypothesized that polycarboxylic high- and low-molecular-weight root exudates successfully inhibit the slow phosphate sorption reaction of goethite due to the clogging of micro- and mesopores. First, I studied the effect of macromolecular polygalacturonate (PGA) coatings on the porosity of goethite, and compared the phosphate sorption kinetics of pure goethites with those of PGA-coated goethites. Polygalacturonate was chosen as a model substance for mucilage (Morel et al., 1987; Gessa and Deiana, 1992; Ciurli et al., 1996). Results of these experiments are presented in Chapter 2 and 3.

Secondly, I tested whether polycarboxylic LMWOA anions inhibit the diffusion of phosphate into micropores of pure goethite and goethite that was pre-equilibrated with dissolved organic matter. Citrate was chosen as a model LMWOA anion as its release is enhanced by several plant species in response to environmental stimuli like P and Fe deficiency or Al toxicity (Ryan et al., 2001, Table 2 therein). Results of this experiment are addressed in Chapter 4.

Another objective of this thesis was to elucidate whether root exudates are capable of entrapping phosphate in pores of goethite, and conversely, whether pre-sorbed root exudates result in an enrichment of phosphate on external goethite surfaces due to pore clogging. Lang and Kaupenjohann (2003) reported an enrichment of molybdate on external goethite surfaces after pre-equilibration of goethite with dissolved organic matter. Additionally, I compared the efficacy of PGA as a model compound for ‘mucilage’ to clog goethite pores and to inhibit the diffusion of phosphate into/out of goethite pores with that of mucigel obtained from maize plants (*Zea mays* L., cv. Marshal). Mucigel is defined as mu-

cilage of soil-grown plants that includes microorganisms and soil particles (Jenny and Grossenbacher, 1963). The comparison between PGA and mucigel was done in order to validate the transferability of results obtained from PGA experiments reported in Chapter 2 and 3 to 'real world' macromolecular root exudates. This experiment is described in Chapter 5.

In soils, organic coatings on minerals are subject to moisture fluctuations. There is growing evidence that the structure of soil organic matter changes when water is absorbed (Schaumann, 2005; Schaumann and LeBoeuf, 2005; Schaumann et al., 2004, 2005). Equilibrating samples of soil A horizon and peat in water led to a swelling of organic matter, which changed the pore size of the samples with time (Schaumann et al., 2004, 2005). Similarly, maize root-cap mucilage is able to hydrate extensively with water contents of up to 99.9% on a wet basis (Guinel and McCully, 1986). The swelling-induced change in pore size of organic matter associated with mineral surfaces may affect the immobilization of oxyanions by sesquioxides. Accordingly, the third objective of this thesis was to elucidate if the hydration-induced swelling of acid polysaccharide coatings changes the permeability of organic coatings for oxyanions. Specifically, I hypothesized that the hydration of PGA coatings on alumina (Al_2O_3) increases their permeability for phosphate. Alumina was taken as a non-paramagnetic adsorbent that could be used in ^{1}H-NMR relaxometry experiments. This experiment is subject matter of Chapter 6.

All experiments were conducted at pH 5 in order to (i) resemble the acidic conditions in the growth media of P starved plants supplied with NO_3-N (Neumann and Römheld, 1999), (ii) minimize interference with bicarbonate, and (iii) ensure the comparability of different kinds of experiments conducted in this thesis.

2 Kinetics of phosphate sorption to polygalacturonate-coated goethite

Christian Mikutta[1], Friederike Lang[1], Martin Kaupenjohann[1]

Soil Science Society of America Journal 2006; 70: 541-549

[1] Department of Soil Science, Institute of Ecology, Berlin University of Technology, Salzufer 12, D-10587 Berlin, Germany

2.1 Abstract

Biogenetic polysaccharides may affect the sorption characteristics of soil mineral particles in the rhizosphere. We hypothesized that polygalacturonate [PGA, $(C_6H_7O_6)^-_n$] coatings on goethite reduce the diffusion of phosphate into the pores of the adsorbent. Goethite was preloaded with PGA (0-10 mg C g^{-1}). The samples were characterized by N_2 and CO_2 adsorption, electrophoretic mobility measurements, and scanning electron microscopy/energy dispersive X-ray analysis (SEM-EDX). The phosphate sorption kinetics were studied with batch experiments over two weeks at pH 5 and an initial phosphate concentration of 250 µM. Pore volume and specific surface area of the goethite samples declined after PGA addition. The PGA coatings reduced the ζ-potential of goethite from 42.3 mV to -39.6 mV at the highest C loading. With increasing PGA-C content and decreasing ζ-potential the amount of phosphate sorbed after two weeks decreased linearly (P <0.001). Sorption of phosphate to pure and PGA-coated goethite showed an initial fast sorption followed by a slow sorption reaction. At the smallest C loading (5.5 mg C g^{-1}) the portion of phosphate retained by the slow reaction was smaller than for the treatment without any PGA, while at higher C loadings the fraction of slowly immobilized phosphate increased. Our results suggest that at low C loadings PGA impaired the intraparticle diffusion of phosphate. In contrast, the slow step-by-step desorption of PGA (<52% within two weeks) or the diffusion of phosphate through PGA coatings or both are rate limiting for the slow phosphate reaction at C loadings >5.5 mg C g^{-1}.

2.2 Introduction

Organic coatings have been identified and characterized on mineral surfaces of various soils (Courchesne et al., 1996; Yuan et al., 1998; Mayer and Xing, 2001; Amelung et al., 2002). Recently, X-ray photoelectron spectroscopy (XPS) data have shown that the surfaces of soil particles are covered with organic substances, even at low bulk organic C contents (<0.1 g kg^{-1}, Gerin et al., 2003). Carbohydrates, which are important constituents of soil organic matter (5-25 %, Stevenson, 1994), are dominated by polysaccharides that can contribute to organic coatings in soils (Miltner and Zech, 1998; Schmidt et al., 2000; Wattel-Koekkoek et al., 2001; Gerin et al., 2003). Many studies on the effect of low-molecular-weight organic acids like malic, citric or oxalic acid on phosphate sorption to soils and minerals are available (Jones, 1998; Jones and Darrah, 1994; Liu et al., 1999), but scant attention has been paid to high-molecular-weight biomolecules released by plants and/or microorganisms. Root apices of many plant species are covered by granular or fibrillar gelatinous materials (Greaves and Darbyshire, 1972). These high-molecular-weight materials (mucilages) exuded by plant's root cap or epidermal cells (Mollenhauer et al., 1961; Vermeer and McCully, 1982) consist mainly of polysaccharides (Paull and Jones, 1975; Moody et al., 1988). For example, mucilage of corn comprised about 90-95% polysaccharides with about 20-35% of polyuronic acids (Cortez and Billes, 1982; Morel et al., 1986). The actual amount of mucilage produced in soils still remains unknown (Nguyen, 2003). Reported polysaccharide-C contents (neutral sugar-C + galacturonic acid-C) of arable soils range from 0.22 to 3.83 mg C g^{-1} (Kiem and Kögel-Knabner, 2003). Studying organic coatings of soils with X-ray photoelectron spectroscopy (XPS), Gerin et al. (2003) found that particle surfaces were strongly enriched in organic C with surface concentrations in the range 50-500 mg C g^{-1}. Therefore, it seems reasonable to assume that mineral surfaces adjacent to plant's root caps have at least C loadings in the range reported by Gerin et al. (2003). As the macromolecular root exudates are supposed to not be diffusible in soils, or if so very slowly (Rovira, 1969; Sealey et al., 1995), their spatial distribution in soils is primarily confined to the soil-root interface. Cross-linked polysaccharide chains of exocellular slimes produced by plants or microbes act to bind soil or sediment minerals into microaggregates (Chenu, 1993; Ransom et al., 1997, 1999; Grimal et al., 2001). Organic coatings on Fe or Al oxide particles or their microaggregation by sorbed acid polysaccharides may decrease the immobilization of phosphate and hence increase its bioavailability.

Grimal et al. (2001) and Gaume et al. (2000) showed that polysaccharides decreased the phosphate sorption capacity of goethite and ferrihydrite. In addition, phosphate mobiliza-

tion from ferrihydrite increased in the presence of maize mucilage (*Zea mays*) and PGA (Gaume et al., 2000). This has been explained - but not yet proven - by the competition for sorption sites and the decrease in oxide surface charge by PGA (Grimal et al., 2001). Lang and Kaupenjohann (2003) recognized that adsorbed natural organic matter extracted from an acid forest floor layer affected the sorption of molybdate by clogging the pores of goethite. Yet, this mechanism has not been proven for mucilage components. Generally, polysaccharide coatings may decrease the sorption of phosphate to mineral surfaces by direct blocking of adsorption sites for phosphate, or by decreasing the accessibility of external or intraparticle sorption sites for phosphate.

We tested the hypothesis that acid polysaccharide coatings prevent phosphate from diffusion into intraparticle pores of goethite. We used synthetic goethite because it represents the most widespread Fe oxide in the soil environments (Cornell and Schwertmann, 2003). Polygalacturonate was taken as a model substance for macromolecular, pectin-like polysaccharides in the rhizospheric soil because it comprises similar structural characteristics like mucilage (Gessa and Deiana, 1992). The experiment was conducted at pH 5 in order to resemble pH conditions of the soil rhizosphere and the bulk of acid soils. The relevance of our study is confined to conditions where the pH of soil solution is lower than the isoelectric point (pH_{iep}) of Fe or Al oxides (typically pH_{iep} >7), and hence the availability of phosphate to plants is strongly reduced because of its sorption to positively charged Fe and Al oxide surfaces.

2.3 Materials and Methods

2.3.1 Goethite

Goethite was synthesized by ageing of ferrihydrite, which precipitated after mixing $Fe(NO_3)_3 \cdot 9H_2O$ and KOH solutions at a molar Fe/OH ratio of 0.05 (Schwertmann and Cornell, 1991). The solutions were aged at 333 ± 1 K for up to 16 days, dialyzed against deionized water until electric conductivity was below 10 µS cm^{-1}, dried at 333 K, softly ground, sieved <200 µm and stored in PE-bottles. Powder X-ray diffraction patterns of the samples were obtained using a Siemens D5005 instrument (Siemens AG, Germany) with CuKα-radiation of wavelength 0.15406 nm (40 kV, 30 mA). The measurement ranged from 5 to 50° 2θ, step size was 0.05° 2θ and step time was 30 s. The goethite was mixed with 25% SiO_2 as an internal standard. The scans indicated pure goethite with no detectable contamination (XRD spectra not shown). Oxalate soluble Fe of the goethite according

to Blakemore et al. (1987) was 9.9 mg g^{-1} and total Fe according to Schulze (1984) was 619 mg g^{-1}.

2.3.2 Polygalacturonic acid (PGA)

Polygalacturonic acid, $(C_6H_8O_6)_n$, with a purity of 86% (dry matter base) was purchased from Sigma (P-3889). Total acidity of PGA estimated from the structure is 5.7 mol_c kg^{-1} provided all acidity comes from COOH groups. The pK_a of PGA is reported to be 3.5 (Grimal et al., 2001) or 3.9 (Au et al., 1998). The molecular weight approximates 4,000-6,000 g mol^{-1} (Aldrich). The PGA did not contain other sugars. The C content was 374 ± 4 mg g^{-1} on a dry matter basis measured with a Carlo Erba C/N NA 1500N Analyzer. The most prominent polyvalent cation in the PGA determined after acid digestion in conc. HNO_3 was Ca with 12 mmol kg^{-1} PGA. This content was too low to cause precipitation of Ca phosphates in the phosphate sorption experiment as calculated with MINTEQ (Allison et al., 1991).

Polygalacturonic acid was dispersed in doubly deionized water by adding 10 µL 1 M KOH per milligram PGA. Six stock solutions containing 0, 20, 40, 80, 160 and 320 mg C L^{-1} were prepared. The pH value of the PGA solutions was adjusted to 5.0 with 0.1 M HNO_3 prior to sorption experiments. Because of pH adjustment the ionic strength in the stock solutions increased to ~0.005 M. The size of PGA in the stock solutions was measured by dynamic light scattering using a high performance particle sizer (HPPS, Malvern, U.K.). The average diameter of the PGA ranged from 560 ± 12 nm at 160 mg C L^{-1} to 1287 ± 14 nm at 320 mg C L^{-1}, but about 88% of the PGA in each treatment was smaller than 450 nm as determined after membrane filtration.

2.3.3 Sorption of PGA to goethite

Goethite (1.30 g) was placed in a 2-L glass volumetric flask. Then 1000 mL of 20 mM KNO_3 solution were added, and the pH was adjusted to pH 5.0 using 0.1 M HNO_3. The suspensions were sonicated for 20 min and shaken on a reciprocating shaker at 140 rev min^{-1} for 24 hours to ensure aggregate dispersion and hydration of adsorption sites. The goethite suspensions were added to 1000 mL of PGA solution in a 2-L PE bottle to yield an ionic strength of background electrolyte of I = 0.01 M and C concentrations between 0 and 160 mg L^{-1}. The suspensions were shaken on an end-over-end shaker at 20 rev min^{-1} and at 293 ± 2 K. The pH was maintained at 5 ± 0.2 using 0.1 M HNO_3 or 0.1 M KOH. After 45 hours the goethite suspensions were filtered through a 0.45-µm cel-

lulose nitrate membrane filter (Sartorious, Germany). The filter residue was rinsed with 800 mL 0.01 M KNO_3 solution (pH 5.0), freeze-dried (Christ, alpha 2-4 freeze drier), and C contents of the samples were determined with a Carlo Erba C/N NA 1500N Analyzer. PGA-C contents of the samples are given in Table 2.1. For convenience the different C treatments are termed according to the rounded C loading, i.e., G6 and G8 represent goethite with 5.5 and 7.6 mg C g^{-1}. In order to measure dissolved Fe concentrations after 45 hours of PGA sorption, three 5-mL aliquots were taken from each PE-bottle and ultracentrifuged at 300,000 x g for one hour and Fe concentrations in the supernatant were determined with atom absorption spectrometry (Perkin-Elmer 1100B).

We calculated the fraction of total mineral surface covered by organic matter, f_{cov}, by the relation

$$f_{cov} = (SSA_{naked} - SSA_{coated}) / SSA_{naked}, \quad [2.1]$$

where SSA_{naked} and SSA_{coated} are the BET surface areas of uncoated and coated goethite, respectively (Mayer and Xing, 2001). Equation [2.1] assumes that the difference in *SSA* between coated and uncoated samples represents surface area that is occluded by organic matter. This mechanism might impair the diffusion of N_2 at 77 K into inter- and intraparticle pore space (Mayer and Xing, 2001).

2.3.4 SEM Analysis

Freeze-dried samples were analyzed with Scanning Electron Microscopy (Hitachi S-2700) to identify organic coatings and structural changes induced by PGA. The specimens were placed on conductive carbon tape, surface-sputtered with Au and measured in the secondary electron detection mode (Evenhart-Thornley detector). The elemental composition of PGA-coated surfaces was estimated by an energy dispersive X-ray detector (EDX) fitted to the microscope.

2.3.5 Phosphate sorption kinetics

Phosphate was provided as KH_2PO_4 p.a. (Merck, Germany). Triplicate samples of uncoated and PGA coated goethite (20 mg) were weighed into 50-mL polypropylene centrifuge tubes (Nalgene, USA), which contained an agate ball of 10-mm size to ensure good mixture. Subsequently, 40 mL of 0.01 M KNO_3 solution with a phosphate concentration of 250 µM (pH 5.0) were added. At pH 5 the predominant chemical species of phosphate pre-

sent is $H_2PO_4^-$. Fifty microliters of 0.05 M $AgNO_3$ were added per liter phosphate solution in order to inhibit microbial activity.

The suspensions were reacted in the dark at room temperature 293 ± 2 K on a rotary shaker at 22 rev min^{-1} for 0.5, 1, 2, 4, 8, 16, 48, 168 and 336 hours. After each reaction period, the pH was recorded and 10-mL aliquots were membrane filtered (0.45 µm), ultracentrifuged at 300,000 x g for one hour and phosphate and Fe concentrations were measured in the supernatant. The filter residue was washed with 40 mL doubly deionized water to remove excess phosphate and freeze-dried. The phosphate concentration was determined photometrically at 710 nm by the method of Murphy and Riley (1962) using a Specord 200 spectralphotometer (Analytik Jena AG). The accuracy of this method was tested to be <1.5%; precision of the measurements was <1%. Subsample variability was generally <2%. We checked the possibility that PGA is precipitated during ultracentrifugation, which would decrease phosphate concentration in solution if phosphate was bound to polyvalent cations associated with the carboxylic groups of PGA. We found no statistical significant indication of a matrix interference by PGA.

The amount of phosphate sorbed was calculated as the difference between phosphate in solution prior and after each reaction time interval. Iron concentrations were measured by furnace atomic absorption spectrometry (Perkin Elmer AAnalyst 700). The Fe concentrations were less than 3 µM, and hence goethite dissolution by PGA desorption was negligible. The amount of PGA-C desorbed was calculated from the initial PGA-C content in the sample and the total organic C concentration measured in the 0.45-µm filtrate using a Shimadzu TOC-5050A Autoanalyzer.

2.3.6 Modeling of phosphate sorption kinetics

Two kinetic models were used to describe the phosphate sorption data. The fitting was performed with SigmaPlot for Windows (SPSS Inc.).

1. Combined model. We combined a first-order model and the parabolic diffusion model (Crank, 1976) in order to account for fast sorption to external sorption sites and diffusion limited slow sorption of phosphate to goethite (Lang and Kaupenjohann, 2003). In PGA-coated samples a portion of phosphate reacted instantaneously. For this reason we permitted a positive intercept:

$$q_t = c_m - a_0 e^{-kt} + bt^{0.5}, \qquad [2.2]$$

where q_t is the amount of phosphate sorbed at time t (µmol m^{-2}), c_m is the maximum amount of phosphate sorbed by the fast reaction (µmol m^{-2}), (c_m-a_0) is the amount of phosphate sorbed instantaneously (faster than could be quantified by the batch approach in µmol m^{-2}), k is the rate constant of the initial fast phosphate sorption (h^{-1}), b is the apparent rate constant of the slow reaction (µmol m^{-2} $h^{-0.5}$), and t is time (h). The parameters c_m, a_0, k and b were determined by fitting Eq.[2.2] to the sorption data. We used q_{336h} corrected for the total amount of phosphate rapidly sorbed (c_m) as an approximation for the fraction of phosphate sorbed slowly (*Fraction* P_{slowly}).

2. Diffusion in heterogeneous medium. Differentiation of the parabolic diffusion equation explicitly expressed as the reciprocal of the rate of diffusion in a heterogeneous medium yields (Aharoni et al., 1991):

$$Z = (dq/dt)^{-1} = ln\,(\tau_m/\tau_i)\; t\,/q_\infty\,[1 - (4t/(\pi\tau_m))^{1/2} - 8/\pi^2\; exp(-\pi^2\, t/(4\,\tau_i))]^{-1}, \qquad [2.3]$$

where $\tau = r^2/D$ with D = diffusion coefficient and r = length of diffusion, τ_i = smallest r and τ_m = largest r. Equation [2.3] yields S-shaped plots of $(dq/dt)^{-1}$ vs. t which are concave to the t axis at small times, convex at large times and linear in between. For diffusion in heterogeneous medium, the linear part of the Z-plots is most prominent, i.e., for τ_i and τ_m there is a large range of t at which the two negative terms in Eq.[2.3] become negligible. Hence, Eq.[2.3] can be reduced to (Aharoni et al., 1991):

$$d(q/\,q_\infty)/dln\; t = 1/\rho = [ln(\tau_m/\tau_i)]^{-1}. \qquad [2.4]$$

The ratio τ_m/τ_i is taken as a measure of the heterogeneity of diffusion pathways (Aharoni and Sparks, 1991).

2.3.7 Model evaluation

The models applied to kinetic data were judged on the basis of the coefficient of determination and the standard error statistics. Model parameters were evaluated by their standard errors using the *t*-statistics, which tests the null hypothesis that the parameter is zero by comparing the parameter value with its standard error. Standard errors of derived parameters were calculated according to the rules of error propagation.

2.3.8 Surface area and pore analysis

Specific surface area (*SSA*) and pore volume were determined with a Quantachrome Autosorb-1 automated gas sorption system (Quantachrome, Syosset, NY) using N_2 as an adsorbate. Approximately 100 mg of sample were degassed until the rate of pressure increase by vapor evolution was below about 1.3 Pa min^{-1} within a 1-min interval. Helium was used as a backfill gas. We used 67-point N_2 adsorption and desorption isotherms from 1.0×10^{-5} to 0.995 P/P_0. Specific surface area was calculated from the BET equation (Gregg and Sing, 1982).

Micropore (<2 nm) porosity and average micropore diameter were determined according to the Dubinin-Radushkevic method (DR, Gregg and Sing, 1982). Because samples showed a large adsorption-desorption hysteresis suggesting network effects during desorption that cause overestimation of surface area (Lowell and Shields, 1984), the mesopore size distribution (2-50 nm) was calculated on the adsorption leg using the BJH method (Barrett et al., 1951). Separation between small (2-10 nm) and large mesopores (10-50 nm) was achieved by linear interpolation of the BJH adsorption data. Total pore volume was taken at 0.995 P/P_0. We also determined the micropore volume using CO_2 as an adsorbate at 273 K with a NOVA gas sorption system (Quantachrome, Syosset, NY). A 25-point adsorption was performed from 1.0×10^{-3} to 3.0×10^{-2} P/P_0 and analyzed using the Dubinin-Radushkevic equation (Gregg and Sing, 1982). All isotherms were recorded in duplicate.

2.3.9 Electrophoretic mobility measurements

Sorption of anionic polyelectrolytes like PGA to goethite may alter its surface charge and thus affect the kinetics of phosphate immobilization. Therefore, we determined the initial ζ-potential of the pure and PGA-coated goethites in 0.01 M KNO_3 solution at pH 5.0. Changes in ζ-potential during phosphate sorption were monitored after resuspending about 200 µg of freeze-dried 0.45-µm filter residue into 4 mL of phosphate equilibrium solution of a respective point in time. Preliminary tests showed no statistically significant difference between ζ-potentials obtained from freeze-dried and non-dried pure and PGA-coated goethites (unpaired *t*-test, $P < 0.05$). The electrophoretic mobility was determined at 298 K with a Malvern Zetasizer 2000 (Malvern Instruments, UK). Before starting the measurements the calibration of the instrument was validated with a ζ-potential transfer reference, which is referenced to the NIST goethite standard SRM1980 (Malvern Instruments, UK). Ten measurements were performed within less than 8 minutes and the average

value was recorded. The ζ-potential was calculated from the electrophoretic mobility using the Smoluchowski approximation (Hunter, 1988). It is generally assumed that the ζ-potential represents the potential at a shear plane located in the diffuse layer close to the Stern layer (Hunter, 1988).

2.4 Results and Discussion

2.4.1 Fractional PGA coverage and surface loadings

Fractional coverage values of our goethite samples indicate that about one third of the goethite surface area is lost due to polysaccharide coatings regardless of the amount of PGA addition (Table 2.1). A negative correlation was observed between the amount of PGA-C sorbed and the coating-efficiency of PGA (i.e., loss of surface area per milligram PGA-C sorbed, r^2 = 0.93, P <0.01). The coating efficiency decreased from 4.42 ± 0.3 m^2 mg^{-1} PGA-C for G6 to 2.68 ± 0.16 m^2 mg^{-1} PGA-C for G10 (mean ± standard deviation). At similar C loadings per unit mass, PGA decreased the *SSA* of goethite more effectively than sorbed dissolved organic matter (approximately factor 2; Fig. 5a in Kaiser and Guggenberger, 2003). Kaiser and Guggenberger (2003) explained the increasing coating efficiency with decreasing C loading of surfaces by varying surface arrangements of organic molecules (see also Theng, 1979, p. 42; Saito et al., 2004), organic multilayer formation or preferential sorption at specific reaction sites, i.e., micropores.

Scanning electron microscopy images of pure goethite show the elongated acicular crystals with up to 2 µm length and 0.2 µm width. Large fibrous multidomain crystallites are well visible (Fig. 2.1a). The images of PGA treated goethite samples reveal the occlusion of the goethite needles by organic matter (Fig. 2.1b, c). Cotton-wool like agglomerations dominate besides larger areas where no coatings can be inferred, possibly because of insufficient coating thickness. Energy dispersive X-ray analysis indicated that even surfaces where no coating was visible contained appreciable amounts of PGA-C (not shown).

Table 2.1. PGA-C content (n = 3), fractional coverage f_{cov} (n = 2), and ζ-potential (n = 10) of pure and PGA-coated goethite. The fractional coverage calculated from Eq.[2.1] represents the fraction of total surface area that is not accessible by N_2 adsorption at 77 K. Values in parentheses represent mean range for the fractional coverage and standard error for C contents and ζ-potentials, respectively. ζ-Potentials followed by the same letter are not statistically different at P <0.05 (unpaired t-test).

Sample	PGA-C content[†]		Fractional Coverage f_{cov}	ζ-Potential at pH 5 in 0.01 M KNO_3
	mg g^{-1}	mg m^{-2}		mV
G0				42.3 (0.4)a
G6	5.5 (0.04)	0.075 (0.001)	0.33 (0.01)	-20.0 (1.5)b
G7	7.2 (0.05)	0.100 (0.001)	0.35 (0.01)	-37.6 (0.3)c
G8	7.6 (0.04)	0.105 (0.001)	0.36 (0.03)	-37.9 (0.2)c
G9	8.5 (0.02)	0.117 (0.001)	0.35 (0.01)	-38.6 (0.2)d
G10	10.0 (0.02)	0.138 (0.001)	0.37 (0.01)	-39.6 (0.2)e

[†] PGA-C contents were obtained by substracting the background C-content.

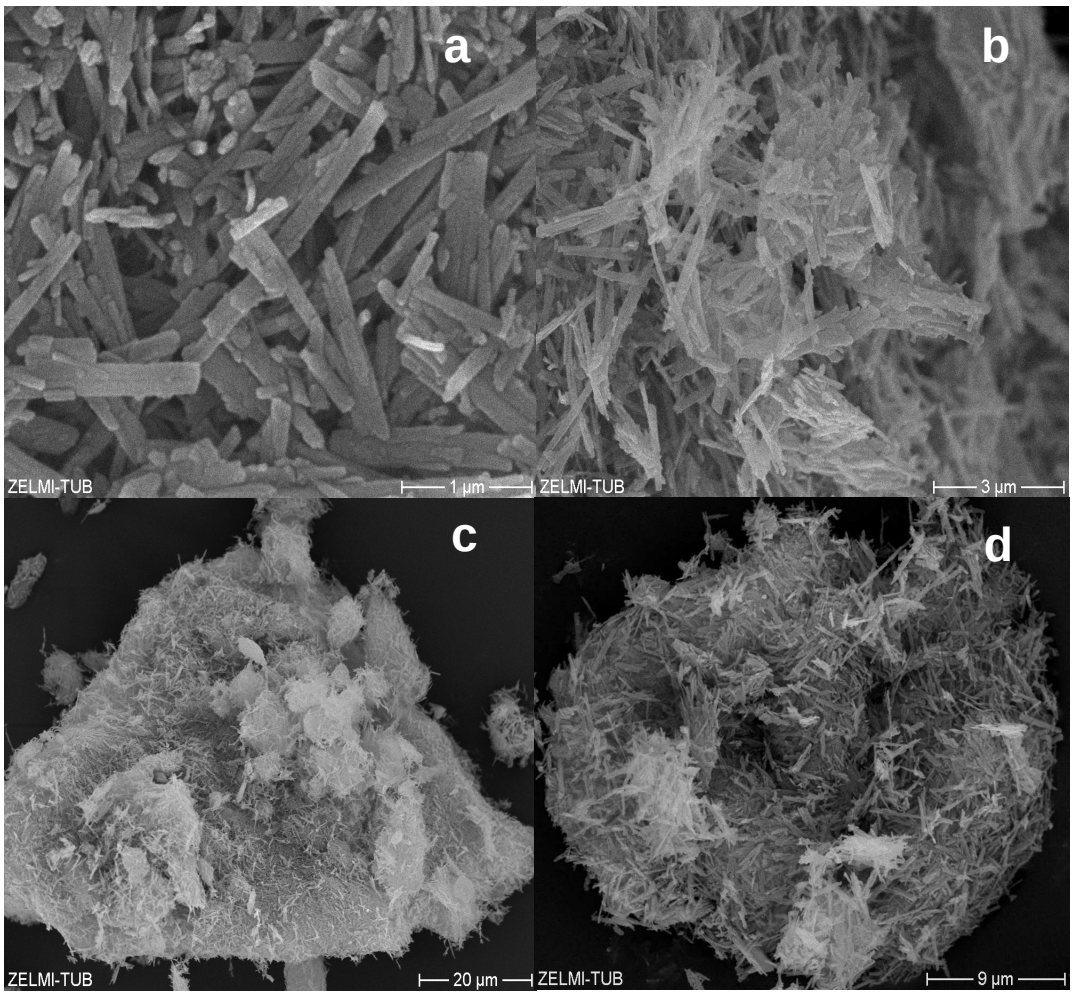

Fig. 2.1. Scanning electron microscopy images of pure goethite (a), and PGA-coated goethite with different C loadings: b = 5.5 mg C g^{-1}, c = 7.6 mg C g^{-1}, and d = 10 mg C g^{-1}. Multidomainic goethite crystals are visible in Fig. 2.1a; Fig. 2.1b shows in more detail the clustering of goethite crystals induced by PGA at low PGA-C content; Fig. 2.1c and 2.1d give overviews of PGA-goethite clusters on differently sized aggregates of goethite.

2.4.2 Porosity changes by PGA

Polygalacturonate coatings reduced the total pore volume by 85 $mm^3\ g^{-1}$ (24%) on average. The N_2 micropore- and small mesopore volumes declined to 65 and 51% of the initial values, respectively (Table 2.2). Our CO_2 adsorption study showed that pores <0.5 nm, into which N_2 diffusion at 77 K is kinetically restricted, existed in samples with intermediate and high PGA loadings (Table 2.2, G7, G8, G10). Upon PGA sorption, the *SSA* declined on average by 35%, independent of the C loading (Table 2.2).

Table 2.2. Specific surface area (*SSA*) and porosity data of pure and PGA-coated goethite obtained by N_2 adsorption at 77 K and CO_2 adsorption at 273 K (n = 2). Figures after 'G' refer to the rounded C content of the sample in mg C g^{-1}. Values in parentheses are given as mean range.

Sample	SSA	Total Pore Volume	Micropore Volume		AMD†	Mesopore Volume	
			N_2	CO_2		2-10 nm	10-50 nm
	$m^2\ g^{-1}$	———	$mm^{-3}\ g^{-1}$	———	nm	$mm^3\ g^{-1}$	
G0	72.5 (0.6)	356 (51)	18.0 (0.1)	17.9 (1.9)	0.92 (0.02)	61.4 (2.3)	97.0 (7.8)
G6	48.4 (1.0)	266 (21)	14.5 (0.6)	14.4 (0.8)	1.02 (0.01)	35.5 (1.5)	73.4 (8.0)
G7	47.1 (0.7)	280 (3)	14.3 (0.1)	15.7 (1.3)	1.02 (0.00)	32.6 (0.0)	78.3 (0.0)
G8	46.5 (1.8)	263 (13)	12.8 (0.5)	16.4 (0.5)	0.94 (0.02)	33.7 (3.2)	75.3 (2.1)
G9	47.4 (1.0)	287 (16)	11.7 (0.4)	12.2 (0.7)	0.91 (0.02)	32.8 (1.4)	79.8 (3.5)
G10	45.6 (1.0)	261 (12)	11.6 (0.3)	16.7 (0.7)	0.93 (0.02)	31.1 (0.5)	75.5 (2.7)

† Average micropore diameter.

2.4.3 Phosphate sorption

Various phosphate adsorption studies on Al oxides (Chen et al., 1973), Fe oxides (Madrid and Arambarri, 1985; Strauss et al., 1997) or soils (Torrent, 1987; Sanyal et al., 1993; Freese et al., 1995) show an initial rapid sorption, which is followed by a slow sorption. The rapid sorption to Fe oxides has been attributed to the adsorption of phosphate on outer mineral surfaces, while the slow immobilization of phosphate has been shown to be caused by the diffusion of phosphate into particle pores (Strauss et al., 1997). Similarly, the diffusion of phosphate into micropores has been confirmed for drinking-water treatment residuals that comprise amorphous Fe and Al oxides (Makris et al., 2004). This typical sorption pattern was also observed in our study (Fig. 2.2). Phosphate sorption onto G0, G6 and G10 attained apparent equilibrium within two weeks. This finding is in agreement with Strauss et al. (1997) who found that phosphate sorption onto pure goethite was complete within two weeks. However, sorption of phosphate onto goethite samples with intermediate PGA loadings (G7-9) continued and did not reach apparent equilibrium within two weeks (Fig. 2.2).

The combined model provided a reasonable fit of the data with r^2 values between 0.94-1.00 (Table 2.3), which is in agreement with the conceptual model of diffusion limited slow sorption. An exception was treatment G6, where no slowly continuing phosphate sorption could be observed. Sorption was nearly completed after 48 hours, pointing out that diffusion was greatly reduced as indicated by a strong decrease in the rate constant of the slow phosphate reaction (Table 2.3, *b*). We will discuss the reason for this observation in a separate paragraph later on.

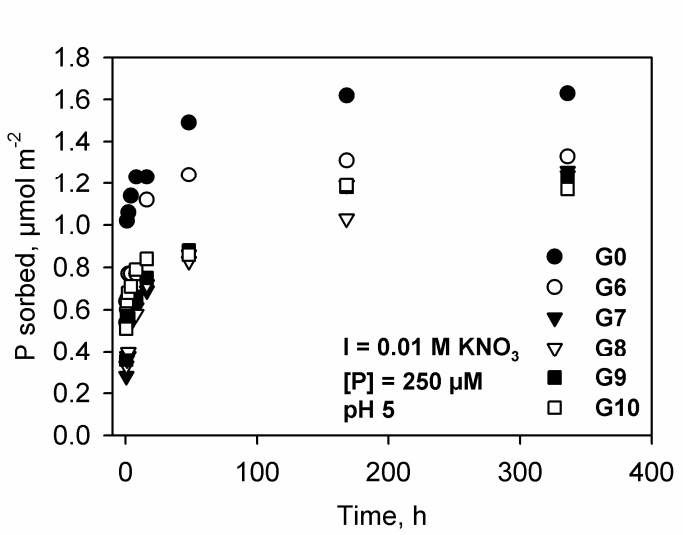

Fig. 2.2. Changes in phosphate sorption with time of PGA-coated and pure goethite. The solid concentration was 0.5 g L^{-1}. Subsample variability was typically less than 2%. Figures after 'G' refer to the rounded C content of the sample in milligram C per gram.

Table 2.3. Fit parameters of the regression of phosphate sorption vs. time of pure and PGA-coated goethite using the combined model, Eq.[2.2], and the diffusion in heterogeneous medium model, Eq.[2.4]. Also given are the slope parameters ($1/\rho$) and heterogeneity indices (τ_m/τ_i) obtained from the heterogeneous diffusion model. Figures after 'G' refer to the rounded C content of the sample in milligram C per gram. Values in parentheses represent standard error.

Sample	Combined Model						Heterogeneous Diffusion		
	c_m †	a_0 ‡	k §	b ¶	Fraction P_{slowly} #	r^2	$1/\rho$	(τ_m/τ_i)	r^2
	µmol m^{-2}	µmol m^{-2}	h^{-1}	µmol m^{-2} $h^{-0.5}$ x 10^{-3}					
G0	1.13 (0.06)	1.13 (0.63)	1.69 (0.99)	31.9 (6.6)	0.31 (0.04)	0.94	0.072	1.13 x 10^6	0.97
G6	1.24 (0.16)	0.67 (0.15)	0.08 (0.03)	5.3 (11.4)	0.07 (0.12)	0.96	0.100	2.23 x 10^4	0.91
G7	0.57 (0.07)	0.34 (0.08)	0.23 (0.14)	40.6 (6.0)	0.54 (0.06)	0.98	0.126	2.74 x 10^3	0.97
G8	0.58 (0.03)	0.31 (0.03)	0.18 (0.05)	35.6 (2.6)	0.53 (0.03)	1.00	0.117	5.15 x 10^3	0.98
G9	0.57 (0.04)	0.57 (0.53)	1.90 (1.69)	39.8 (4.3)	0.54 (0.03)	0.97	0.101	2.05 x 10^4	0.94
G10	0.70 (0.05)	0.31 (0.18)	0.92 (0.90)	29.2 (4.8)	0.40 (0.04)	0.95	0.082	1.86 x 10^5	0.92

† Total amount of phosphate sorbed fast.

‡ Parameter related to the amount of phosphate sorbed instantaneously (c_m-a_0) according Eq.[2.2].

§ Rate constant of the fast phosphate sorption.

¶ Rate constant of the slow phosphate sorption.

Fraction of phosphate slowly immobilized, calculated as (q_{336h}-c_m)/q_{336h}, where q_{336h} is the amount of phosphate sorbed after two weeks, and c_m is the total amount of phosphate sorbed fast.

In the presence of PGA the amount of phosphate sorbed via the fast reaction decreased by up to 50% (Table 2.3, c_m). The rate constants of the fast reaction varied greatly (Table 2.3, k). Sensitivity analyses, however, showed that the amount of phosphate sorbed was rather insensitive to changes in k. The rate constant of the slow reaction increased in the treatments G7-9 compared with pure goethite (Table 2.3, b).

Also, the heterogeneous diffusion model provided an adequate fit of the data with r^2 values ranging from 0.91 to 0.98 (Table 2.3). Aharoni and Sparks (1991) predicted that a slope <0.24 for the relationship $d(q/q_\infty)$ vs. ln t is indicative of heterogeneous diffusion. Using Eq.[2.4], we obtained slopes ($1/\rho$) between 0.072 and 0.126, suggesting heterogeneous diffusion (Table 2.3). The ratio τ_m/τ_i differed by three orders of magnitude: 10^6 (G0) – 10^3 (G7 and G8), indicating that the heterogeneity, i.e., the range of reciprocal apparent diffusion constants, $(D/r^2)_{app}$, of goethite decreased by PGA coatings (Table 2.3). For those samples, where equilibrium was not reached after two weeks, only a minimum value of τ_m/τ_i can be estimated from q/q_{max} (Aharoni et al., 1991).

2.4.4 Electrophoretic mobility measurements

Phosphate sorption to pure goethite reversed its ζ-potential from positive to negative values (Fig. 2.3). After about 16 hours of phosphate sorption, the ζ-potential of the goethite increased again by approximately 20 mV. The increase in ζ-potential of goethite with time has been documented in other phosphate sorption studies using lower and higher phosphate concentrations compared to this study (Ler and Stanforth, 2003, Mikutta et al., 2006a). There are several possible explanations including the surface precipitation of Fe phosphates or the formation of ternary surface complexes with dissolved Fe. The dissolution of goethite in the presence of phosphate increased the dissolved Fe concentrations in G0 samples up to 2.7 µM. The increase in ζ-potential observed (Fig. 2.3) might reflect the increase in the total dissolved Fe concentrations after 16 hours and hence indicate the formation of ternary surface complexes as proposed by Ler and Stanforth (2003). However, no Fe phosphates were observed by XANES in a study by Khare et al. (2005) who used a much higher concentration than applied in our study (0.01 M phosphate). Also, no Fe phosphate precipitates on natural goethite were observed after 90 days at elevated phosphate concentrations (0.001 M, pH 4.5; Martin et al., 1988). Thus, the surface precipitation of Fe phosphates seems unrealistic.

With increasing PGA loadings the ζ-potential decreased to negative values (Table 2.1). At a PGA loading of 7.2 mg C g^{-1} the ζ-potential dropped markedly from 42.3 to

-37.6 mV; any additional amount of PGA altered the ζ-potential only slightly (Table 2.1). This result may be explained in terms of multilayer sorption of polyprotic PGA molecules, which can also be inferred from similar fractional surface coverages (Table 2.1), our SEM observations (Fig. 2.1), and the presence of polyvalent cations in the PGA (see section 2.3.2).

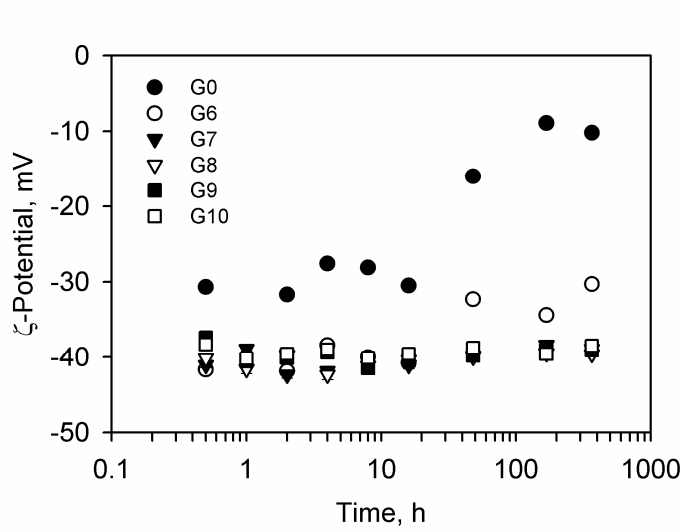

Fig. 2.3. Changes in ζ-potential of pure and PGA-coated goethite during phosphate sorption (I = 0.01 M KNO_3, pH 5). Note that x-axis is log scale. Error bars indicating the standard error of 10 replicate measurements are within the symbol size. Initial ζ-potentials of the samples (no phosphate contact) are presented in Table 2.1. Figures after 'G' refer to the rounded C content of the sample in milligram C per gram.

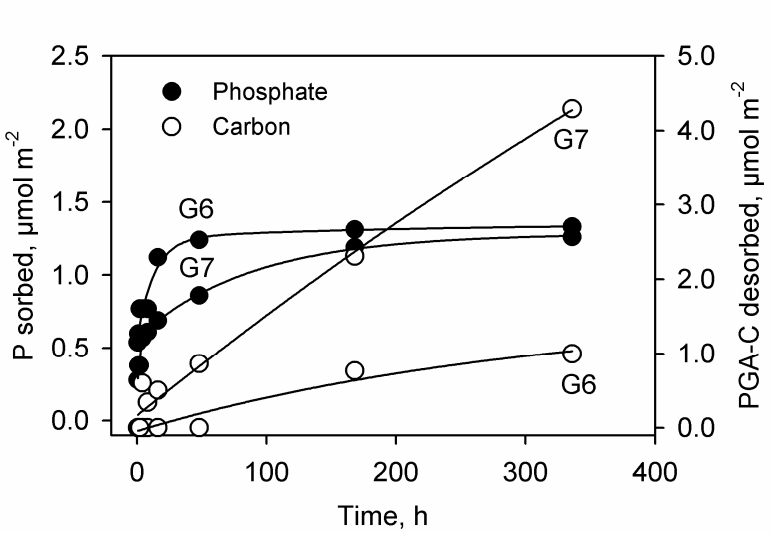

Fig. 2.4. Kinetics of phosphate sorption and PGA-C desorption in samples with low (G6) and intermediate PGA-C content (G7) at an initial phosphate concentration of 250 µM in 0.01 M KNO_3 at pH 5 with a solid concentration of 0.5 g L^{-1}. Figures after 'G' refer to the rounded C content of the sample in milligram C per gram.

In all cases except those with no and small PGA content (G0, G6) the ζ-potential was independent of phosphate sorption, staying constant around –39 mV after contact with

phosphate solution (Fig. 2.3). The most likely explanation is that the negative charge of phosphate ions conveyed to the surface was counterbalanced by a release of PGA into solution. This assumption is supported by the increasing C concentrations in solution with increasing phosphate sorption (Fig. 2.4). Up to 52% of PGA-C (G7) was desorbed by phosphate indicating the high competitiveness of phosphate for sorption sites (Fig. 2.5).

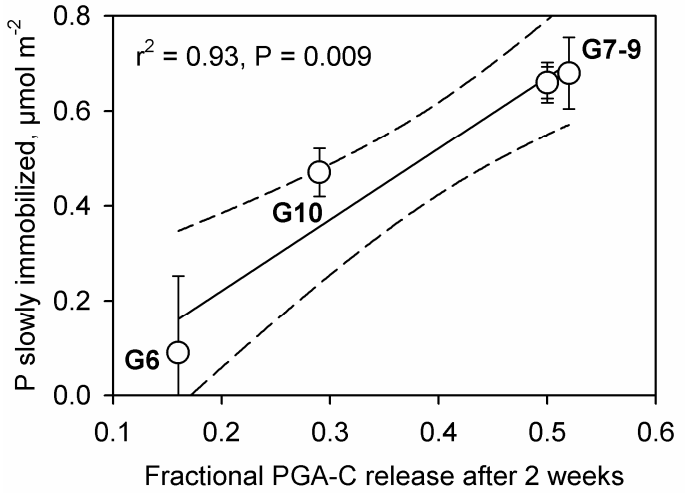

Fig. 2.5. Amount of phosphate slowly immobilized versus fractional PGA-C release after two weeks. The amount of phosphate slowly immobilized was calculated as the difference between the total amount of phosphate sorbed after two weeks and the total amount sorbed fast (c_m of Eq.[2.2]). Figures after 'G' refer to the rounded C content of the sample in milligram C per gram. Error bars represent standard error.

2.4.5 Rate-limiting processes of the slow phosphate sorption

Polysaccharide coatings on goethite reduced the amount of phosphate sorbed and also affected the rate at which equilibrium with phosphate solution was attained. With increasing PGA-C content the amount of phosphate sorbed after two weeks decreased linearly (r^2 = 0.98, P <0.001). One reason might be the decreasing accessibility of intraparticle pores caused by the PGA coating as reflected by porosity measurements (Table 2.2). Phosphate sorption after two weeks was positively related to the amount of micropore (r^2 = 0.90, P <0.01) and small mesopore volume (r^2 = 0.97, P <0.001, Fig. 2.6). The statistical relationship for the latter pores persisted when the G0 sample was removed from the data set (P <0.05). Figure 2.6 reveals that a portion of the surface area belonging to pores <10 nm was either inaccessible or hardly accessible to phosphate because of PGA coatings. However, no relationship existed between the pore volumes of <10-nm pores and the amount of phosphate slowly immobilized (P >0.73). The finding indicates that the slow phosphate immobilization by PGA-coated goethites was not primarily controlled by the diffusion of phosphate into intraparticle pores. In addition, the amount of phosphate sorbed

after two weeks was positively related to the initial ζ-potential (r^2 = 0.97, P <0.001), suggesting that the initial surface charge is a determinant of the amount of phosphate sorbed after two weeks.

The applicability of diffusion-based models to our data indicates diffusion-limited phosphate sorption. The samples differed significantly in the fractions of phosphate slowly immobilized after two weeks (Table 2.3, *Fraction* P_{slowly}), and the rate constants of the slow reaction (Table 2.3, *b*). For pure goethite intraparticle diffusion is rate limiting because phosphate diffuses into the micropores of goethite located between the crystal's domains (Strauss et al., 1997). At the lowest C loading (G6) the continuing phosphate reaction stopped after ~48 hours (Fig. 2.2), and the rate constant of the slow phosphate reaction strongly decreased in comparison with the control treatment (Table 2.3, *b*). Thus, at low C loading, PGA seems to act as an intraparticle diffusion barrier preventing phosphate ions from penetrating into micro- and small mesopores because of a preferential sorption of PGA to micropores and small mesopores (Kaiser and Guggenberger, 2003). This interpretation is in line with Scheinost et al. (2001) who suggest that fulvic acid acts as a diffusion barrier for Cu and Pb between the solution and sorption sites of ferrihydrite.

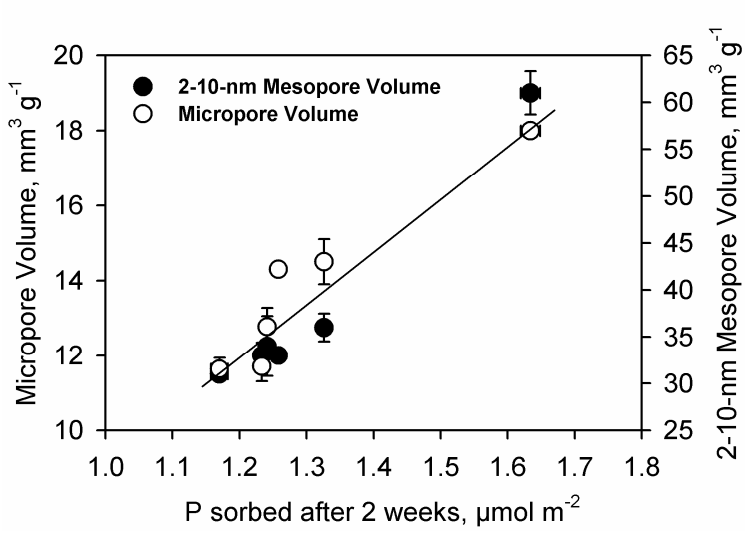

Fig. 2.6. Relationship between the amount of phosphate sorbed after two weeks and the micro- (<2 nm) and small mesopore volume (2-10 nm) of the samples analyzed with N_2 adsorption at 77 K. Horizontal error bars indicate standard error, vertical error bars indicate mean range.

Contrary to our expectation, the fraction of slowly immobilized phosphate at higher C loadings exceeded that of pure goethite (Table 2.3, *Fraction* P_{slowly}). Figure 2.5 shows that the amount of phosphate slowly immobilized was related to the fractional PGA-C release after two weeks. Additionally, the rate constants, *b*, of both phosphate sorption and PGA-C desorption obtained from fitting Eq.[2.2] to both data sets were significantly correlated

(P <0.01, n = 5). The findings support the idea that sorption competition between phosphate and PGA and hence the step-by-step desorption of PGA from external goethite surfaces governed the rate of the slow phosphate sorption. Unfortunately, no data are available in the literature on the kinetics of the exchange between oxyanions and high-molecular-weight biopolymers bound at the Fe oxide interface via polynuclear surface complexes. Therefore, we cannot rule out the possibility that the rate of the slow phosphate sorption to PGA-coated goethite was limited by the diffusion of phosphate to external goethite surfaces. If a diffusion limitation of phosphate by sorbed PGA existed, it is less likely due to electrostatic but rather sterical interactions between PGA and phosphate because the slow phosphate sorption was independent of the ζ-potential (Table 2.3, Fig. 2.3).

2.5 Conclusion

Our results showed that naturally ubiquitous acid polysaccharides coatings on Fe oxides may increase the bioavailability of phosphate in natural systems. The increase in bioavailability of phosphate possibly results from a combination of several processes including (i) the decrease in surface charge of the adsorbent upon PGA sorption, (ii) clogging of pores <10 nm at low C loading (5.5 mg C g^{-1}) with a subsequent decrease in intraparticle diffusion of phosphate, and (iii) sorption competition between phosphate and pre-sorbed PGA or the diffusion of phosphate to external goethite surfaces or both at C loadings >5.5 mg C g^{-1}. As PGA is slowly displaced by phosphate due to sorption competition, the increase in the bioavailability of phosphate to plants following the exudation of acid polysaccharides may only be transient.

3 Acid polysaccharide coatings on microporous goethites – controls of the slow phosphate sorption

Christian Mikutta[1], Jaane Krüger[1], Friederike Lang[1], Martin Kaupenjohann[1]

Accepted for publication in the Soil Science Society of America Journal

[1] Department of Soil Science, Institute of Ecology, Berlin University of Technology, Salzufer 12, D-10587 Berlin, Germany

3.1 Abstract

Organic coatings on Fe oxides can decrease the accessibility of intraparticle pores for oxyanions like phosphate. We hypothesized that the slow sorption of phosphate to goethite coated with polygalacturonate (PGA) is controlled by the accessibility of external goethite surfaces to phosphate rather than by diffusion of phosphate into micropores (Ø <2 nm). Therefore, we studied the phosphate sorption kinetics of pure and PGA-coated goethites that differed in their microporosity (N_2 at 77 K, 46 vs. 31 $mm^3\ g^{-1}$). As drying may affect the structure or surface coverage of PGA, we also tested the effect of freeze-drying on the slow phosphate sorption. The samples were examined by gas adsorption (N_2, CO_2), and electrophoretic mobility measurements. Phosphate sorption and PGA-C desorption were studied in batch experiments for three weeks at pH 5. In PGA-coated samples, the slow phosphate sorption was independent of micropore volume. Phosphate displaced on average 57% of PGA-C within three weeks. Similar to phosphate sorption, the PGA-C desorption comprised a rapid initial desorption which was followed by a slow C desorption. Sorption competition between phosphate and pre-sorbed PGA depended on the <10-nm porosity and the C loading of the adsorbent. The efficacy of phosphate to desorb PGA generally increased after freeze-drying. We conclude for PGA-coated goethites that (i) freeze-drying biased the slow phosphate sorption by changing the structure/surface coverage of PGA, and (ii) within the time frame studied, micropores did not limit the rate of the slow phosphate sorption. Rather, the slow gradual desorption of PGA and/or the diffusion of phosphate through PGA coatings controlled the slow phosphate sorption to PGA-coated goethite.

3.2 Introduction

In soils and sediments, minerals are partially covered with organic matter (Ransom et al., 1997; Yuan et al., 1998; Mayer and Xing, 2001; Gerin et al., 2003). This coverage may drastically change the physico-chemical properties of the mineral phases such as surface charge (Heil and Sposito, 1993a; Kaiser and Zech, 1999; Mikutta et al., 2004) or colloidal stability (Heil and Sposito, 1993b; Kretzschmar et al., 1997). As a consequence, the presence of organic coatings on soil minerals may affect the sorption of nutritional or environmentally hazardous elements.

In the rhizosphere, organic coatings on mineral surfaces may be dominated by organic compounds released by plant roots and microorganisms. Root apices of most plant species are covered by granular or fibrillar gelatinous materials (mucilage) (Greaves and Darbyshire, 1972; Knee et al., 2001). Mucilage exuded by plant's root cap or epidermal cells (e.g. Vermeer and McCully, 1982) is confined to the soil-root interface because mucilage components are supposed to diffuse very slowly into the soil (Rovira 1969; Sealey et al., 1995). Mucilage components consist mainly of polysaccharides with a notable proportion of polygalacturonic acid. For example, mucilage of maize comprised 90-95% polysaccharides with about 20-35% of uronic acids (Cortez and Billes, 1982; Morel et al., 1986). The effect of mucilage sorbed to Fe or Al oxides on the immobilization of oxyanions like phosphate is still poorly understood.

Phosphate sorption to Fe oxides usually comprises two stages. A rapid initial sorption to external surfaces is generally followed by a slow sorption that can last for days or weeks (Barrow et al., 1981; Torrent et al., 1990). The slow phosphate sorption has been attributed to the diffusion of phosphate into microporous imperfections of the crystals, micro- and mesopores between the crystal domains (Torrent, 1991; Barrow et al., 1993; Strauss et al., 1997; Makris et al., 2004), or the diffusion into aggregates of particles (Anderson et al., 1985; Willet et al., 1988). The sorption of high-molecular-weight biomolecules to porous Fe oxides may impair the diffusion of phosphate into intraparticle pores of these adsorbents. In a previous study we observed that polygalacturonate (PGA) coatings impaired the diffusion of phosphate into pores of goethite (α-FeOOH) at a low C loading of 6.3 µmol m^{-2} (Mikutta et al., 2006b). Phosphate, however, was highly competitive at higher C loadings, being able to desorb up to 52% of the polysaccharide C within two weeks (Mikutta et al., 2006b). Our results implied that processes other than micropore diffusion could control the slow phosphate immobilization of PGA-coated goethites. The diffusion of phosphate to external goethite surfaces and/or the desorption of organic matter by

phosphate might be possible controls of the slow phosphate sorption. Both processes are expected to be influenced by the state of hydration of organic coatings. In the presence of free water, maize mucilage is able to hydrate extensively. Fully hydrated root-cap mucilage can have water contents of up to 100,000 wt% of its dry weight (Guinel and McCully, 1986). Reversible structural changes of pectin-like biomolecules upon hydration/dehydration or irreversible structural changes through physico-chemical alterations of the molecular framework upon drying (Wedlock et al., 1983; Jouppila and Roos, 1997; Allison et al., 1998; Souillac et al., 2002) may change the coverage of mineral surfaces by organic matter and/or the desorbability of organic matter by phosphate. Porosity measurements by ^{1}H-NMR relaxometry and N_2 adsorption have indicated that labile interparticle pores created by PGA coatings may be destroyed during freeze-drying (Mikutta et al., 2004), thus possibly reducing the effectiveness of organic coatings as diffusion barriers for phosphate and/or changing the sorption competition between phosphate and PGA sorbed to Fe oxides.

The objective of this study was to elucidate whether micropores of PGA-coated goethite are responsible for the slow sorption reaction of phosphate. Specifically, we hypothesized that the slow phosphate sorption to PGA-coated goethite is not controlled by the diffusion of phosphate into micropores but by the accessibility of external goethite surfaces to phosphate. The accessibility of external goethite surfaces to phosphate should be directly influenced by the structural arrangement of PGA at the surface. To test our hypothesis we coated two goethites differing in their micro- and mesoporosity (<10 nm) with PGA and conducted phosphate sorption experiments using freeze-dried and non-dried samples. Polygalacturonate was used as a simplified model substance for macromolecular root exudates (Morel et al., 1987; Gessa and Deiana, 1992). The experiment was conducted at pH 5 in order (i) to resemble pH conditions observed for soybean plants fertilized with NH_4-N (Riley and Barber, 1971) and P-starved tomato, chickpea and lupin plants fertilized with NO_3-N (Neumann and Römheld, 1999), and (ii) to minimize interference with bicarbonate.

3.3 Materials and Methods

3.3.1 Goethites

Microporous goethite (G1) was synthesized by oxidative hydrolysis of Fe(II) ($FeSO_4 \cdot 7H_2O$, Merck, extra pure) at pH 7 using H_2O_2 as an oxidant. The precipitate was washed until the electric conductivity was below 10 µS cm^{-1}, freeze-dried, softly ground and sieved to a particle size <200 µm. The oxalate-soluble Fe content determined accord-

ing to Blakemore et al. (1987) was 4.9%. Goethite G2 was obtained by autoclaving G1 for two hours (9 times) and four hours (8 times) at 1 bar and 120°C. After autoclaving, the goethite was put into a microwave (Mars XPress, CEM, Kamp-Lintfort, Germany) for two hours (4 times) at 2.8 bar and 150°C. After each run the goethite was oven-dried at 50°C.

The goethites were characterized by X-ray diffraction analysis (Siemens D5005) and scanning electron microscopy (Hitachi S-4000). Potentiometric titrations of the goethites (~0.01 g L^{-1}) in 0.01 *M* KNO_3 using a Zetasizer 2000 connected with a MPT-1 autotitrator (Malvern Instruments, U.K) were carried out to determine the charge characteristics of both adsorbents. During titration, the ζ-potential was analyzed in triplicate at each target pH and the average value was recorded.

3.3.2 Preparation of polygalacturonate coatings

Polygalacturonic acid was purchased from Fluka (P81325, $(C_6H_5O_2(OH)_2COOH)_n$, >95%, M = 25-50 kDa) and comprised 37.2 % C and 0.05% N as determined with an Elementar Vario EIII C/N/S analyzer. To achieve high and low organic C surface loadings on goethite, solutions with 1010 and 50.5 mg C L^{-1} were prepared. Polygalacturonic acid was dissolved in 1 L 0.01 M KNO_3 solution after adding 10 µL 1 M KOH mg^{-1} PGA to enhance PGA solubility. One hundred microliters of 0.05 M $AgNO_3$ solution were added to eliminate microbial activity. The PGA solutions were titrated back to pH 5 using 1 M HNO_3 without any visible flocculation occurring. The final ionic strength of the solutions was ≤0.02 M.

Five grams of goethite were placed into 1-L centrifuge PE-bottles and 10 mL 0.01 M KNO_3 solution (pH 5) were added. To ensure particle disaggregation and hydration of adsorption sites, the goethites were shaken on a reciprocating shaker at 85 rev min^{-1} for 48 hours and pH was readjusted to 5 with dilute HNO_3 or KOH. Subsequently, PGA solutions (990 mL) were added to achieve C concentrations of 50 or 1000 mg C L^{-1} in 0.01 M KNO_3 background electrolyte. The bottles were transferred onto a rotary shaker running at 20 rev min^{-1}. The pH was manually kept within 5 ± 0.2 using dilute HNO_3. After 24 hours the goethite suspensions were repetitively centrifuged at 5,500 x g for 20 min (RC-3B Refrigerated Centrifuge, Sorvall Instruments) and washed with 500 mL doubly deionized water until the total organic C (TOC) concentration in supernatant solutions was <5 mg C L^{-1} (Shimadzu TOC-5050A Autoanalyzer). The goethite residue was either freeze-dried, softly homogenized in an agate mortar and stored in the dark until use or instantaneously used in the phosphate sorption experiment without any freeze-drying.

Freeze-drying was always accomplished after freezing the PGA-coated goethites at -80°C in an Christ alpha 2-4 freeze drier (Osterode, Germany).

3.3.3 Phosphate sorption kinetics

The phosphate sorption was conducted in batch systems in 0.01 M KNO_3 solution at pH 5. Phosphate was used in the form of KH_2PO_4 p.a. (Merck, Germany). At pH 5 the predominant phosphate species is $H_2PO_4^-$ (99%). Triplicate 0.625-g samples of pure and PGA-coated goethites (moist or freeze-dried) were weighed into 2-L HD-PE bottles (Nalgene, USA), which were coated with Al-foil to exclude light. Then 250 mL of background electrolyte with pH 5 were added and the bottles were shaken on a reciprocating shaker at 150 rev min^{-1} for one hour in order to facilitate dispersion and hydration. Afterwards, 1 L background electrolyte solution (pH 5) containing 500 µM phosphate was added to achieve a phosphate concentration of 400 µM and a solid concentration of 0.5 g L^{-1}. Additionally, 50 µL 0.1 M $AgNO_3$ solution were added to reduce microbial activity. The bottles were rotary-shaken at 20 rev min^{-1} and at 298 ± 2 K. The pH was maintained manually at 5 ± 0.2 using dilute HNO_3 or KOH. After 0.5, 1, 2, 4, 8, 24, 48, 168, 336 and 504 hours a 10 mL aliquot was removed, 0.45-µm membrane-filtered (polyethersulfone, Supor-450, Pall Life Science, USA) and total organic C was measured in the filtrate. A 2.5-mL aliquot of the 0.45-µm filtrate was ultracentrifuged at 440,000 x g for one hour and phosphate was measured photometrically in the supernatant by the ascorbic-molybdenum blue method of Murphy and Riley (1962) at 710 nm. The amount of phosphate sorbed was calculated from its loss in solution. Adsorption of phosphate on container walls could be ruled out by checking blank solutions for dissolved phosphate. The analytical precision of the photometric determination of phosphate was <1%. Subsample variability was generally <1.5%. Preliminary tests showed that matrix interferences of phosphate with polyvalent cations bound in the PGA structure did not occur during ultracentrifugation, i.e., phosphate concentrations in solution did not decrease due to sedimentation of PGA during ultracentrifugation.

After sampling, the 0.45-µm filter residue was washed with 20 mL doubly deionized water, freeze-dried and stored in the dark in a desiccator until use for electrophoretic mobility measurements. The amount of phosphate sorbed was corrected for the water content of the samples (13 ± 1 wt%), which was determined by outgassing the samples in an Autosorb-1 gas sorption system (Quantachrome, Syosset, NY) until the rate of pressure increase by vapor evolution was below about 1.3 Pa min^{-1} within a 0.5-min test interval. Due to possible damage to PGA coatings, outgassing was not performed at elevated temperatures.

The phosphate sorption data were fitted with a linear combination of a modified first-order rate equation and the parabolic rate law (Crank, 1976) in order to account for the fast and the slow sorption of phosphate to goethite, respectively (Lang and Kaupenjohann, 2003):

$$q_t = c_m - a_0\, e^{-kt} + bt^{0.5}, \qquad [3.1]$$

where q_t is the amount of phosphate sorbed at time t (µmol g^{-1}), c_m is the maximum amount of phosphate sorbed by the fast reaction (µmol g^{-1}), (c_m-a_0) is the amount of phosphate operationally defined as 'sorbed instantaneously' (faster than could be quantified by the batch approach, µmol g^{-1}), k is the rate constant of the initial fast phosphate sorption (h^{-1}), t is time (h), and b is the apparent rate constant of the slow sorption (µmol g^{-1} $h^{-0.5}$). The parameters c_m, a_0, k and b were determined by minimizing the sum of the squared differences between the observed and predicted values of the phosphate sorption data using the Marquardt-Levenberg algorithm implemented in SigmaPlot for Windows (SPSS Inc.). In most cases, parameters were significant at the $P = 0.05$ level, which was tested with the t-statistics implemented in SigmaPlot.

The rate constant of the slow phosphate sorption, b, is related to the apparent diffusion constant $(D/r^2)_{app}$ (h^{-1}) (Lang and Kaupenjohann, 2003):

$$b = 4q_\infty \pi^{-0.5} (D/r^2)_{app}^{0.5}, \qquad [3.2]$$

where q_∞ is the amount of phosphate diffused at infinite time (µmol g^{-1}), D is the apparent diffusion coefficient (m^2 h^{-1}), and r is the radius of diffusion (m). Unlike Lang and Kaupenjohann (2003), we accounted for cylindrical pore geometry by using a factor of 4 instead of 6 in Eq.[3.2]. We used the total amount of phosphate present at t = 0 hours (µmol g^{-1}) corrected for the total amount of phosphate sorbed to external surfaces (c_m) as an approximation for q_∞ in Eq.[3.2] to calculate the apparent diffusion constant $(D/r^2)_{app}$. This calculation accounts for differing phosphate concentration gradients in the samples after the fast sorption of phosphate to external goethite surfaces but may lead to a systematic underestimation of $(D/r^2)_{app}$.

3.3.4 Surface area and porosity measurements

Specific surface area (*SSA*) and pore volume were determined with a Quantachrome Autosorb-1 automated gas sorption system (Quantachrome, Syosset, NY) using N_2 as an

adsorbate. Approximately 80 mg of pure and PGA-coated goethite were degassed until the rate of pressure increase by vapor evolution was below about 1.3 Pa min^{-1} within a 0.5-min test interval. Helium was used as a backfill gas. We analyzed N_2 adsorption and desorption at 79 points in the partial pressure range 1.0×10^{-5} - 0.995 P/P_0. Specific surface area was calculated from the BET equation (Brunauer et al., 1938).

Micropore (<2 nm) volume and average micropore diameter were determined according to the Dubinin-Radushkevic method (Gregg and Sing, 1982). The mesopore (2-50 nm) size distribution was calculated on the desorption leg using the BJH method (Barrett et al., 1951). Separation between small (2-5 nm), medium (5-10 nm) and large mesopores (10-50 nm) was achieved by linear interpolation of the BJH desorption data. Total pore volume was taken at 0.995 P/P_0 and the average pore diameter was calculated as $D_p = 4V_{liq}/SSA$, where V_{liq} is the volume of liquid N_2 contained in pores at 0.995 P/P_0 and SSA is the BET surface area. We also performed 16-point CO_2 adsorption measurements from 1.0×10^{-3} to 3.0×10^{-2} P/P_0 at 273 K to obtain the CO_2 micropore volume and average micropore diameter according to the Dubinin-Radushkevic method (Gregg and Sing, 1982). All isotherms were recorded in triplicate.

3.3.5 Electrophoretic mobility measurements

The electrophoretic mobility was determined at the start of the phosphate sorption experiment and over the entire phosphate sorption run. After each reaction time about 200 µg of freeze-dried 0.45-µm filter residue were resuspended into 4 mL of 0.01 M KNO_3 at pH 5. In order to facilitate sample handling we used dried solids for electrophoretic mobility measurements. Preliminary tests revealed that during phosphate sorption for one week electrophoretic mobilities of pure and PGA-coated goethites in aqueous suspensions (0.01 M KNO_3, pH 5) did not significantly differ from those obtained from samples that where freeze-dried after 0.45-µm membrane filtration and resuspended in background electrolyte for electrophoretic measurements (t-test, $P < 0.05$). The electrophoretic mobility was determined at 298 K with a Zetasizer 2000 (Malvern Instruments, U.K.). Before the measurements, the accuracy of the measurements was checked with a transfer standard which is referenced to the NIST goethite standard SRM1980 (Malvern Instruments, UK). Ten measurements were performed and the average value was recorded. The ζ-potential was calculated from the electrophoretic mobility using the Smoluchowski equation (Hunter, 1988).

3.4 Results and Discussion

3.4.1 Effects of hydrothermal treatment on goethite properties

Powder X-ray diffraction analysis of G1 goethite showed typical reflexes of goethite without any detectable contamination. In addition, differential X-ray analysis after oxalate treatment according to Schwertmann (1964) did not indicate the presence of ferrihydrite. Powder X-ray diffraction analysis of G2 goethite showed that traces of hematite appeared after hydrothermal treatment of G1. The [hematite/(hematite + goethite)] XRD intensity ratio calculated from the ratio of areas under the 110 reflection of goethite and the 102 reflection of hematite according to Ruan and Gilkes (1995) was 0.05. Scanning electron microscope images obtained on a Hitachi S-4000 microscope at high resolution (x 150,000) showed no visible difference in the crystal habit between G1 and G2 (not shown).

Potentiometric titrations of the goethites indicated that at the pH chosen for this study, their ζ-potentials were essentially identical (~30 mV). However, above pH 5 the ζ-potential of G2 was approximately 5 mV lower than that of G1. Hence, a slight decrease in the isoelectric point (pH_{iep}) from 7.6 to 7.2 was noticed after hydrothermal treatment of G1. The pH_{iep} of G1 was within the range of pH_{iep}'s and points of zero charge reported for goethites (Kosmulski et al., 2003). The shift in the pH_{iep} of G2 might be due to the presence of traces of hematite, because published points of zero charge of synthetic hematites are on average lower than those of goethites (Kosmulski et al., 2003).

Hydrothermal treatment of G1 mainly affected pores <10 nm. The N_2 micropore volume decreased by 33%, and the mesopore volumes of <10-nm pores decreased by up to 46% (Table 3.1). The loss in micro- and mesoporosity was accompanied by a considerable drop in *SSA* (31%). In addition, the average pore size increased by 34% (Table 3.1). Micropore volumes of pure goethite samples determined with CO_2 adsorption at 273 K were about 30% higher than micropore volumes determined with N_2 adsorption at 77 K. De Jonge and Mittelmeijer-Hazeleger (1996) showed that CO_2 is capable of penetrating into pores of soil organic matter <0.5 nm at 273 K, whilst pores of this size remain inaccessible to N_2 at 77 K. Therefore, it might be concluded that in both goethite samples approximately one-fifth of micropores have diameters <0.5 nm.

3.4.2 Porosity and surface area changes upon PGA sorption

Carbon loadings of the goethites are presented in Table 3.1. At low C loadings, no or only tiny porosity and *SSA* changes were noticed for both goethites, with the total pore volume being reduced most effectively (Table 3.1). At higher C loadings, however, *SSA* as

well as micropore volume decreased significantly. The effect was stronger for the more microporous G1 compared to its less porous analogue. While average micropore diameters remained constant at low C loadings, they increased at high C loadings independent of the adsorbate used (Table 3.1). Contrary to the stronger decrease in micropore volumes for G1 than for G2, the relative reduction in 5-10-nm pore volume was five-fold greater for G2 (Table 3.1). The decrease in pore volume of <10-nm pores with increasing C loading suggests a preferential sorption of PGA in or at these small pores. A pore filling mechanism by organic matter has been advocated by several researchers (Kaiser and Guggenberger, 2003; Mikutta et al., 2004; Zimmerman et al., 2004a).

Table 3.1. Carbon loadings of freeze-dried goethite samples, their specific surface areas and porosity properties obtained from N_2 and CO_2 adsorption measurements. Values in parentheses represent standard error.

Sample	C loading[†]	SSA[‡]	Total Pore Volume	D_P[§]	Micropore Volume		AMD[¶]		Mesopore Volume		
					N_2	CO_2	N_2	CO_2	2-5 nm	5-10 nm	10-50 nm
	µmol C m^{-2}	m^2 g^{-1}	mm^3 g^{-1}	nm	mm^3 g^{-1}		x 10^{-2} nm		mm^3 g^{-1}		
G1		148 (1)	583 (3)	15.8 (0.1)	46.4 (0.2)	58.5 (0.8)	87 (0)	56 (1)	46.7 (1.0)	74.5 (1.1)	419 (2)
G1-low PGA	2.5 (0.0)	147 (2)	557 (3)	15.2 (0.1)	44.1 (0.1)	54.7 (0.3)	86 (1)	58 (1)	45.9 (1.2)	72.6 (0.5)	400 (1)
G1-high PGA	11.9 (0.1)	130 (1)	511 (3)	15.7 (0.2)	37.5 (0.2)	44.5 (0.8)	91 (0)	60 (0)	38.2 (1.6)	67.0 (0.9)	367 (3)
G2		102 (1)	543 (4)	21.2 (0.1)	31.1 (0.2)	41.3 (0.4)	82 (1)	58 (0)	25.3 (0.6)	42.7 (0.4)	433 (5)
G2-low PGA	3.0 (0.1)	100 (1)	510 (2)	20.4 (0.1)	28.8 (0.3)	40.2 (0.4)	82 (1)	59 (0)	23.7 (1.5)	41.4 (0.2)	409 (5)
G2-high PGA	13.9 (0.1)	97 (1)	488 (1)	20.1 (0.2)	27.1 (0.3)	32.4 (0.7)	91 (1)	62 (0)	21.4 (0.8)	21.4 (0.8)	387 (3)

[†] C loadings were corrected for the C in pure goethite samples (0.6 and 0.2 µmol C m^{-2} for G1 and G2, respectively).

[‡] Specific surface area.

[§] Average pore diameter.

[¶] Average micropore diameter.

3.4.3 Controls of the slow phosphate sorption in PGA-coated samples

The phosphate sorption kinetics of freeze-dried and non-dried PGA-coated goethites are shown in Fig. 3.1. Equilibrium was not reached within three weeks in all samples. Increasing amounts of sorbed PGA decreased the total amount of phosphate being rapidly immobilized (Table 3.2, c_m), indicating sorption competition of PGA and phosphate at external goethite surfaces. In all PGA-coated samples with high C loading, the rate constant of the slow phosphate sorption was higher compared to the C-free control treatment, irrespective of pre-drying the samples or not (Table 3.2, *b*).

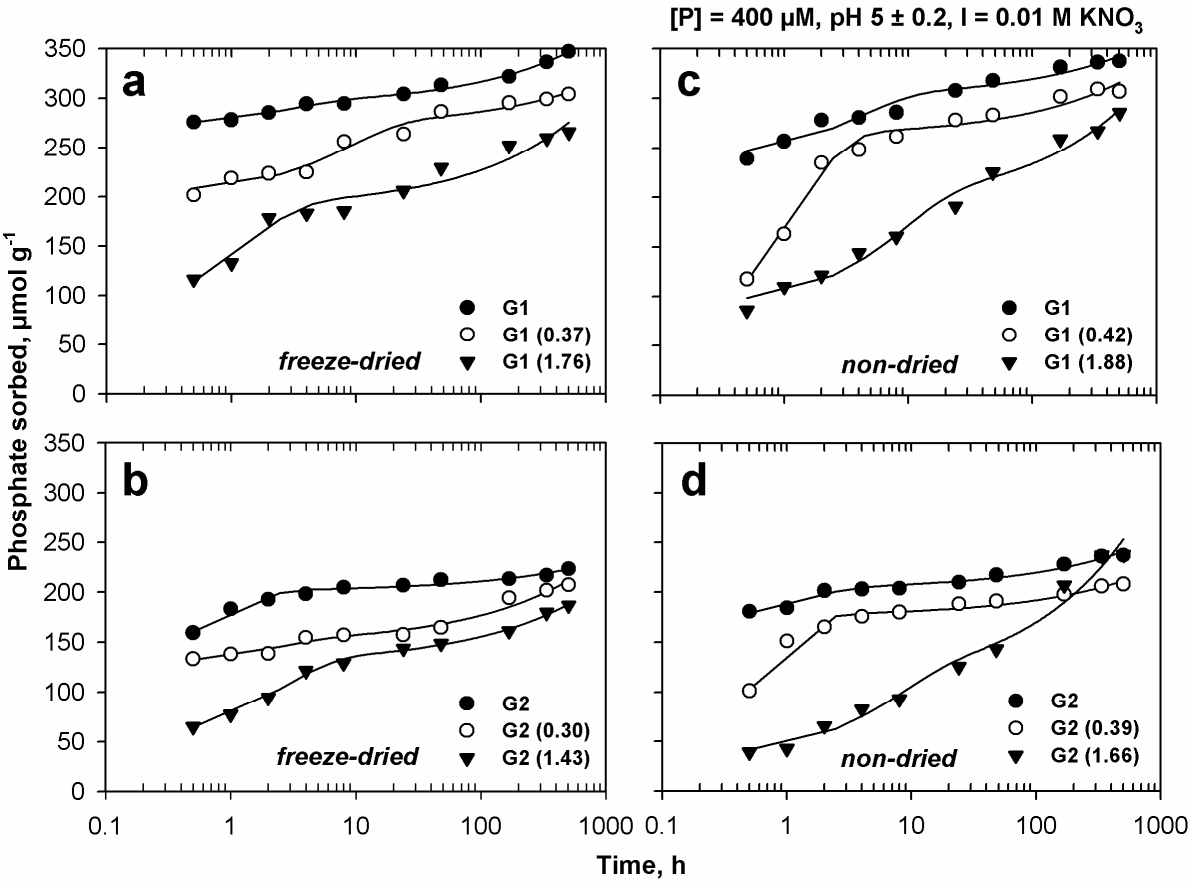

Fig. 3.1. Phosphate sorption kinetics of freeze-dried and non-dried pure and PGA-coated goethites. (a) G1, freeze dried; (b) G1, non-dried; (c) G2, freeze-dried; (d) G2, non-dried. Solid lines show the predicted values using the combined model of Eq.[3.1]. Values in parentheses refer to the initial C contents in mmol C g^{-1}.

Can these high rate constants of the slow phosphate sorption be ascribed to micropore clogging by PGA? Micropores being not detectable by CO_2 at 273 K are likely not accessible to phosphate because of the smaller molecular size of CO_2 as compared to phosphate (0.28 vs. 0.45 nm). Hence, a decreased accessibility of CO_2 to micropores due to PGA sorption in goethite pores should be reflected in a decreased accessibility of micropores to phosphate. Accordingly, if microporosity limits the rate of the slow phosphate sorption to

PGA-coated goethites, one would expect decreased $(D/r^2)_{app}$ values with decreasing microporosity, i.e., with increasing diffusion resistance for phosphate ions. Values presented in Fig. 3.2 are inconsistent with this idea because (i) $(D/r^2)_{app}$ values of PGA-coated goethites with the lowest CO_2 micropore volume were higher than values for uncoated goethites, and (ii) $(D/r^2)_{app}$ values were independent of the CO_2 micropore volume of PGA-coated G2 samples (Fig. 3.2). In contrast to our initial reasoning, higher $(D/r^2)_{app}$ values for PGA-coated than for pure goethites might be explained by a preferential clogging of small pores by PGA because phosphate diffusion would then be confined to the remaining larger pores. As a consequence, equilibrium would be reached faster in samples with high C loading than in C-free samples as the diffusion of phosphate into pores occupied by PGA would be impaired. This reasoning, however, disagrees with Fig. 3.1 showing that at high C loadings phosphate sorption proceeded at a rate similar to or higher than in the C-free controls. Therefore, we conclude that in PGA-coated goethite samples, micropore diffusion of phosphate does not control the slow phosphate sorption.

Table 3.2. Kinetic parameters obtained by fitting the combined model to the phosphate sorption data of freeze-dried and non-dried pure and PGA-coated goethites. Apparent diffusion constants, $(D/r^2)_{app}$, were calculated according Eq.[3.2]. Values in parentheses represent standard error. Also given is the fractional PGA-C release after three weeks of phosphate sorption.

Treatment[†]	c_m[‡]	c_m-a_0[§]	k[¶]	b[#]	r^2	$(D/r^2)_{app}$	Fractional C release after 3 weeks
	µmol g^{-1}	µmol g^{-1}	h^{-1}	µmol g^{-1} $h^{-0.5}$		x 10^{-6} h^{-1}	
freeze-dried							
G1/0.0	293 (2)	270 (4)	0.4 (0.1)	2.4 (0.2)	0.99	4.4 (0.4)	0.00
G1/0.37	271 (10)	204 (14)	0.1 (0.0)	1.6 (0.6)	0.97	1.7 (0.9)	0.59
G1/1.76	188 (9)	76 (29)	0.8 (0.3)	3.9 (0.7)	0.96	7.9 (1.9)	0.52
G2/0.0	201 (2)	125 (14)	1.2 (0.3)	1.0 (0.2)	0.98	0.5 (0.1)	0.00
G2/0.30	149 (5)	126 (10)	0.5 (0.4)	2.8 (0.3)	0.97	3.7 (0.6)	0.87
G2/1.43	129 (2)	48 (5)	0.4 (0.1)	2.6 (0.2)	1.00	3.0 (0.3)	0.59
non-dried							
G1/0.0	301 (9)	239 (14)	0.2 (0.1)	1.9 (0.6)	0.96	2.7 (1.2)	0.00
G1/0.42	262 (7)	33 (26)	0.9 (0.2)	2.4 (0.5)	0.99	4.0 (1.2)	0.29
G1/1.88	190 (13)	89 (19)	0.1 (0.0)	4.4 (0.8)	0.99	10.3 (2.7)	0.62
G2/0.0	203 (3)	165 (10)	0.8 (0.4)	1.7 (0.2)	0.98	1.6 (0.3)	0.00
G2/0.39	176 (3)	0 (34)	1.7 (0.3)	1.6 (0.3)	0.98	1.3 (0.3)	0.42
G2/1.66	103 (14)	32 (21)	0.1 (0.1)	6.7 (0.9)	0.98	18.2 (3.5)	0.67

[†] Numbers after forward slash indicate PGA-C sorbed in mmol C g^{-1}.

[‡] Total amount of phosphate sorbed fast.

[§] Amount of phosphate operationally defined as 'instantaneously sorbed' according Eq.[3.1].

[¶] Rate constant of the fast phosphate sorption.

[#] Rate constant of the slow phosphate sorption.

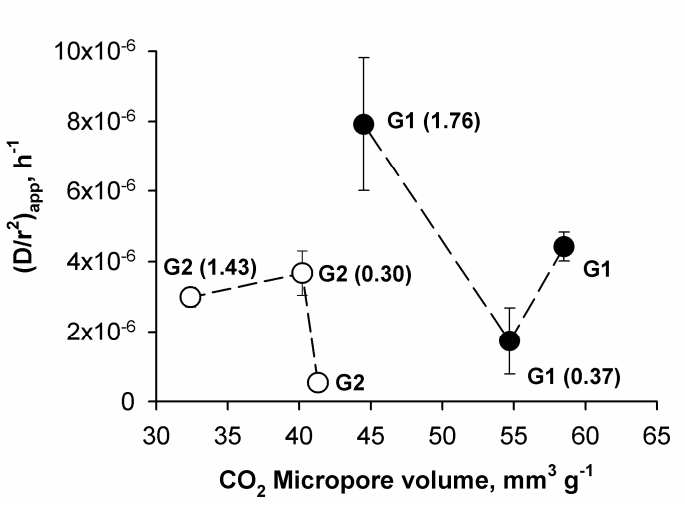

Fig. 3.2. Apparent diffusion constants $(D/r^2)_{app}$ of freeze-dried pure and PGA-coated goethites versus the CO_2 micropore volume present prior to phosphate sorption. Bi-directional error bars indicate standard error. Values in parentheses indicate the C content in mmol C g^{-1}.

Up to 87% of C was displaced by phosphate within three weeks, showing the high competitiveness of phosphate (Table 3.2). Similar to the phosphate sorption kinetics, the C desorption kinetics was biphasic; an initial rapid C desorption was followed by a slow C desorption (Fig. 3.3). Approximately 50% of the total desorbed C was desorbed after 24 h (Fig. 3.3).

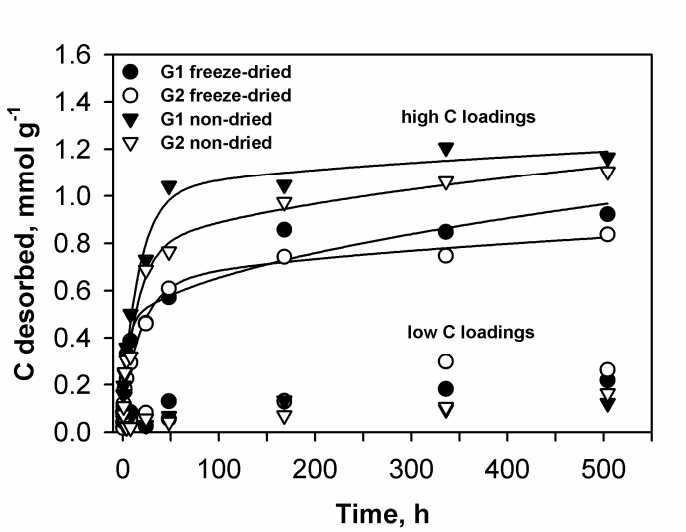

Fig. 3.3. Polygalacturonate-C desorption from goethites during phosphate sorption for three weeks. Solid lines indicate the fit of Eq.[3.1] to the C desorption data of goethites with high C loadings. Coefficients of determination were always >0.97. Average standard error of total organic C measurements was 27 µmol g^{-1}; maximal standard error recorded was 78 µmol g^{-1} (n = 80).

The increasing molar ratios of phosphate sorbed and PGA-C desorbed with increasing time (Fig. 3.4) indicate that phosphate was more effective in triggering PGA desorption at longer sorption times either by direct ligand-exchange or by decreasing the surface potential of PGA-coated goethites. Off-sets in molar C_{des}/P_{sorb} ratios between freeze-dried and non-dried samples are due primarily to higher C loadings of non-dried goethites (Table

3.2). The plateaus in Fig. 3.4 that were reached after about one week indicate that every phosphate desorbed on average two-thirds of a carboxyl group when we assume that the amount of esterified carboxyls is low (one carboxyl-C per six C atoms in the structure of PGA).

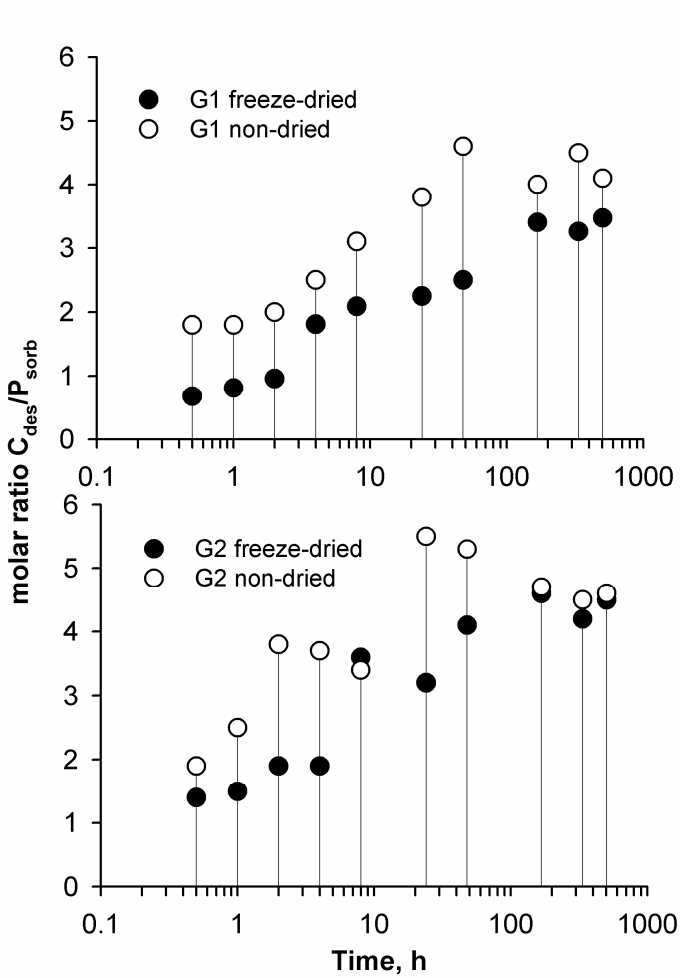

Fig. 3.4. Changes in the molar ratio of PGA-C desorbed and phosphate sorbed of freeze-dried and non-dried PGA-coated goethites with high C loadings during phosphate sorption over three weeks. The mean standard error of the molar C_{des}/P_{sorb} ratios was 0.2. Note that x-axis is in logarithmic scale.

As a consequence of the ion exchange at the goethite surface, the ζ-potential of PGA-coated goethites remained relatively constant during the phosphate sorption run (Fig. 3.5). Noteworthy, the ζ-potential of pure goethites increased again after about 24 hours of phosphate sorption (Fig. 3.5). This observation was reported before (Ler and Stanforth, 2003; Mikutta et al., 2006b) and explained by the formation of ternary phosphate surface complexes (Ler and Stanforth, 2003).

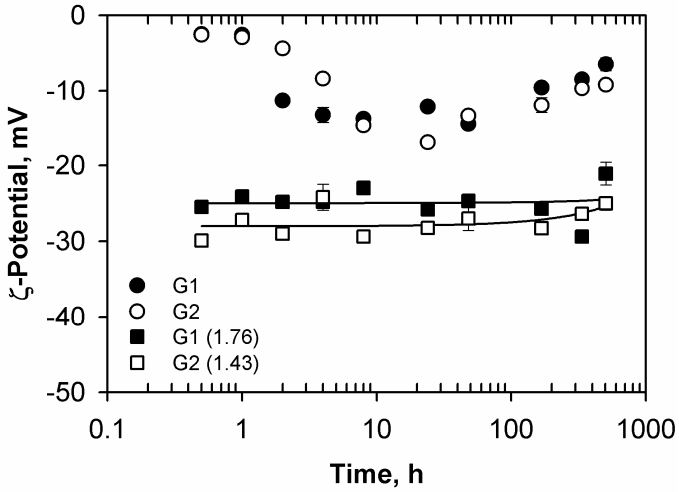

Fig. 3.5. ζ-Potential changes during phosphate sorption of freeze-dried uncoated and PGA-coated goethites at the highest PGA-level. The solid lines show linear regressions. Error bars are standard error. Values in parentheses represent the C loading in mmol C g^{-1}. Initial ζ-potentials (mV) at pH 5 in 0.01 M KNO_3 were G1: 29.8 ± 3.5, G2: 29.1 ± 0.5, G1 (1.76): -29.0 ± 3.6, G2 (1.43): -28.5 ± 1.2. Note that x-axis is in logarithmic scale.

Figure 3.6 shows the relationship between the amount of phosphate sorbed and C desorbed. Although these relations were not strictly linear, we fitted the data with a linear function in order to obtain information on the average desorbability of PGA by phosphate. Slopes of non-dried samples with low C loadings were not statistically different from zero at the 0.05 probability level and are thus not presented in Fig. 3.6b. The slope of regressions presented in Fig. 3.6 can be taken as a measure of the average competitiveness of phosphate with pre-sorbed PGA. Accordingly, in freeze-dried samples with low C loading, phosphate was less able to displace PGA from the more micro- and mesoporous G1 than from G2 (Fig. 3.6a). On the contrary, at higher C loadings the reduced desorbability of PGA by phosphate in the more nanoporous G1 samples diminished (Fig. 3.6a). In addition, Fig. 3.6 indicates that the desorbability of C by phosphate was larger at high compared with low C loadings, indicating that at higher C loadings polymers were less intimately associated with mineral surfaces (Theng, 1979; Kaiser and Guggenberger, 2003; Saito et al., 2004).

In summary, we found that (i) the apparent diffusion constant of PGA-coated samples was independent of the CO_2 micropore volume and (ii) the C desorption showed a kinetic pattern similar to the phosphate sorption. These findings imply that the slow gradual desorption of PGA and/or the transport of phosphate to external goethite surfaces controlled the slow phosphate sorption to PGA-coated goethites. The ability of phosphate to diffuse through PGA networks at pH ≤4.5 and a phosphate concentration of 150 µM has recently been demonstrated by Gessa et al. (2005).

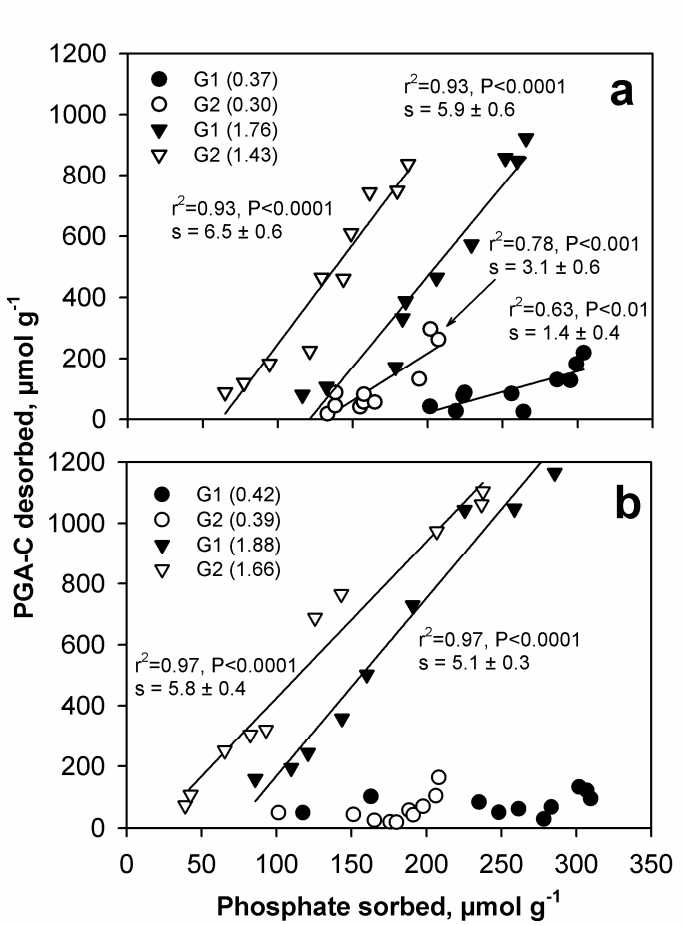

Fig. 3.6. Plots of phosphate sorbed versus PGA-C desorbed for (a) freeze-dried and (b) non-dried PGA-coated goethites. Values in parentheses refer to the amount of PGA-C initially present in the samples in mmol C g^{-1}.

3.4.4 Effects of drying on the phosphate sorption kinetics

The rate constant *b* of the slow phosphate sorption to C-free, freeze-dried G2 was significantly lower than for freeze-dried G1 (Table 3.2). This finding agrees with the diffusion of phosphate into pores of Fe oxides (Torrent, 1991; Barrow et al., 1993; Strauss et al., 1997; Makris et al., 2004), because the strong reduction in the pore volume of <5-nm pores upon hydrothermal treatment of G1 has rendered less pores accessible to phosphate in G2 samples (Table 3.1). In contrast, we found equal rate constants for pure G1 and G2 in non-dried systems (Table 3.2). Also, similar apparent diffusion constants, $(D/r^2)_{app}$, for non-dried G1 and G2 samples indicate a similar diffusion resistance for phosphate in both samples (Table 3.2). It appears that freeze-drying has induced an aggregation of G2, which partly explains its loss in micro- and mesoporosity. The aggregation of G2 upon freeze-drying probably led to an occlusion of mineral surfaces that were neither accessible to N_2 and CO_2 nor by phosphate. In non-dried systems, however, G2 samples were shaken in background electrolyte for 72 hours prior to phosphate addition. This treatment likely

caused a sufficient re-dispersion of G2 and hence a similar slow phosphate sorption in G1 and G2 samples (Table 3.2). Therefore, the observed decrease in the apparent diffusion constant of dried G2 samples with respect to dried G1 (Table 3.2) was most probably caused by a reduced intra-aggregate diffusion.

Freeze-drying PGA-coated goethites altered the phosphate sorption pattern especially at short times <10 hours (Fig. 3.1). The amount of phosphate instantaneously sorbed (Table 3.2, c_m-a_0) increased significantly after freeze-drying samples with low C content, which implies that the coatings impaired the sorption of phosphate to external surfaces less effectively than in non-dried samples (Fig. 3.1).

At high C loading, the sorption kinetics of non-dried G1 was similar to its freeze-dried counterpart (Table 3.2). On the contrary, the rate constant of the slow phosphate sorption to non-dried G2 at high C loading increased anomalously (Table 3.2, *b*). The reason for this observation is unclear; possible explanations may include discontinuous PGA desorption and particle disaggregation.

Freeze-drying also changed the average desorbability of PGA by phosphate as indicated by the slopes in Fig. 3.6. At low C loadings, PGA was more prone to desorption by phosphate in freeze-dried compared to non-dried samples (Fig. 3.6). For example, 45% PGA-C were less desorbed within three weeks in non-dried compared to freeze-dried G2 samples (Table 3.2). At higher C loadings, freeze-drying only increased significantly the average desorbability of PGA by phosphate in G2 samples (Fig. 3.6). These results suggest that freeze-drying PGA-coated goethites alters the ability of phosphate to displace pre-sorbed PGA. This finding may be attributed to physico-chemical changes in the structure of sorbed PGA due to dehydration/hydration processes, which have been reported for pure organics including proteins and polysaccharides (Wedlock et al., 1983; Jouppila and Roos, 1997; Allison et al., 1998; Souillac et al., 2002) and PGA coatings on γ-AlOOH (Mikutta et al., 2004).

3.5 Conclusions

Our results show that micropores of PGA-coated goethite do not significantly contribute to the slow and continuous phosphate sorption. Instead, sorption competition and/or the diffusion of phosphate through PGA coatings controlled the slow phosphate sorption to PGA-coated goethite. With increasing <10-nm porosity, the ability of phosphate to displace PGA decreased for freeze-dried goethites with low C loading (0.30 and 0.37 mmol C g^{-1}). However, the stabilization of PGA against desorption by phosphate ex-

erted by nanoporous surfaces diminished at higher C loadings (1.43 and 1.76 mmol C g^{-1}). In freeze-dried samples, PGA was less easily desorbed by phosphate at low C loadings compared with high C loadings, indicating a stronger attachment of PGA to goethites at low C loadings. Microaggregation of goethite upon freeze-drying can affect the slow phosphate sorption. In addition, freeze-drying C-coated goethites can change the competition between phosphate and pre-sorbed organic matter. Thus freeze-drying may lead to errors in the interpretation of sorption studies when only freeze-dried pure and organic matter-coated Fe oxides are used.

4 Citrate impairs the micropore diffusion of phosphate into pure and C-coated goethite

Christian Mikutta[1], Friederike Lang[1], Martin Kaupenjohann[1]

Geochimica et Cosmochimica Acta 2006; 70: 595-607

[1] Department of Soil Science, Institute of Ecology, Berlin University of Technology, Salzufer 12, D-10587 Berlin, Germany

4.1 Abstract

Anions of polycarboxylic low-molecular-weight organic acids (LMWOA) compete with phosphate for sorption sites of Fe and Al oxides. To test whether the sorption of LMWOA anions decrease the accessibility of micropores (<2 nm) of goethite (α-FeOOH) for phosphate, we studied the kinetics of citrate-induced changes in microporosity and the phosphate sorption kinetics of synthetic goethite in the presence and absence of citrate in batch systems for three weeks (500 µM of each ion, pH 5). We also used C-coated goethite obtained after sorption of dissolved organic matter (DOM) in order to simulate organic coatings in the soil. We analyzed our samples with N_2 adsorption and electrophoretic mobility measurements. Citrate clogged the micropores of both adsorbents by up to 13% within one hour of contact. The micropore volume decreased with increasing concentration and residence time of citrate. In the absence of citrate, phosphate diffused into micropores of the pure and C-coated goethite. The C coating (5.6 µmol C m^{-2}) did not impair the intraparticle diffusion of phosphate. In the presence of citrate the diffusion of phosphate into the micropores of both adsorbents was strongly impaired. We attribute this to the micropore clogging and the ligand-induced dissolution of goethite by citrate. While the diffusion limitation of phosphate by citrate was stronger when citrate was added before phosphate to pure goethite, the order of addition of both ions to C-coated goethite had only a minor effect on the intraparticle diffusion of phosphate. Micropore clogging and dissolution of microporous Fe and Al oxides may be regarded as potential strategies of plants to cope with phosphate deficiency in addition to ligand-exchange.

4.2 Introduction

Phosphate sorption to Fe oxides comprises a rapid initial adsorption to external surfaces followed by a slow reaction, which can last for days or weeks (Barrow et al., 1981; Torrent et al., 1990). The slow phosphate immobilization has been attributed to the diffusion of phosphate into microporous imperfections of the crystals, micro- and mesopores located between the crystal domains (Torrent, 1991; Barrow et al., 1993; Strauss, 1992; Fischer et al., 1996; Strauss et al., 1997; Makris et al., 2004), or the diffusion into aggregates of particles (Anderson et al., 1985; Willet et al., 1988). Torrent et al. (1990, 1992) observed that a portion of phosphate sorbed to microporous Fe oxides was not desorbable in 0.1 M KOH. This finding was attributed to both the slow rediffusion of phosphate out of micropores and the formation of binuclear surface complexes of phosphate. Also, Fuller et al. (1993) showed that the rate of the slow sorption of arsenate to ferrihydrite was limited by intraparticle diffusion.

Polycarboxylic low-molecular-weight organic acids (LMWOA) successfully compete with phosphate for sorption sites (Violante et al., 1991; Bhatti et al., 1998; Geelhoed et al., 1998). This is especially relevant for the soil rhizosphere where exudation of LMWOA anions by plants and microorganisms is high. When polycarboxylic LMWOA anions are added to Al and Fe oxides or soils before phosphate, a decrease in phosphate sorption is generally noticed (Hue, 1991; Violante et al., 1991; Geelhoed et al., 1998; Hu et al., 2001). This may be attributed to direct site blocking, electrostatic repulsion or diffusion of LMWOA anions into small nm-pores of the adsorbent, which may result in a steric and/or electrostatic diffusion impedance for phosphate ions. Considering the volume of anhydrous citric acid (0.775 nm^3, Nordman et al., 1960), a decreased accessibility of micropores (<2 nm) to phosphate due to the sorption of citrate in micropores can be expected. Here we hypothesized that citrate clogs the micropores of goethite, thus reducing the diffusion of phosphate into the adsorbent.

In the soil environments, microbes rapidly consume LMWOA anions, causing average half lives of LMWOA anions in the soil solution to be fairly low. For example, Jones and Darrah (1994) and Jones (1998) reported half lives of less than 12 hours for citrate. If our proposed mechanism was relevant *in vivo*, the micropore clogging of Fe oxides by citrate should proceed within hours. Therefore, we tested the micropore clogging kinetics of pure and C-coated goethite by citrate within up to 12 hours.

In soils and sediments clean oxide surfaces seldom exist as they are partly coated with organic matter (Mayer, 1999; Mayer and Xing, 2001; Gerin et al., 2003). Coatings created

by dissolved organic matter (DOM) and polygalacturonate (PGA) have been shown to clog micropores of Fe and Al oxides (Lang and Kaupenjohann, 2003; Kaiser and Guggenberger, 2003; Mikutta et al., 2004). The micropore clogging of goethite by polygalacturonate at a low surface loading (6.3 µmol C m^{-2}) has been shown to decrease the slow phosphate sorption, i.e., the diffusion of phosphate into intraparticle pores of goethite (Mikutta et al., 2006b).

The presence of C-coatings on the surface of pedogenic Fe oxides may change the effect of LMWOA anions in different ways: LMWOA anions may exchange for pre-sorbed macromolecular natural organic matter by sorption competition, or be able to disrupt organo-mineral associations either by complexation of bridging multivalent cations (Edwards and Bremmer, 1967) or by dispersion (Pinheiro-Dick and Schwertmann, 1996). These processes may liberate diffusion pathways for phosphate, thus enhancing the slow, continuous and strong phosphate fixation in intraparticle pores. Alternatively, LMWOA anions may further increase the micropore clogging already induced by the sorption of high-molecular-weight compounds, thereby impairing the diffusion of phosphate into micropores. For this reason, we studied the phosphate immobilization kinetics of pure and C-coated goethite in the presence and absence of citrate for three weeks. The changes in specific surface area (*SSA*), porosity, and electrophoretic mobility of pure and C-coated goethite upon sorption of phosphate and/or citrate were also analyzed. All experiments were conducted at pH 5 in order to resemble pH conditions of the soil rhizosphere and the bulk of acid soils. At conditions where the pH of soil solution is lower than the isoelectric point of Fe and Al oxides ($pH < pH_{iep}$), the availability of phosphate to plants is strongly reduced because of its sorption to positively charged Fe and Al oxide surfaces. In addition, goethite dissolution by protonation and the inference with bicarbonate in the sorption experiments should be kept to a minimum.

4.3 Materials and Methods

4.3.1 Preparation and characterization of the adsorbents

Goethite was synthesized in one batch by oxidative hydrolysis of Fe(II) ($FeSO_4 \cdot 7H_2O$, Merck, extra pure) at pH 7 using H_2O_2 as an oxidant. The precipitate was washed until the electric conductivity was below 10 µS cm^{-1}, freeze-dried, softly ground and sieved to a particle size <200 µm. Powder X-ray diffraction analysis (Siemens D5005, CuKα radiation) showed typical reflections of goethite without any detectable contamination. The goethite was analyzed with transmission electron microscopy (JEOL JSEM 200B). Transmis-

sion electron microscopy images showed a broad size distribution of crystallites due to differing rates of Fe(II) oxidation during synthesis. Larger acicular crystallites are accompanied by smaller ones having no particular habit (Fig. 4.1). The acid-ammonium oxalate-soluble Fe content (Blakemore et al., 1987) of the goethite was 4.9 wt%. The acid-ammonium oxalate-soluble Fe is usually ascribed to Fe contained in amorphous or poorly crystalline Fe minerals (e.g., Olson and Ellis, 1982). However, there is evidence that this treatment will also dissolve crystalline Fe oxides (McKeague et al., 1971; Schwertmann, 1973; Walker, 1983; Borggaard, 1988, 1990; Fine and Singer, 1989). Hence, an acid ammonium-oxalate soluble Fe content of ~5 wt% indicates that the content in residual ferrihydrite is low in our goethite sample. Possible effects of residual ferrihydrite on porosity changes induced by phosphate/citrate are accounted for in the results and discussion section. The isoelectric point, pH_{iep}, of the goethite used was 7.6 as determined by potentiometric titration of the goethite in 0.01 M KNO_3 solution (~0.01 g L^{-1} goethite) using a MPT-1 autotitrator connected with a Zetasizer 2000 (Malvern Instruments, U.K.). The density of goethite was found to be 4.2 ± 0.1 g cm^{-3} as determined with a Quantachrome He-pycnometer.

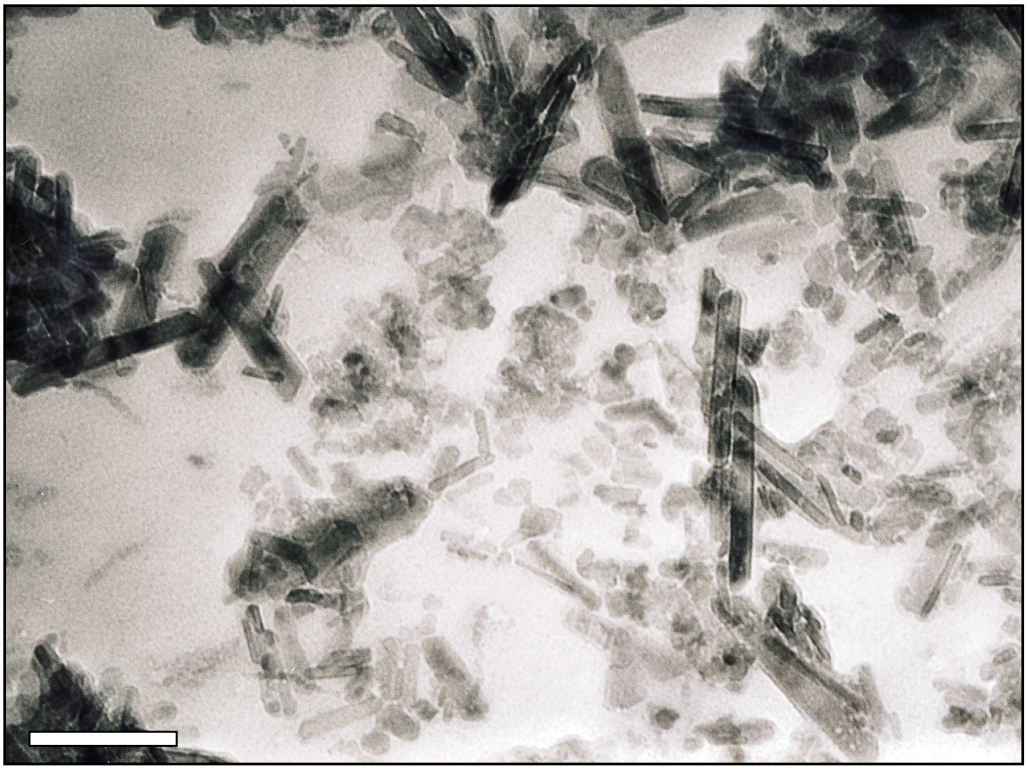

Fig. 4.1. Transmission electron micrograph of the goethite used in this study (x 102,000). The bar indicates 100 nm.

In order to simulate organic coatings of the mineral, the goethite was coated with dissolved organic matter. The DOM solution was obtained from an aqueous extract of a forest-floor soil sample of an O-horizon of a Haplorthod. The forest-floor material was extracted in doubly deionized water for 20 hours at pH 5 (1:6/w:v). The extract was membrane filtered (0.45-µm) and analyzed for total organic C (TOC) using a Shimadzu TOC-5050A Autoanalyzer. The TOC concentration was 220.1 ± 4.9 mg C L^{-1}. The average size of colloids in the DOM filtrate was 191 ± 18 nm as measured by dynamic light scattering (Malvern HPPS, U.K.). Phosphate in the DOM solution was measured photometrically at 710 nm using the method of Murphy and Riley (1962) after ultracentrifugation at 440,000 x g for one hour. The phosphate concentration found would have led to a maximal possible preloading of ~0.08 µmol P m^{-2} when goethite was equilibrated with DOM, which is low compared to the maximal sorption capacity of goethite of 2.5 µmol P m^{-2} (Torrent et al., 1990). Multivalent cations in the DOM extract were determined with atomic absorption spectrometry (Perkin Elmer 1100B). The amount of charge equivalents in the DOM extract was 71 $\mu mol_c\ L^{-1}$ Ca, 11 $\mu mol_c\ L^{-1}$ Mg, and 33 $\mu mol_c\ L^{-1}$ Fe.

Prior to sorption of DOM to goethite, the Fe oxide was ultrasonicated for 30 min and hydrated in doubly deionized water for 48 hours in a glass volumetric flask in order to hydrate adsorption sites (2:25/w:v). The pH of the stock suspension was adjusted to 5.0 ± 0.02 with diluted HNO_3. Goethite was reacted with DOM solution (179.5 mg C L^{-1}) in the dark (1:100/w:v, pH 5 ± 0.2) under magnetic stirring in a 2-L PE bottle. After 24 hours the suspension was membrane filtered (0.45 µm). The filter residue was washed with 2.5 L doubly deionized water adjusted to pH 5 with dilute HNO_3 or KOH to remove excess DOM-C and freeze-dried. The C content of the goethite was 12.1 mg g^{-1} as determined with a Carlo Erba C/N NA 1500N Analyzer. The C-coated goethite was stored in the dark until use.

4.3.2 Analysis of porosity changes induced by citrate

Citrate was used in the sodium form $C_6H_5Na_3O_7 \cdot 2H_2O$ (Merck, p.a.). The effect of citrate on the accessibility of micropores was studied at different citrate concentrations for C-coated goethite only and different contact times for both adsorbents.

Citric acid concentrations in the soil solution are typically less than 370 µM (Jones, 1998 and references therein). Hence, for studying the concentration effect of citrate, the C-coated goethite (2 g L^{-1}) was reacted with solutions containing 20, 100 and 300 µM citrate in 2-L PE bottles at pH 5 on a reciprocating shaker at 130 rev min^{-1}. Potassium nitrate

(0.01 M) was used as background electrolyte. The dominating citrate species at pH 5 are H_2Cit^- (28.3%) and $HCit^{2-}$ (66.9%). Since the average half life of citrate in soils is 2-3 hours (Jones, 1998) or larger (11.7 hours; Jones and Darrah, 1994), we chose a contact time of three hours. After three hours the suspensions were filtered (0.45 µm), washed with 1 L 0.01 M KNO_3 solution (pH 5), freeze-dried, softly ground to <200-µm particle size and further analyzed by N_2 adsorption.

The influence of residence time of citrate on nanoporosity of pure and C-coated goethite was tested at a citrate concentration of 300 µM in 0.01 M KNO_3 solution (pH 5) with a solid concentration of 1 g L^{-1}. The suspensions were reacted on a reciprocating shaker at 130 rev min^{-1}. After 1, 6 and 12 hours the suspensions were membrane filtered (0.45 µm), the filter residues were washed with 1 L 0.01 M KNO_3 solution (pH 5) and freeze-dried. The freeze-dried filter residues were further analyzed by N_2 adsorption after soft grinding to <200-µm particle size.

In both experiments the reaction vessels were coated with Al-foil in order to inhibit the photochemical dissolution of goethite in the presence of citrate. The pH was manually maintained with dilute HNO_3 or KOH at pH 5 ± 0.2. Citrate, TOC and Fe were measured in the 0.45-µm filtrates. The citrate concentration was determined photometrically at 340 nm by measuring the stoichiometric decrease in nicotinamide-adenin dinucleotide (NADH) concentration in an enzymatic reaction with a Specord 200 spectralphotometer (Analytik Jena AG) (Möllering and Gruber, 1966). The detection limit of this method is 2.6 µM citric acid and linearity of the determination ranges from 2.6 to 2.08 x 10^3 µM citric acid (Boehringer Mannheim/R-Biofarm, Germany). Matrix interferences with dissolved Fe did not occur. Additionally, the amount of citrate-C sorbed onto pure goethite was measured with an Elementar Vario EIII C/N/S Analyzer. Iron was analyzed with graphite furnace AAS (Perkin Elmer AAnalyst 700). All experiments were conducted in triplicate.

4.3.3 Phosphate sorption kinetics in the absence and presence of citrate

Phosphate sorption onto pure and C-coated goethite was measured for three weeks in batch experiments at pH 5 in a temperature-controlled room at 298 K. Phosphate was used as KH_2PO_4 (Merck, p.a.). The predominant species of phosphate at pH 5 is $H_2PO_4^-$. In order to hydrate adsorption sites and disperse particles, 200 mL of background electrolyte (pH 5) were given to 0.6 g adsorbent. The samples were then shaken on a horizontal shaker at 100 rev min^{-1} for three hours. Then 1 L of 600 µM phosphate solution in 0.01 M KNO_3 (pH 5) was added to get a final phosphate concentration of 500 µM and a solid concentra-

tion of 0.5 g L^{-1}. Reaction vessels were coated with Al foil and 100 µL 0.05 M $AgNO_3$ were added to inhibit microbial activity. Samples were then shaken on a rotary shaker at 10 rev min^{-1}. The pH was manually maintained at 5 ± 0.2 using dilute HNO_3 or KOH. After 0.5, 1, 2, 4, 8, 24, 48, 168, 336 and 504 hours a 10 mL-aliquot was removed and 0.45-µm membrane filtered. An ultracentrifuged (one hour at 440,000 x g) subsample of the 0.45-µm filtrate was analyzed for phosphate and Fe. Additionally, total organic C was measured in the 0.45-µm filtrate (Shimadzu TOC-5050A Autoanalyzer). We ensured that sampling did not result in a relative enrichment of the adsorbent in the reaction vessels. The solid concentrations of the subsamples varied by less than 5 wt%. The 0.45-µm filter residue was washed with 40 mL doubly deionized water and freeze-dried for electrophoretic mobility measurements. The 0.45-µm filtrates were stored at -18°C until they were defrosted for electrophoretic mobility measurements. After three weeks of phosphate (citrate) sorption, goethite suspensions were 0.45-µm membrane filtered, washed with doubly deionized water, freeze-dried, and further characterized by N_2 adsorption.

The influence of citrate on the kinetics of phosphate sorption to pure and C-coated goethite was studied at equimolar ion concentrations of 500 µM. In one experiment phosphate and citrate were added simultaneously '(C+P)'. After equilibration of goethite and C-coated goethite in the background electrolyte as described above, 1 L of 0.01 M KNO_3 solution containing equimolar amounts of phosphate and citrate (600 µM) were added to obtain a concentration of 500 µM of each ion. Phosphate sorption was again monitored for three weeks.

In a second experiment citrate was added before phosphate ('C+P'). Six hundred milligrams of pure and C-coated goethite were equilibrated in 1.2 L 0.01 M KNO_3 solution (pH 5) containing 500 µM citrate. After three hours the solution was spiked with 10 mL phosphate solution to give a phosphate concentration of 500 µM and analyzed for phosphate, Fe and citrate as described above. All sorption experiments were performed in triplicate.

In all experiments, concentrations expressed on a unit mass or surface area basis were corrected for the water content in pure and C-coated samples. The water content was determined by outgassing the sample in a Quantachrome Autosorb-1 automated gas sorption system (Quantachrome, Syosset, NY) at room temperature until the pressure increase rate by vapor evolution was below about 1.3 Pa min^{-1} within a 0.5-min test interval. This was done in order to avoid phase transformations and the loss of structural water. The water content of both microporous adsorbents was 17 wt%.

4.3.4 Phosphate sorption data interpretation

We combined a modified first-order rate equation with the parabolic rate law (Crank, 1976) in order to account for the fast and the slow sorption of phosphate to goethite, respectively (Lang and Kaupenjohann, 2003):

$$q_t = c_m\text{-}a_0\, e^{-kt} + bt^{0.5}, \qquad [4.1]$$

where q_t is the amount of phosphate sorbed at time t (µmol m^{-2}), c_m is the maximum amount of phosphate sorbed by the fast reaction (µmol m^{-2}) and represents the portion of phosphate that is sorbed to external goethite surfaces, (c_m-a_0) is the amount of phosphate sorbed instantaneously (faster than could be quantified by the batch approach, µmol m^{-2}), k is the rate constant of the initial fast phosphate sorption (h^{-1}), t is time (h), and b is the apparent rate constant of the slow sorption (µmol m^{-2} $h^{-0.5}$).

The rate constant of the slow phosphate sorption, b, is related to the apparent diffusion constant $(D/r^2)_{app}$ (h^{-1}):

$$b = 4q_\infty \pi^{-0.5} (D/r^2)_{app}^{0.5}, \qquad [4.2]$$

where q_∞ is the amount of phosphate diffused at infinite time (µmol m^{-2}), D is the apparent diffusion coefficient (m^2 h^{-1}), and r is the radius of diffusion (m). In order to obtain parameters c_m, a_0, k and b, Eq.[4.1] was fitted to our phosphate sorption data using SigmaPlot for Windows (SPSS Inc.). We used the total amount of phosphate present at t = 0 hours (µmol m^{-2}) corrected for the total amount of phosphate sorbed to external surfaces (c_m) as an approximation for q_∞ in Eq.[4.2] to calculate the apparent diffusion constant $(D/r^2)_{app}$. The amount of phosphate sorbed by the slow reaction was approximated by

$$P_{slowly} = q_{504h} - c_m, \qquad [4.3]$$

where q_{504h} is the amount of phosphate sorbed after 504 hours (µmol m^{-2}) and c_m is the total amount of phosphate sorbed by the fast phosphate reaction.

4.3.5 Surface area and porosity measurements

Specific surface area and pore volume were determined with a Quantachrome Autosorb-1 automated gas sorption system (Quantachrome, Syosset, NY) using N_2 as an adsorbate. Approximately 80 mg sample were degassed until the pressure increase rate by vapor evolution was below about 1.3 Pa min^{-1} within a 0.5-min test interval. Helium was used as a backfill gas. We used 71-point N_2 adsorption and desorption isotherms from 1.0×10^{-5} to 0.995 P/P_0. Specific surface area was calculated from the BET equation (Brunauer et al., 1938).

Micropore (<2 nm) porosity and average micropore diameter were determined according to the Dubinin-Radushkevic method (DR method; Gregg and Sing, 1982). The mesopore size distribution (2-50 nm) was calculated on the desorption leg using the BJH method (Barrett et al., 1951). Separation between small (2-5 nm), medium (5-10 nm) and large mesopores (10-50 nm) was achieved by linear interpolation of the BJH desorption data. Total pore volume was taken at 0.995 P/P_0 and the average pore diameter was calculated as $D_p = 4V_{liq}/SSA$, *w*here V_{liq} is the volume of liquid N_2 contained in the pores at 0.995 P/P_0 and *SSA* is the BET surface area. All isotherms were recorded in triplicate.

4.3.6 Electrophoretic mobility measurements

The electrophoretic mobility, μ, was monitored over the entire phosphate/citrate sorption run. After each reaction time, about 200 µg of freeze-dried 0.45-µm filter residue were resuspended into 4 mL of phosphate/citrate solution obtained after 0.45-µm membrane filtration of the goethite suspension.

In order to facilitate sample handling, we used dried solids that were stored in the dark at ambient relative humidity (~30%) for electrophoretic mobility measurements. Preliminary tests revealed that during phosphate sorption for one week electrophoretic mobilities of pure and C-coated goethite in aqueous suspensions (0.01 M KNO_3, pH 5) did not significantly differ from those obtained from samples that where freeze-dried after 0.45-µm membrane filtration and resuspended in background electrolyte for electrophoretic measurements (*t*-test, $P < 0.05$).

The electrophoretic mobility was determined at 298 K with a Zetasizer 2000 (Malvern Instruments, U.K.). Before the measurements the instrument was calibrated with a ζ-potential transfer reference, which is referenced to the NIST goethite standard SRM1980 (Malvern Instruments, UK). Ten measurements were performed within less than 8 min and the average value was recorded. The ζ-potential was calculated from the electrophoretic

mobility using the Smoluchowski equation (Hunter, 1988) with $\mu = \varepsilon_0 D \zeta / \eta$, where ε_0 is the permittivity of vacuum, D is the dielectric constant of water, ζ is the ζ-potential and η is the coefficient of viscosity. It is generally assumed that the ζ-potential represents the potential at a shear plane located in the diffuse layer close to the Stern layer (Hunter, 1988).

4.4 Results and Discussion

4.4.1 Pore clogging of goethite by DOM and citrate

Sorption of DOM to goethite led to a significant decrease in the volume of micropores and small mesopores <10 nm (Table 4.1). Similar results have been obtained by several researchers (Kaiser and Guggenberger, 2003; Lang and Kaupenjohann, 2003; Mikutta et al., 2004). In contrast, the average micropore diameter was not affected by the DOM treatment. This observation might be explained in two ways: (i) DOM sorption might cause a complete clogging of some micropores for N_2 at 77 K, while other micropores remained free of any organic matter, or (ii) DOM treatment might induce an occlusion of mineral surfaces upon drying.

The amount of citrate sorbed onto pure and C-coated goethite after 12 hours at pH 5 was 1.7 and 1.6 µmol m^{-2}, respectively, which is close to the reported maximum level of citrate sorption onto goethite with 1.9 µmol m^{-2} (Cornell and Schindler, 1980). Citrate sorption to both adsorbents resulted in a pronounced decrease in the micropore volume and the average micropore diameter (Table 4.1). The effect increased with increasing contact time of citrate and, in the case of C-coated goethite, increased with increasing citrate concentration (Table 4.1). The results indicate a micropore clogging by citrate within less than one hour of citrate sorption. Absolute changes in micropore volumes upon sorption of citrate were highly significant but about as small as changes reported for Fe and Al oxides of drinking-water treatment residuals after sorption of phosphate for 80 days (Makris et al., 2004).

The micropore volumes of pure goethite decreased in the background electrolyte, even without the addition of DOM or citrate (see 'Goethite Control', Table 4.1). However, the decrease in micropore volume was significantly larger in the citrate treatments (Table 4.1).

Ligand-promoted dissolution of goethite can be ruled out as a course for the porosity changes detected in the presence of citrate as Fe concentrations determined in solution were small. For example, the addition of 300 µM citrate to C-coated goethite for three hours resulted in a goethite dissolution of only 0.3 mol% Fe. Taking an average N_2-BET

surface area of 242 m^2 g^{-1} of ten synthetic 2-line and 6-line ferrihydrites (Cornell and Schwertmann, 2003, Table 5.1, p. 106; Liang et al., 2000), and assuming (i) a molecular weight of ferrihydrite of 480 g mol^{-1} ($Fe_5HO_8 \cdot 4H_2O$, Towe and Bradley, 1967) and (ii) that all acid-ammonium oxalate-soluble Fe (4.9 wt%) comes from residual ferrihydrite still present in our solid, a simple alligation calculation shows that maximal 6 m^2 per gram solid could be attributed to residual ferrihydrite. The decrease in the DR-micropore surface area after sorption of citrate to pure and C-coated goethites for 12 hours was 23 and 16 m^2 g^{-1}, respectively. Therefore, we take the statistically significant decreases in micropore volumes and micropore diameters obtained from applying the DR model to the N_2 adsorption data of citrate-treated goethites as direct evidence for pore clogging by citrate. It should be noted that these micropore diameters are average diameters. From a chemical standpoint, the tiny decreases observed (<0.1 nm, Table 4.1) suggest that no monolayer sorption by citrate in micropores occurred. Our results show that the sorption of citrate in micropores is a fast process being detectable by N_2 adsorption just one hour after citrate addition to both adsorbents.

4.4.2 Phosphate sorption kinetics in the absence of citrate

Pure and C-coated goethite sorbed 2.1 and 1.8 µmol P m^{-2}, respectively. The value for pure goethite is smaller than the 2.5 µmol P m^{-2} that are maximal expected to sorb on a (101) goethite surface with two singly coordinated surface hydroxyls per 0.68 nm^2 at a maximum loading (Torrent et al. 1990; Cornell and Schwertmann, 2003). Sorption of phosphate to pure and C-coated goethite did not reach an equilibrium within three weeks and showed a biphasic pattern (Fig. 4.2), which is commonly observed for phosphate sorption to soils and Fe oxides (Torrent, 1987; Barrow et al., 1993; Strauss et al., 1997). The slowly continuing phosphate immobilization over weeks by goethite has been verified to be due to diffusion of phosphate into micropores (Strauss et al., 1997). Similarly, a clogging of micropores of drinking-water treatment residuals that comprise amorphous Fe and Al oxides by phosphate has recently been confirmed (Makris et al., 2004).

The micropore diffusion of phosphate in our study is further evidenced by decreasing average micropore diameters when phosphate was added to pure and C-coated goethite (Table 4.2). It is important to note, however, that the high-surface-area goethite used partially recrystallized in solution. This is shown by the decrease in the micropore volume and a concomitant increase in the average micropore diameter after three weeks compared with the initial goethite (Table 4.2). Accordingly, the healing of the smallest surface inhomoge-

neities (micropores) increased the average micropore diameter as well as decreased the micropore volume.

Table 4.1. Concentration and residence time effects of citrate on meso- and microporosity of pure and C-coated goethite at pH 5. Goethite-initial and Goethite/DOM-initial give the goethite properties at the beginning of the sorption experiments, i.e., no solution contact. Means were compared with the unpaired *t*-test. Values in the same column that are followed by the same letter are not statistically different at $P < 0.05$. Values are given as mean ± standard deviation. In the citrate residence time experiment, means of each residence time were compared (+ citrate vs. respective control treatment).

Treatment	Mesopore Volume			Micropore Volume	Average Micropore Diameter
	2-5 nm	5-10 nm	10-50 nm		
	——— $mm^3 g^{-1}$ ———			$mm^3 g^{-1}$	nm
Citrate Concentration †					
Goethite-initial‡	75 (6)a	89 (3)a	420 (12)a	57 (1)a	0.87 (0.01)a
Goethite/DOM-initial‡	53 (5)b	76 (2)b	417 (9)a	44 (0)b	0.87 (0.01)a
Goethite/DOM + 20 µM Citrate	48 (3)b	78 (4)b	401 (7)ab	42 (0)c	0.85 (0.01)ab
Goethite/DOM + 100 µM Citrate	46 (2)b	76 (3)b	395 (13)a	40 (0)d	0.84 (0.00)bc
Goethite/DOM + 300 µM Citrate	45 (0)b	79 (4)b	393 (9)b	37 (1)e	0.82 (0.01)d
Citrate Residence Time §					
Goethite Control					
1 h	62 (4)	82 (1)	359 (2)	53 (1)	0.88 (0.01)
6 h	61 (2)	82 (0)	342 (4)	52 (0)	0.87 (0.02)
12 h	58 (1)	79 (1)	345 (13)	51 (1)	0.88 (0.01)
Goethite + Citrate					
1 h	58 (4)NS	80 (3)NS	361 (4)NS	46 (0)***	0.83 (0.00)**
6 h	56 (3)NS	83 (3)NS	356 (5)*	44 (0)***	0.82 (0.01)*
12 h	53 (3)*	80 (3)NS	360 (3)NS	42 (0)***	0.81 (0.01)***
Goethite/DOM Control					
1 h	46 (27)	77 (2)	387 (6)	41 (0)	0.86 (0.01)
6 h	49 (3)	77 (3)	374 (5)	42 (1)	0.87 (0.01)
12 h	48 (3)	75 (2)	383 (1)	43 (0)	0.87 (0.00)
Goethite/DOM + Citrate					
1 h	47 (4)NS	76 (3)NS	369 (3)**	38 (0)***	0.83 (0.00)**
6 h	45 (3)NS	78 (3)NS	373 (6)NS	37 (0)***	0.83 (0.01)**
12 h	51 (4)NS	80 (2)*	355 (8)**	37 (0)***	0.82 (0.00)***

† three hours contact time, 2 g L^{-1} solid concentration and I = 0.01 M KNO_3.

‡ initial = no solution contact.

§ 300 µM citrate addition, 1 g L^{-1} solid concentation and I = 0.01 M KNO_3.

*,**,*** Significant at the 0.05, 0.01, and 0.001 probability level, respectively.

NS indicates nonsignificance at $P = 0.05$.

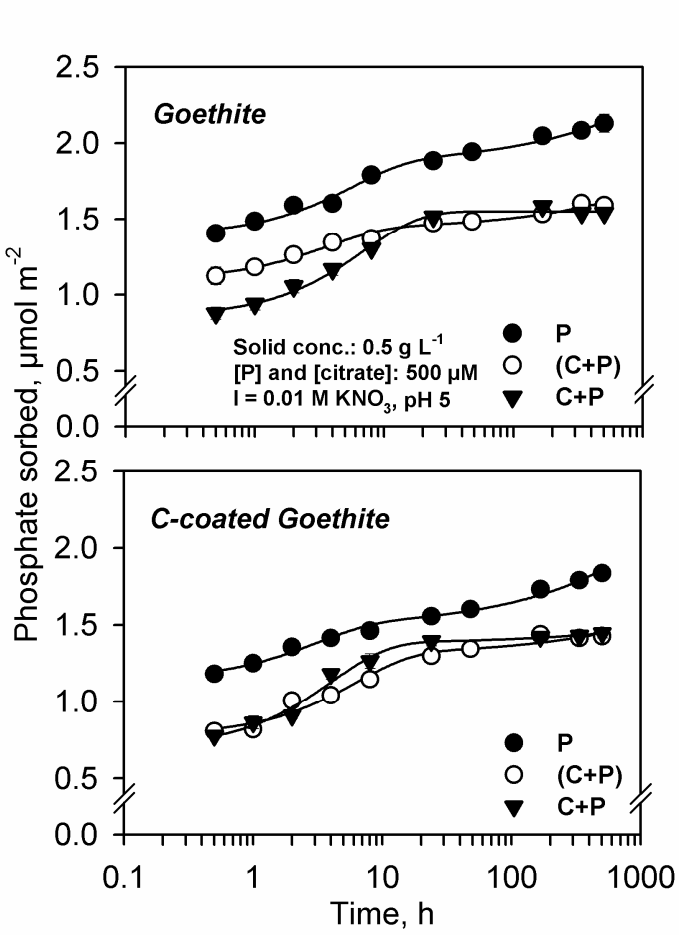

Fig. 4.2. Phosphate sorption versus time of pure goethite and C-coated goethite. The lines show the fits of Eq.[4.1] to the phosphate sorption data. Treatments: P, phosphate addition; (C+P), simultaneous addition of citrate and phosphate; C+P, citrate added three hours before phosphate. Number of replicates was 3; subsample variability was <2% on average. Error bars representing standard deviation are within the symbol size.

The strongly complexing phosphate counteracted the goethite transformation to some extent, which resulted in greater micropore volumes of phosphate-treated samples relative to the controls (Table 4.2, no P). This inhibitory effect of specifically sorbing ligands like phosphate has also been shown to retard ferrihydrite transformation (Barrón et al., 1997). Despite the dynamic nature of the goethite surface it can be unambiguously concluded that phosphate penetrated into micropores as their average diameters decreased during three weeks with respect to the initial goethite's average micropore diameter (Table 4.2).

While the sorption of phosphate to external surfaces was reduced by 21% due to the DOM coating (Table 4.3, c_m), the amount of slowly sorbing phosphate, P_{slowly}, and the apparent diffusion constant $(D/r^2)_{app}$ were not significantly affected (Table 4.3). Therefore, the diffusion of phosphate into micropores of goethite was likely not restricted by DOM as shown by a similar decrease in average micropore diameter compared with pure goethite (Table 4.2). It is particularly noteworthy that the ζ-potential of goethite was reversed upon DOM sorption from +29 mV to -32 mV and remained negative upon phosphate sorption (Fig. 4.3B), and that 43% of C were desorbed from C-coated goethite after three weeks of

phosphate sorption. Consequently, the phosphate diffusion into micropores of C-coated goethite was hardly influenced by the decreased ζ-potential caused by sorbed DOM molecules. The phosphate sorption kinetics of C-coated goethite is clearly inconsistent with the preferential sorption and stabilization of organic matter in pores <10 nm (Kaiser and Guggenberger, 2003; Zimmerman et al., 2004a, b).

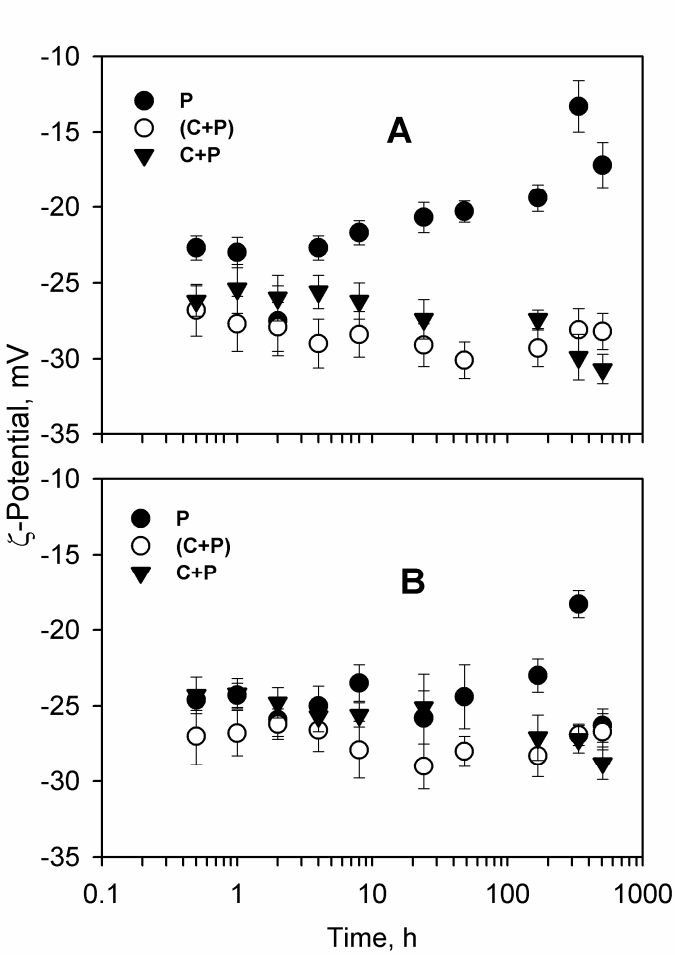

Fig. 4.3. Change of ζ-potential with time of (A) pure goethite and (B) C-coated goethite during three weeks. Treatments: P, phosphate addition; (C+P), simultaneous addition of citrate and phosphate; C+P, citrate added three hours before phosphate. The initial ζ-potential of pure and C-coated goethite in 0.01 M KNO_3 (pH 5) was +29 and -32 mV, respectively. Error bars represent standard deviation.

The proposed preferential sorption of DOM molecules in or at the mouths of micropores (Kaiser and Guggenberger, 2003) should render these organic molecules less desorbable by phosphate, and – more important – should decrease the accessibility of these pores to phosphate ions. Therefore, the observed inconsistency between the strong reduction in pore volume of pores <10 nm in C-coated goethite samples (Table 4.1) and both a similar change in average micropore diameter after phosphate sorption and slow phosphate sorption kinetics compared with pure goethite (Table 4.2, 4.3) might be best explained by structural changes of organic molecules at the goethite surface upon drying. Drying of or-

ganic coatings might decrease the accessibility of pores <10 nm for N_2 at 77 K. In a previous study Mikutta et al. (2004) showed that mesopores of a Al oxide sample coated with polygalacturonate decreased upon drying.

4.4.3 Citrate-promoted goethite dissolution during phosphate sorption

Iron concentrations in solution increased linearly in the presence of citrate, and up to 2.3 mol% Fe of pure and C-coated goethite were dissolved within three weeks (Fig. 4.4). The zero-order dissolution kinetics of goethite complies with a surface-controlled, ligand-promoted dissolution that has been described by Stumm and coworkers (Furrer and Stumm, 1986; Zinder et al., 1986; Stumm and Furrer, 1987). This effect was greater for C-coated goethite and samples to which citrate was added before phosphate (Fig. 4.4). Dissolution of pure and C-coated goethite proceeded at higher rates at times <~24 hours. The initial fast dissolution was followed by a slower linear dissolution pattern; a finding that was also reported for lepidocrocite (Bondietti et al., 1993) and hematite (Sulzberger et al., 1989). The initial fast dissolution is attributed to the rapid dissolution of surface irregularities of crystals or to the dissolution of small particles (Ostwald ripening), like for instance ferrihydrite particles in goethite/ferrihydrite mixtures (Schwertmann et al., 1982). The initial fast dissolution step was small compared with the linear dissolution pattern in our and related studies on crystalline Fe oxides (Sulzberger et al., 1989; Bondietti et al., 1993), but became the controlling process in the citrate-mediated dissolution of ferrihydrite (Liang et al., 2000).

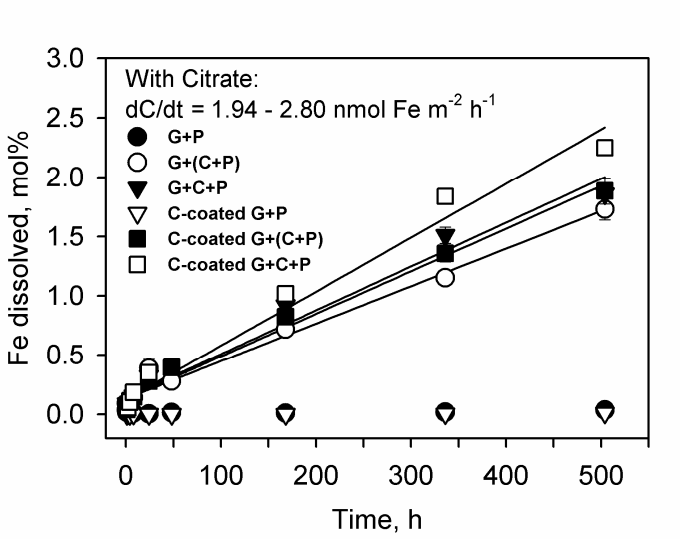

Fig. 4.4. Iron release kinetics of pure (G) and C-coated goethite (C-coated G) in the presence of citrate following different modes of addition (I = 0.01 M, pH 5). The solid lines were obtained by linear curve fitting. Coefficients of determination were ≥0.98. Treatments: P, phosphate addition; (C+P), simultaneous addition of citrate and phosphate; C+P, citrate added three hours before phosphate. The Fe release rates of pure and C-coated goethite were normalized to the N_2-BET surface area of pure goethite (179 m^2 g^{-1}). Error bars representing standard deviation are smaller than the symbol size.

If the Fe dissolved rapidly is attributed to residual ferrihydrite, the contribution of dissolved residual ferrihydrite to the sample's mass would be 0.44 wt% in the treatment with maximal Fe release (C-coated goethite, 'C-coated G+C+P' in Fig. 4.4). This value corresponds to a maximal ferrihydrite contribution of <1 m^2 g^{-1} to the total N_2-BET surface area – a value, which cannot be resolved by N_2 surface area measurements. As changes in micropore surface area were larger than 1 m^2 g^{-1} in the presence of citrate, microporosity data discussed hereafter are likely not biased by the presence of residual ferrihydrite.

Sorption of citrate before phosphate to pure goethite decreased the ability of phosphate to compete with citrate for sorption sites (Table 4.4). In accordance with the ligand-promoted, nonreductive dissolution of Fe oxides by organic ligands, R_L, that is linearly dependent on the concentration of the adsorbed ligand (L_{ads}):

$$R_L = d[Fe(III)_{aq}]/dt = k_L\,[L_{ads}], \qquad [4.4]$$

where k_L is the rate constant of ligand-promoted dissolution (Stumm, 1992), higher adsorption densities of citrate in the 'C+P' treatment (Table 4.4) facilitated the partial dissolution of pure goethite. As a consequence, higher Fe concentrations were measured in solution in the 'C+P' treatment (Fig. 4.4). When both ions were added simultaneously, citrate sorption was strongly reduced (Table 4.4) and the dissolution of goethite was less distinct (Fig. 4.4). Our results are in line with Watanabe and Matsumoto (1994) and Hiradate and Inoue (1998) who observed that the dissolution of Fe oxides by mugineic acid was inhibited by phosphate due to sorption competition.

While the amount of citrate sorbed to C-coated goethite after one hour, 24 hours (Table 4.4) and 504 hours (not shown) were similar in both citrate treatments, TOC concentrations in solution were 23% higher in the 'C+P' treatment compared to the '(C+P)' treatment after three weeks. Likewise, Fe concentrations in solution after three weeks were 19% higher when citrate was added before phosphate to C-coated goethite (Fig. 4.4). These findings indicate that either citrate alone or in combination with phosphate promoted the partial dissolution of C-coated goethite by favoring the release of Fe(III)-organic matter complexes from the goethite surface. A similar synergistic effect of LMWOA anions on the ligand-promoted dissolution of goethite has been reported for oxalate, which enhanced the rate of goethite dissolution by the fungal siderophore desferrioxamine B (Cervini-Silva and Sposito, 2002; Cheah et al., 2003).

Table 4.2. Specific surface area and porosity after three weeks of sorption of phosphate, citrate, and both ions using differing addition modes. Treatments: Goethite-initial and Goethite/DOM-initial; goethite properties at the beginning of the sorption experiments, i.e., no solution contact; no P, samples in background electrolyte (control); P, phosphate addition; (C+P), simultaneous addition of citrate and phosphate; C+P, citrate added three hours before phosphate. Means were compared using the unpaired *t*-test. For each adsorbent, values in the same column that are followed by the same letter are not statistically different at $P < 0.05$. Values in parentheses represent standard deviation.

Treatment	Specific Surface Area	Total Pore Volume	D_p[†]	Mesopore Volume			Micropore Volume	Average Micropore Diameter
				2-5 nm	5-10 nm	10-50 nm		
	$m^2\ g^{-1}$	$mm^3\ g^{-1}$	nm	——— $mm^3\ g^{-1}$ ———			$mm^3\ g^{-1}$	nm
Goethite								
initial[‡]	178.8 (5.9)	647 (15)	14.5 (0.2)	75 (6)	89 (3)	420 (12)	57 (1)	0.87 (0.01)
no P	136.7 (1.6)a	538 (15)a	15.7 (0.4)a	45 (3)a	77 (1)a	346 (2)a	41 (0)a	0.91 (0.01)a
P	151.1 (1.3)bc	540 (9)a	14.3 (0.1)b	45 (3)a	79 (1)a	358 (4)b	44 (1)b	0.75 (0.02)b
(C+P)	155.5 (2.0)b	529 (3)a	13.6 (0.1)c	48 (4)a	84 (1)b	354 (5)a	40 (0)c	0.71 (0.00)c
C+P	150.7 (1.6)c	565 (20)a	15.0 (0.7)ab	47 (2)a	77 (2)a	364 (12)a	39 (0)d	0.72 (0.01)bc
Goethite/DOM								
initial[‡]	149.3 (4.2)	620 (7)	16.6 (0.3)	53 (5)	76 (2)	417 (9)	44 (0)	0.87 (0.01)
no P	135.8 (0.9)a	581 (2)a	17.1 (0.1)a	41 (0)a	74 (1)a	367 (1)a	38 (0)a	0.90 (0.01)a
P	149.9 (1.7)bc	579 (6)a	15.5 (0.1)b	45 (3)a	80 (2)b	370 (4)a	40 (0)b	0.73 (0.01)b
(C+P)	153.6 (1.9)b	566 (13)a	14.7 (0.2)c	53 (5)b	80 (2)b	354 (6)b	39 (0)b	0.73 (0.01)b
C+P	146.2 (4.0)c	574 (9)a	15.7 (0.2)b	43 (3)a	76 (4)ab	368 (9)ab	38 (1)a	0.74 (0.03)b

[†] Average pore diameter.

[‡] initial = no solution contact.

Table 4.3. Parameter obtained from fitting the combined model to the phosphate sorption data, apparent diffusion constant $(D/r^2)_{app}$ and the amount of phosphate slowly immobilized during three weeks. Treatments: P, phosphate addition; (C+P), simultaneous addition of citrate and phosphate; C+P, citrate added three hours before phosphate. Values in parentheses represent standard error.

Treatment	c_m †	a_0 ‡	k §	b ¶	r^2	$(D/r^2)_{app}$	P_{slowly} $q_{504h} - c_m$
	µmol m^{-2}		h^{-1}	µmol m^{-2} $h^{-0.5}$ x 10^{-3}		h^{-1} x 10^{-7}	µmol m^{-2}
Goethite							
P	1.85 (0.04)	0.46 (0.04)	0.18 (0.04)	13 (2)	0.99	23.7 (8.8)	0.29 (0.05)
(C+P)	1.42 (0.02)	0.33 (0.03)	0.29 (0.07)	9 (2)	0.98	8.4 (3.1)	0.17 (0.02)
C+P	1.55 (0.04)	0.70 (0.04)	0.14 (0.02)	NS	0.99	NS	0.00 (0.04)
Goethite/DOM							
P	1.47 (0.02)	0.34 (0.04)	0.36 (0.10)	17 (2)	0.99	34.7 (6.8)	0.36 (0.03)
(C+P)	1.30 (0.05)	0.52 (0.06)	0.16 (0.04)	7 (3)	0.98	4.8 (4.7)	0.13 (0.05)
C+P	1.38 (0.04)	0.69 (0.05)	0.25 (0.05)	NS	0.99	NS	0.07 (0.05)

† Total amount of phosphate sorbed rapidly.

‡ Constant related to the amount of phosphate instantaneously sorbed according Eq.[4.2].

§ Rate constant of the fast phosphate reaction.

¶ Rate constant of the slow phosphate reaction.

NS indicates nonsignificance at the $P = 0.10$ level.

Table 4.4. Amounts of phosphate and citrate sorbed after one hour and 24 hours. Treatments: P, phosphate addition; (C+P), simultaneous addition of citrate and phosphate; C+P, citrate added three hours before phosphate. Values in parentheses denote standard deviation.

Treatment	Sorption after 1 h			Sorption after 24 h		
	P	Citrate	∑(P+Citrate)	P	Citrate	∑(P+Citrate)
	µmol m^{-2}					
Goethite						
P	1.49 (0.03)		1.49 (0.03)	1.88 (0.02)		1.88 (0.02)
(C+P)	1.18 (0.05)	0.30 (0.10)	1.48 (0.11)	1.48 (0.01)	0.16 (0.00)	1.64 (0.01)
C+P	0.94 (0.04)	0.69 (0.05)	1.62 (0.06)	1.51 (0.02)	0.62 (0.07)	2.13 (0.08)
Goethite/DOM						
P	1.25 (0.02)		1.25 (0.02)	1.56 (0.02)		1.56 (0.02)
(C+P)	0.82 (0.01)	0.30 (0.03)	1.12 (0.03)	1.30 (0.04)	0.27 (0.01)	1.57 (0.04)
C+P	0.86 (0.04)	0.40 (0.04)	1.26 (0.06)	1.40 (0.03)	0.25 (0.02)	1.65 (0.04)

4.4.4 Phosphate sorption kinetics in the presence of citrate

Phosphate sorption induced the desorption of citrate from pure and C-coated goethite (Table 4.4). Despite the strong competition between both ions, citrate decreased the amount of phosphate sorbed to pure and C-coated goethites after three weeks by up to 28% and 22%, respectively. The result complies with Geelhoed et al. (1998) who reported a

pronounced decrease in phosphate sorption at pH 5 when citrate was present at equimolar concentration.

The effect of citrate on the phosphate sorption kinetics of goethite can be slit up into two separate processes: First, citrate reduced the amount of phosphate sorbed to external surfaces of both adsorbents (Table 4.3, c_m), which can be attributed to direct site blocking. Secondly, citrate reduced the amount of phosphate sorbed to internal sorption sites (Table 4.3, P_{slowly}). The latter effect of citrate was more pronounced compared with the sorption competition between phosphate and citrate for external surface sites.

The rate constant of the slow phosphate immobilization, *b*, decreased for pure and C-coated goethite in the order P > (C+P) >> C+P (Table 4.3). The amount of phosphate diffused, approximated as P_{slowly}, decreased for pure goethite in the order P > (C+P) >> C+P, but no statistically significant effect of the order of addition on the slow phosphate immobilization could be found for C-coated goethite (P > (C+P) = C+P; Table 4.3). Apparent diffusion constants, $(D/r^2)_{app}$, reported in Table 4.3 comply well with apparent diffusion constants reported for molybdenum desorption from pure and C-coated goethites (Lang and Kaupenjohann, 2003), but are 3-4 orders of magnitude lower than those reported for phosphate sorption to goethites (Strauss et al., 1997), which may be caused by a systematic overestimation of q_∞ as an approximation for the amount of phosphate diffused at infinite time in Eq.[4.2]. Apparent diffusion constants decreased in the presence of citrate and became statistically insignificant at $P = 0.10$ when citrate was added before phosphate (Table 4.3). This finding indicates that the diffusion resistance of phosphate increased in the citrate treatments as a consequence of the micropore volume and micropore diameter reduction (Table 4.2). The stronger the reduction in micropore volume was for pure goethite, i.e., C+P >> (C+P), the less phosphate was slowly immobilized during three weeks (Fig. 4.5).

We observed an inverse relationship between the amount of Fe dissolved (µmol g^{-1}) after three weeks and the specific micropore volume still present after three weeks (n = 5, $r^2 = 0.97$, $P = 0.003$). The treatment 'C-coated goethite + P' had to be excluded from the regression analysis, because the Fe release in this treatment was possibly impaired by sorbed DOM, thus producing an outlier in the data. Despite that, the observed relationship implies that in the presence of citrate both the clogging of micropores as shown in the short-term citrate sorption experiment (Table 4.1) and the partial dissolution of goethite proceeding at external goethite surfaces may account for (i) the reduction in micropore volume and average micropore diameter (Table 4.2), and hence (ii) the reduction in the rate

constant of the slow phosphate sorption and the amount of slowly sorbing phosphate (Table 4.3). However, as the slow phosphate sorption in the presence of citrate decreased by up to 100% and both adsorbents were dissolved by citrate by only up to 2.3 mol% (Table 4.3, Fig. 4.4), we conclude that the micropore clogging prevailed over the ligand-induced dissolution as a cause for the diffusion inhibition of phosphate.

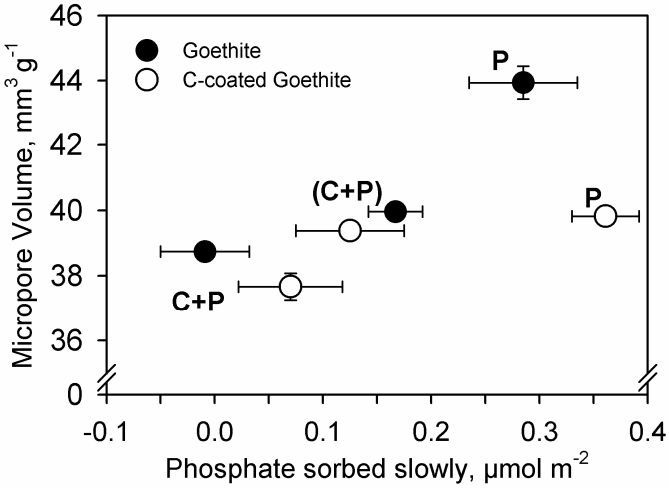

Fig. 4.5. Phosphate sorbed slowly calculated according Eq.[4.3] vs. the micropore volume present after three weeks of sorption. Treatments: P, phosphate addition; (C+P), simultaneous addition of citrate and phosphate; C+P, citrate added three hours before phosphate. Error bars indicate standard error.

4.4.5 Electrophoretic mobility measurements

The ζ-potential kinetics are presented in Fig. 4.3. Phosphate sorption to pure goethite reversed its ζ-potential to negative values, which accords with the finding that specifically sorbing anions lead to a reversal of the ζ-potential with increasing ion concentration (Hunter, 1988; Goldberg et al., 1996; Su and Suarez, 2000). With increasing sorption time, the ζ-potential of pure goethite increased by about 6 mV during phosphate sorption, which was not noticeable for C-coated goethite (Fig. 4.3). Possible explanations include surface precipitation of Fe phosphates (Ler and Standforth, 2003; Kim and Kirkpatrik, 2004), disaggregation of goethite particles (Lima et al., 2000), or diffusion of phosphate into pores of the adsorbent (Strauss et al., 1997; Makris et al., 2004), where it does no more contribute to the electrophoretic mobility. We favor the latter explanation because (i) phosphate clogged micropores of pure goethite and C-coated goethite in the absence of citrate (Table 4.4, average micropore diameter), (ii) no surface precipitation of phosphate on goethite could be detected by XANES over a broad range of phosphate solution concentrations (0-1.4 mM) (Khare et al., 2005), and (iii) the Fe release kinetics were not related to the ζ-potential kinetics (Fig. 4.3, 4.4).

In the presence of citrate, the ζ-potential of the adsorbents declined when compared with samples to which only phosphate was added, showing that citrate conveyed additional negative charge to the adsorbents surface (Fig. 4.3). This effect was stronger for pure goethite compared with C-coated goethite. The order of addition of both ions to pure goethite did not result in significant differences in the ζ-potential, which accords with the minor effect of the order of addition on the amount of phosphate sorbed to external surfaces (Table 4.3, c_m). This result indicates that externally sorbed ions contribute primarily to the electrophoretic mobility.

4.4.6 Environmental implications

Polycarboxylic low-molecular-weight organic acid anions are excreted by plant roots at rates ranging up to 4000 nmol g^{-1} (fresh weight) h^{-1} depending on environmental conditions (Ryan et al., 2001). Consequently, concentrations of these anions in the rhizosphere soil solution can increase up to 1500 µM (Jones, 1998). Modeling approaches indicate that 99% of these acids remain within 1 mm from the root surface (Jones et al., 1996), which confines their efficiency in nutrient acquisition to the soil-root interface. Phosphate mobilization mediated by LMWOA anions has been documented for soils (e.g., Lopez-Hernandez et al., 1986; Traina et al., 1987; Jungk et al., 1993; Ström et al., 2002), but the mechanisms behind are not easily identifiable in complex systems. The increase in phosphate solution concentration in the presence of LMWOA anions has mostly been ascribed to sorption competition (Lopez-Hernandez et al., 1986; Geelhoed et al., 1998, 1999; see Guppy et al., 2005 for a review) and, less often, to the dissolution of phosphate-bearing minerals (Traina et al., 1987; Bolan et al., 1994, 1997; Bertrand et al., 1999). Although the dissolution of Fe oxides by LMWOA anions is well documented (Stumm et al., 1985; Miller et al., 1986; Zinder et al., 1986; Chiarizia and Horwitz, 1991), its ecological meaning has received much less attention (Jones et al., 1996; Bertrand and Hinsinger, 2000).

In accordance with adsorption studies (e.g., Geelhoed et al., 1998), sorption competition between citrate and phosphate decreased the sorption of phosphate to pure and C-coated goethite by up to 28%. Additionally, citrate clogged the micropores of both adsorbents and enhanced the goethite's dissolution - two mechanisms by which the diffusion of phosphate into mineral pores of <2-nm size and hence its strong fixation can be reduced.

The sorption of citrate in micropores of pure and C-coated goethites was detectable within the maximal average half-life time reported for citrate in soils (<12 hours, Jones and Darrah, 1994) without any significant dissolution of the goethite occurring

(<0.3 mol% Fe). The sorption of citrate in micropores of goethite within hours may partially promote its stabilization against microbial decay by the physical exclusion of enzymes (Adu and Oades, 1978; Mayer, 1994; Zimmerman et al., 2004a, b). Within three weeks of phosphate sorption to pure and C-coated goethite, citrate significantly impaired the slow phosphate reaction. Micropore clogging by citrate and citrate-mediated goethite dissolution (<2.3 mol% Fe) were identified as possible mechanisms by which the diffusion of phosphate into micropores of pure and C-coated goethites can be impaired. As plants under phosphate stress will exude LMWOA anions at high rates and over long periods of time, the micropore clogging or the dissolution of strongly phosphate sorbing Fe and Al oxides adjacent to root surfaces may be regarded as potential strategies of plants to cope with phosphate deficiency in addition to ligand-exchange. The effects of micropore clogging by LMWOA anions and the dissolution of Fe oxides by polyprotic LMWOA anions on the bioavailability of phosphate have yet not been realized, and are therefore still unaccounted for in mathematical models of phosphate mobilization by organic anion excretion by plant roots (Kirk, 1999; Geelhoed et al., 1999).

4.5 Conclusions

Under the experimental conditions chosen, citrate as a common water soluble root exudate has been shown to clog the micropores of both a synthetic pure goethite and one that was coated with natural organic matter. For both adsorbents, the micropore clogging proceeded within only a few hours. The micropore clogging of both adsorbents by citrate increased with time and, for C-coated goethite, with increasing citrate concentration.

During three weeks of phosphate sorption in the presence of citrate at equimolar concentration (500 µM), citrate reduced the amount of phosphate sorbed to both adsorbents by up to 28%, and solubilized Fe from pure and C-coated goethite by up to 2.3 mol%. In addition, citrate led to a reduction in the micropore volume and average micropore diameter of pure and C-coated goethite. Consequently, the slow and continuous phosphate immobilization by both adsorbents via diffusion of phosphate into micropores was strongly impaired. This effect was larger when citrate was added three hours before phosphate to pure goethite, but only a minor effect of the order of addition of both ions was observed for C-coated goethite. As both microporous Fe oxides and LMWOA anions are ubiquitous in soils and sediments, micropore clogging and the partial dissolution of Fe oxides by LMWOA anions might be of significant importance regarding the mobility of nutrient and/or contaminant anions that would otherwise be strongly fixed by Fe oxides in acidic

environments. Due to phase transformations of meta-stable microporous adsorbents in aqueous solutions, the average micropore diameter can be regarded as a better parameter for identifying micropore clogging or dissolution reactions caused by organic compounds than simply micropore volume.

5 Phosphate desorption from goethite in the presence of galacturonate, polygalacturonate, and maize mucigel (*Zea mays* L.)

Christian Mikutta[1]*, Günter Neumann*[2]*, Friederike Lang*[1]

Submitted for publication in the Soil Science Society of America Journal

[1] Department of Soil Science, Institute of Ecology, Berlin University of Technology, Salzufer 12, D-10587 Berlin, Germany

[2] Institute of Plant Nutrition, University of Hohenheim, Fruwirthstr. 20, D-70593 Stuttgart, Germany

5.1 Abstract

Uronates are important constituents of maize mucilage and Polygalacturonate is used as a simplified model of the soil-root interface. We tested whether galacturonate (GA) and polygalacturonate (PGA) impair the diffusion of phosphate into/out of pores <5 nm of a synthetic goethite (147 m^2 g^{-1}) and whether the effect of maize mucigel (MU) is comparable with that of PGA. We measured the phosphate desorption kinetics of goethites in batch experiments over two weeks at pH 5. One part of the goethite was equilibrated with organic substances before phosphate addition, another part after addition of phosphate. Before the desorption experiments, the porosity of our samples was analyzed by N_2 gas adsorption. In each treatment a rapid initial desorption was followed by a slow desorption reaction, which is assigned to the diffusion of phosphate out of goethite pores. No consistent relation between the <5-nm porosity and the rate of the slow phosphate desorption was observed. Compared with the C-free control, only PGA and MU affected the fraction of phosphate mobilized by the fast and slow desorption: When PGA was sorbed to goethite prior to phosphate, twice as much phosphate was mobilized via the fast reaction than in the treatment where phosphate was sorbed prior to PGA, suggesting a decreased accessibility of goethite pores to phosphate. Mucigel, however, showed reversed effects, which is ascribed to its differing chemical composition. In conclusion, PGA seems inappropriate as a model substance for maize MU collected from non-axenic sand cultures. Under the experimental conditions chosen, the efficacy of all organic substances to increase the solution concentration of phosphate by pore clogging and sorption competition is small.

5.2 Introduction

The P reservoir of soils is usually large (Foth and Ellis, 1997), but phosphate concentrations found in the soil solution are generally smaller than 20 µM (Reisenauer, 1964; Barber, 1974). The reason for the low phosphate concentrations under acid conditions is the strong sorption of phosphate to soil minerals, especially Fe and Al oxides. Phosphate ions either adsorb on external surfaces of Fe and Al oxides or in their intra- and interparticle pores that are accessible to phosphate by diffusion (Willet et al., 1988; Torrent et al., 1990; Strauss et al., 1997; Mikutta et al., 2006c). The extent of phosphate diffusion into pores of Fe oxides depends on the volume of micro- and mesopores, and the pore geometry of the adsorbent (Cabrera et al., 1981; Madrid and de Arambarri, 1985; Strauss et al., 1997).

In soils, mineral surfaces are partly covered with organic matter (OM) (Fontes et al., 1992; Heil and Sposito, 1995; Mayer and Xing, 2001; Gerin et al., 2003). Organic coatings of the soil rhizosphere may consist primarily of microbial and phytogenic OM, with polysaccharides being important constituents. Especially mucilages have been implicated to strongly bind soil particles together, thus coating mineral surfaces at the soil-root interface (Vermeer and McCully, 1982; Watt et al., 1993). Mucilages are pectin-like high-molecular-weight root exudates, which are primarily secreted by root cap cells (Paull and Jones, 1975; Rougier, 1981) and comprise about 90-95% polysaccharides with about 20-35% of uronic acids (Cortez and Billes, 1982; Morel et al., 1986). Principal components of maize mucilage identified are glucose, galactose, fucose, xylose, arabinose, and galacturonic acid (Rougier, 1981; Osborn et al., 1999).

The sorption of polygalacturonate (PGA) - as a model substance for root mucilage - to goethite (α-FeOOH) has been shown to reduce the pore volume of <10-nm pores and the amount of phosphate sorbed within two weeks (Mikutta et al., 2006b). Gaume et al. (2000) explained the increase in isotopically exchangeable phosphate after phosphate addition to PGA- and mucilage-treated ferrihydrite with microaggregation of ferrihydrite particles, which decreased the accessibility of sorption sites for phosphate. Apart from these reports, no studies on the effect of mucilage or mucilage-like substances on the accessibility of mineral pores to phosphate or other oxyanions are available. In addition, most studies on the kinetics of oxyanion-mineral interactions are confined to adsorption. To date, only one study is available relating the ‘pore clogging’ of Fe oxides by organic sorbates to the desorption kinetics of oxyanions. Lang and Kaupenjohann (2003) studied the effect of residence time of molybdate on the molybdate desorption kinetics using pure goethites and

goethites incubated with dissolved OM. They found that C coatings prevented molybdate from diffusion into intraparticle pores, thus favoring its enrichment on outer goethite surfaces and hence its fast desorption compared with pure goethites. Until now it has not been studied whether oxyanions might be trapped in micro- and small mesopores (Ø <5 nm) by organic coatings comprising macromolecular root exudates. This situation likely occurs when oxyanions sorb to porous minerals prior to OM. We hypothesized that high-molecular-weight OM entraps phosphate in pores <5 nm of goethite when added after phosphate and, conversely, that the diffusion of phosphate into pores <5 nm is impaired when OM is sorbed prior to phosphate. A pore size boundary of 5 nm was chosen because in preliminary experiments we observed that the volume of <5-nm pores of microporous goethite was significantly reduced by sorbed natural OM or PGA (Mikutta et al., 2006a, c). Polygalacturonate is commonly used as a simplified model of the soil-root interface (Morel et al., 1987; Gessa and Deiana, 1992; Ciurli et al., 1996; Gaume et al., 2000; Grimal et al., 2001; Mikutta et al., 2006a, b). However, well-defined root exudates seldom exist in the rhizosphere, and the ability of PGA or mucilage to affect the kinetics of phosphate sorption and desorption of Fe oxides might depend on the degree of alteration of these substances, e.g., by microbial activity or by complexation with polyvalent cations (Deiana et al., 2001; Mimmo et al., 2003; Gessa et al., 2005). In order to more realistically test the effect of macromolecular root exudates on the phosphate desorption kinetics of Fe oxides, we additionally used mucigel of maize plants. Mucigel is a gelatinous material at root surfaces of plants grown under non-axenic conditions (Jenny and Grossenbacher, 1963). It includes pure and modified mucilage, bacterial cells, their metabolic products (e.g., capsules and slimes) as well as colloidal mineral and/or OM inherited from the sampling environment.

We hypothesized that the phosphate desorption kinetics of goethite treated with PGA is comparable to that of mucigel-treated goethite. Goethite was used because it is the most prominent Fe oxide in soils (Cornell and Schwertmann, 2003). Polygalacturonate and maize mucigel (MU) were taken as phytogenic macromolecular organic sorbates, whereas galacturonate (GA) was used to identify effects arising from the polymeric nature of PGA only. For example, in contrast to GA, sorption of PGA in micropores is unlikely due to size-constraints (Gaume et al., 2000). All experiments were conducted at pH 5 in order to resemble the acidic conditions in the growth media of P starved plants supplied with NO_3-N (Neumann and Römheld, 1999) and to minimize the influence of bicarbonate.

5.3 Materials and Methods

5.3.1 Preparation of goethite

The goethite was synthesized by oxidative hydrolysis of Fe(II) ($FeSO_4 \cdot 7H_2O$, Merck, extra pure) at pH 7 using H_2O_2 as an oxidant. The precipitate was washed until the electric conductivity was below 10 µS cm^{-1}, freeze-dried, softly ground and sieved to a particle size <200 µm. The oxalate-soluble Fe content according to Blakemore et al. (1987) was 4.9%. Powder X-ray diffractograms of the goethites were obtained using a Siemens D5005 instrument (Siemens AG, Germany) with CuKα-radiation of wavelength 0.15406 nm (40 kV, 30 mA). The scans indicated pure goethite with no detectable contamination. Differential X-ray analysis after oxalic acid-ammonium oxalate treatment (Schwertmann, 1964) did not reveal ferrihydrite contaminations. Scanning electron micrographs of pure and OM-treated goethite were obtained with a Hitachi S-4000 microscope fitted with an Energy-dispersive X-ray detector.

5.3.2 Organic substances

The polygalacturonic acid used comprised 37.2% C and 0.05% N [$(C_6H_8O_6)_n$, >95%, M = 25-50 kDa, Fluka P81325]. The most prominent cations of the PGA were Na (192 $mmol_c$ kg^{-1}) and Ca (11.4 $mmol_c$ kg^{-1}). Polygalacturonate solutions were prepared by dissolving PGA in 0.01 M KNO_3 with the help of 10 µL 1 M KOH mg^{-1} PGA. The pH of the solutions was then readjusted to pH 5 with 0.01 M HNO_3 without any visible flocculation occurring. Galacturonic acid was used in the form of D(+) galacturonic acid ($C_6H_{10}O_7 \cdot H_2O$, >93%, Fluka P48280).

Mucigel from maize plants (*Zea mays* L., cv. Marshal) was obtained by the method outlined in Neumann et al. (1999). Twelve maize plants were grown in 2.8-L glass tubes filled with quartz sand under greenhouse conditions with a light period of 16 hours (Fig. 5.1). Using a wick-irrigation system with two drippers per culture vessel for continuous percolation of nutrient solution (1 L per plant, replaced every second day), a nutrient solution was constantly percolated through the tubes containing 2 mM $Ca(NO_3)_2$, 0.1 mM KCl, 0.7 mM K_2SO_4, 0.5 mM $MgSO_4$, 0.5 µM KH_2PO_4, 100 µM FeEDTA, 10 µM H_3BO_3, 0.5 µM $MnSO_4$, 0.5 µM $ZnSO_4$, 0.2 µM $CuSO_4$, and 0.01 µM $(NH_4)Mo_7O_{24}$. After three weeks, the concentration of all components was doubled, except for Fe, which was raised to 150 µM of Sequestren ® (Syngenta) instead of FeEDTA. After approximately eight weeks, fertilization was raised to the maximum level, reaching the five-fold concentration of the initial nutrient supply. Sequestren application was increased to 450 µM. From the

middle of November 2004 until the end of January 2005 (begin of flowering) root MU was collected alternately from six plants every two days: The glass tubes were percolated twice with 500 mL of distilled H_2O to remove accumulated salts originating from the nutrient solution as far as possible and to induce swelling of the mucilage by flushing the roots with water. After two hours, the draining tubes were closed and the tubes were incubated with 500 mL of warm (35-38°C) distilled H_2O for solubilization of mucilage. Thereafter, the solution was collected in PE bottles and percolated twice through the glass tubes. Percolates (approx. 4 L per 6 plants) were subsequently concentrated by rotary-evaporation at 45°C to a volume of approx. 100 mL and stored at -20°C. At the end of the collection period, all pre-concentrated samples were combined and lyophilized to complete dryness.

The mixed lyophilized samples were extracted with ice-cold methanol (80% v/v) to solubilize salts and low-molecular weight organic compounds. Repeated washings of the 80% methanol-insoluble high-molecular-weight fraction were performed by re-suspending in 80 mL 80% methanol and subsequent centrifugation (3,500 x g for 5 min). Washing were performed until the electric conductivity was below 50 µS cm^{-1}.

An attempt to remove cations, originating from the nutrient solution and potentially bound to cation-exchange sites of the mucigel, was performed by re-suspending the MU in 200 mL of 80% methanol. Five membrane bags each containing 2 g of a cation exchange resin (Dowex 50 W X 8", 20-50 mesh, Na^+ form) were added, and the suspension was shaken for 6 hours at room temperature. After final centrifugation, the MU was air-dried at 27°C (approx. 6 g dry matter). For the experiments, we prepared MU solutions by dispersing MU in 0.01 M KNO_3, sonicating the suspension for 40 min, and re-adjusting the pH to 5 with 0.01 M HNO_3.

Characterization of MU. Total C and N content of the MU were determined with an Elementar Vario EIII C/N/S Analyzer. The MU was analyzed in triplicate for the content of sugars, uronic acids and proteins. For the analysis of sugars and uronic acids, 10 mg of the dry MU were hydrolyzed for three hours at 100°C with 1 mL 2 M H_2SO_4 (Harborne, 1984). Insoluble material was removed by centrifugation, and the hydrolysate was analyzed for reducing sugars after 10-fold dilution and pH adjustment to 4-5 using glucose as a standard (Blakeney and Mutton, 1980). Uronic acids were determined with glucuronic acid as standard (Blumenkrantz and Asboe-Hansen, 1973). Proteins were quantified according to Bradford (1976) after resuspending 10 mg of the dry MU in 0.5 mL dest. H_2O.

Whereas no soluble proteins could be detected in the MU suspension, a clearly positive Coomassie-blue staining indicated the presence of insoluble proteins.

Fig. 5.1. Sand-culture system for exudate collection from maize plants.

Cations bound by MU were measured with atomic absorption spectrometry (Perkin Elmer 1100B) after acid digestion of the MU in conc. HNO_3 (10:1/w:v). Total P in the MU was determined photometrically at 710 nm (Murphy and Riley, 1962) after acid hydrolysis in conc. HCl (50:1/w:v). The amount of organically bound P (P_{org}) was operationally defined as the difference between total P and the amount of phosphate bound by MU (P_{inorg}). The latter was determined after ultracentrifugation (440,000 x g, one hour) of an aqueous suspension of MU containing 1 g C L^{-1}. Mineral phases in the MU were identified with powder X-ray diffraction (Siemens D5000). Table 5.1 summarizes the chemical composition of the maize MU used.

Table 5.1. Composition of the maize mucigel used in this study. Values in parentheses indicate standard error of triplicate measurements.

Content in mg g^{-1} (dry weight)					
C	H†	N	S†	Sugar	Uronic acid
118 (0.4)	19.1 (0.3)	8.5 (0.1)	9.4 (2.2)	40 (0.6)	6.3 (0.1)
Na	K	Ca	Mg		
11.4 (0.2)	7.1 (0.1)	19.8 (0.1)	5.7 (0.1)		
Fe	Al	Si‡	P_{org}	P_{inorg}	
1.1 (1.0)	13.8 (0.1)	bdl	17.1 (1.0)	3.3 (0.1)	

† determined with a Leco CHNS-932 analyzer with extension VTF 900.
‡ bdl, below detection limit (<1 mg L^{-1} in the digestion solution).

5.3.3 Sorption of phosphate and organic matter

Goethite (18 g) was weighed into a 2-L HD-PE bottle and equilibrated for 20 hours in 1 L 0.01 M KNO_3 solution at pH 5 on a reciprocating shaker at 130 rev min^{-1} using 0.01 M HNO_3 for pH readjustments. To impair microbial activity the bottle was coated with Al foil and 100 µL 0.1 M $AgNO_3$ solution were added. After 20 hours, 1 L 0.01 M KNO_3 solution (pH 5) containing a phosphate concentration of 8 mM was added. Phosphate was provided as KH_2PO_4 (Merck, p.a.). The sample was then transferred onto a rotary shaker running at 10 rev min^{-1}. The pH was manually maintained at 5 ± 0.2 by addition of 0.01 M HNO_3. After 15 days the suspension was 0.2-µm membrane filtered, and the filter residue was washed with 500 mL doubly deionized water, freeze-dried, and softly homogenized in an agate mortar.

Eight grams of the phosphated goethite were then weighed into a 2-L HD-PE bottle and 1 L of 0.01 M KNO_3 solution (pH 5) containing 1 g C L^{-1} of GA or PGA was added. Because we had only a few grams of MU material at hand, 280 mL MU solution with 1 g C L^{-1} were given to 2.24 g of phosphated goethite. The samples were shaken on a rotary shaker at 20 rev min^{-1} in the dark at 20 ± 2 °C for 12 hours. Afterwards, the samples were 0.2-µm membrane filtered, washed with 500 mL doubly deionized water to remove excess phosphate and organic C, freeze-dried, softly homogenized and stored in the dark until use.

In another treatment we reversed the sequence of OM and phosphate addition to pure goethite. Details of this procedure were identical to the first treatment. After phosphate and/or OM sorption and subsequent freeze-drying of the samples, organic C contents were determined with an Elementar Vario EIII C/N/S Analyzer. Before the freeze-drying commenced, all samples were frozen at -80°C. The dried samples were further examined with N_2 adsorption.

5.3.4 Phosphate desorption kinetics

In order to avoid product limitation in the desorption experiments, we used synthetic Al_2O_3 (Merck, pH 6.0 ± 0.5, 50-150 µm) as an infinitive sink for phosphate that is mobilized in our batch-desorption experiments. The Al_2O_3 was sieved to a particle size of >100 µm. The phosphate sorption capacity of the sieved Al_2O_3 in 0.01 M KNO_3 solution at pH 5 was ~410 µmol P g^{-1} as judged from the phosphate sorption isotherm. The Al_2O_3 'sink' ensured phosphate solution concentrations of less than 2.5 µM, which corresponds

to less than 2% of the total phosphate desorbed. After two weeks of phosphate desorption, phosphate solution concentrations were typically <<0.7 µM in all samples.

Six grams of Al_2O_3 were packed into a 16 x 5 cm polyamide net of 50-µm mesh size, which was sealed with an impulse sealer ME-200HI (MoFix GmbH, Bad Rappenau, Germany). In order to avoid H^+ buffering by dry Al_2O_3, the Al_2O_3-bags were equilibrated at pH 5 in doubly deionized water until the pH was constant. At the beginning of the desorption run, the nets were added simultaneously with the background electrolyte solution (1 L 0.01 M KNO_3, pH 5) to the reaction bottles that contained 2 g of differently treated goethite. Again, in the MU treatments the sample weight had to be reduced to 0.3 g. Therefore, 150 mL of background electrolyte solution were added simultaneously with 0.9 g of pre-equilibrated Al_2O_3 to MU-treated goethites.

Triplicate samples were shaken in the dark on a rotary shaker at 10 rev min^{-1} and at 20 ± 2 °C. To inhibit microbial activity 100 µL 0.1 M $AgNO_3$ were added per liter background electrolyte solution. The pH was manually maintained at pH 5 with 0.01 M HNO_3. Deviations from the target pH were <0.5 for times <24 hours and <0.2 for times >24 hours. After 1, 2, 4, 8, 24, 48, 96, 168 and 336 hours a 10-mL aliquot (5 mL in MU treatments) was removed from the suspensions and 0.45-µm membrane filtered. The filter residue was freeze-dried. Subsequently, 5.0 ± 0.05 mg of the dried filter residue were weighed into a glass vial and dissolved in 100 µL conc. HCl. To ensure a rapid dissolution of the solids, the vials were placed in an oven at 105°C for 3 min. Afterwards, 10 mL doubly deionized water were added and the phosphate concentration was analyzed photometrically by the ascorbic-molybdenum blue method at 710 nm (Murphy and Riley, 1962). Solutions containing MU components were additionally 0.2-µm membrane filtered (cellulose nitrate) in order to obtain clear solutions for the phosphate measurement. Standards were prepared to resemble the matrix of the samples analyzed. The analytical precision of photometric determination of phosphate was ~1%. Subsample variability was 1.4% on average. At the end of the desorption experiments the organic C content of the freeze-dried goethites was measured with an Elementar Vario EIII C/N/S Analyzer. Carbon desorption during the phosphate desorption experiments was less than 9% in all treatments (not shown).

5.3.5 Desorption data evaluation

Desorption of phosphate from goethite was modeled using a linear combination of a first-order rate equation and the parabolic rate law (Lang and Kaupenjohann, 2003). While

the first term describes the fast desorption of phosphate from external goethite surfaces, the diffusion term models the slow transport-controlled desorption of phosphate:

$$P/P_{initial}\,(t) = a_0\text{-}a_0\,e^{-kt} + bt^{0.5}, \qquad [5.1]$$

where $P/P_{initial}\,(t)$ is the fractional amount of phosphate desorbed at time t, a_0 is the fractional amount of phosphate desorbed by the fast reaction, k is the rate constant of the fast desorption (h^{-1}), and b is the rate constant of the slow phosphate desorption ($h^{-0.5}$). The parameters a_0, k and b were determined by minimizing the sum of squared differences between the observed and predicted values of the dependent variable using the Marquardt-Levenberg algorithm implemented in SigmaPlot for Windows Version 7.0 (SPSS, Inc.). Parameters were evaluated with the *t*-statistics, which tests the null hypothesis that the parameter is zero by comparing the parameter value with its standard error. The rate constant of the slow phosphate desorption, b, is related to the apparent diffusion constant $(D/r^2)_{app}$ (h^{-1}):

$$b = 4q_\infty \pi^{-0.5} (D/r^2)_{app}^{0.5}, \qquad [5.2]$$

where q_∞ is the fractional amount of phosphate diffused at infinite time, D is the apparent diffusion coefficient ($m^2\ h^{-1}$), and r is the radius of diffusion (m). To calculate the apparent diffusion constant, $(D/r^2)_{app}$, we used the fraction of phosphate present at t = 0 hours corrected for the fractional amount of phosphate desorbed rapidly (a_0) as an approximation for q_∞ in Eq.[5.2].

5.3.6 Surface area and porosity measurements

We used an Autosorb-1 gas sorption system (Quantachrome, Syosset, NY) to assess porosity and surface area of goethite after addition of phosphate, organic compounds, or both. Helium was used as backfill gas, N_2 was used as adsorbate. Approximately 100 mg sample (~15 m^2) were degassed until the rate of pressure increase by vapor evolution was below about 1.3 Pa min^{-1} within a 0.5-min test interval. Nitrogen adsorption and desorption isotherms were obtained from 79 points in the partial pressure range 3.0 x 10^{-5} to 0.995 P/P_0. Specific surface area was calculated from the BET equation (Brunauer et al., 1938).

Microporosity (<2 nm) and average micropore diameter were determined according to the Dubinin-Radushkevic method (Gregg and Sing, 1982). The mesopore size distribution

(2-50 nm) was calculated on the desorption leg using the BJH method (Barrett et al., 1951). Separation between small (2-5 nm), medium (5-10 nm) and large mesopores (10-50 nm) was achieved by linear interpolation of the BJH desorption data. Total pore volume was taken at 0.995 P/P_0 and the average pore diameter was calculated as $D_p = 4V_{liq}/SSA$, where V_{liq} is the liquid volume of N_2 contained in pores at 0.995 P/P_0 and SSA is the BET surface area. All isotherms were recorded in triplicate.

The MU contributed up to 31% to the sample's mass, which when unaccounted for would *a priori* decrease the adsorption of N_2 at 77 K in these goethite samples because N_2-specific surface areas of OM are generally <5 m^2 g^{-1} (De Jonge and Mittelmeijer-Hazeleger, 1996; Mikutta et al., 2004; Alvarez-Puebla and Garrido, 2005). Therefore, porosity and surface area of MU-treated goethites were corrected for the mass of MU present in the sample:

$$X_{corr} = X / [1- (C_{goethite}/C_{mucigel})], \quad [5.3]$$

where X determines specific pore volume (e.g., mesopore volume) or specific surface area measured with N_2 adsorption, and $C_{goethite}$ and $C_{mucigel}$ denote the organic C content (%) of the MU-treated goethite and the MU, respectively. Because GA and PGA contributed less than 4 wt% to the total sample mass, no corrections were made.

5.4 Results and Discussion

5.4.1 Carbon contents and sorption competition

The C content of 118 mg C g^{-1} (dry weight) of the maize mucigel was significantly lower than values published for maize mucilage (Morel et al., 1986; Gaume et al., 2000; Grimal et al., 2001). Powder diffraction analysis revealed contaminations by mineral matter, including quartz (SiO_2), calcite ($CaCO_3$), gypsum ($CaSO_4 \cdot 2H_2O$), and 1:1 layer silicates (Fig. 5.2). Provided all S in the MU was bound as Ca sulfate, the contribution of carbonate-C to the total MU-C would be 2% (Table 5.1). Contrary, provided all Ca measured in the MU was bound as carbonate, the contribution of carbonate-C to the total MU-C would be 5% (Table 5.1).

The presence of gypsum with its high solubility (log K_0 = -4.64, Lindsay, 1979) is possibly due to inefficient salt removal during the MU purification process. Chemical equilib-

rium calculations with VisualMINTEQ (Allison et al., 1991) showed that at pH 5 precipitation of Ca or Al phosphates was unlikely in our experiments.

Initial C contents of the goethite samples are presented in Table 5.2. For pure and phosphated goethite they increased in the order GA < PGA << MU. Compared with pure goethite systems, sorption of OM to goethite was inhibited by 0% (MU), 41% (PGA), and 89% (GA) by pre-sorbed phosphate (Table 5.2), showing a strong competition of pre-sorbed phosphate with GA and PGA. No effect of pre-sorbed phosphate on MU sorption can be explained by the fact that in the MU treatment MU-C presumably existed partially as a separate solid phase, which was not affected by the addition of phosphate. Phosphate sorbed to OM-treated goethites within 15 days displaced 72% of GA-C, 56% of PGA-C, and 35% of MU-C, showing that phosphate strongly competed with sorbed OM (Table 5.2). The result shows that phosphate was less able to desorb PGA-C compared with GA-C, which can be explained by the multi-site attachment of polymers to mineral surfaces ('octopus' effect, Podoll et al., 1987). Our results comply with Nagarajah et al. (1970) who reported that PGA markedly decreased phosphate sorption to goethite, gibbsite, and kaolinite whereas the monomer hardly influenced phosphate sorption.

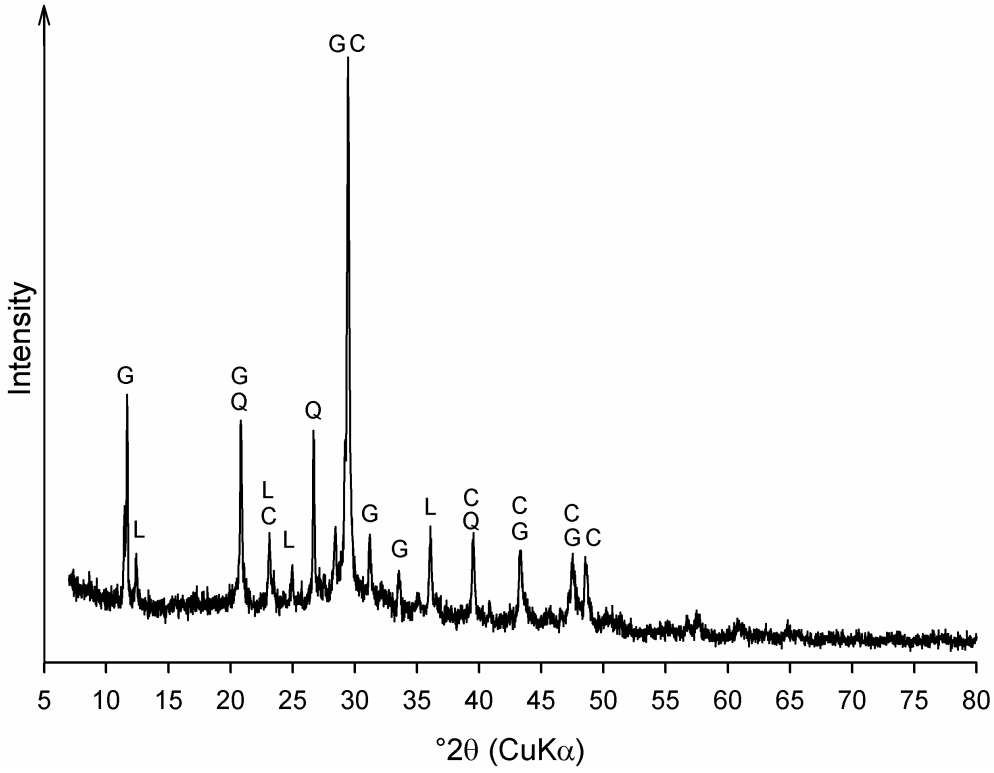

Fig. 5.2. X-ray diffractogram of the maize mucigel used in this study. Abbreviations: C, calcite; G, gypsum; L, 1:1 layer silicate; Q, quartz.

Table 5.2. Carbon content, specific surface area, and porosity characteristics of goethite after sorption of phosphate, organic matter, or both. Abbreviations used: P, phosphate; GA, galacturonate; PGA, polygalacturonate; MU, mucigel. The sequence of abbreviations indicates the sequence of sorbate addition to goethite. Values in parentheses represent standard error.

Treatment	C content[†]	SSA[‡]	D_p[§]	Total Pore Volume	Micropore Volume	Mesopore Volume		
						2-5 nm	5-10 nm	10-50 nm
	mg g^{-1}	m^2 g^{-1}	nm			mm^3 g^{-1}		
Goethite		147 (1)	15.0 (0.1)	555 (3)	45.7 (0.2)	48 (2)	75 (1)	398 (2)
P (Control)		150 (1)	15.1 (0.1)	568 (3)	45.2 (0.2)	42 (2)	70 (1)	405 (1)
GA	7.6 (0.02)	137 (0)	15.6 (0.1)	534 (3)	39.1 (0.1)	38 (0)	71 (2)	401 (1)
PGA	12.5 (0.2)	137 (1)	15.2 (0.0)	518 (3)	41.9 (0.1)	38 (1)	69 (1)	386 (0)
MU	35.8 (0.5)	151 (1)	16.6 (0.3)	627 (12)	38.2 (0.1)	42 (0)	80 (2)	448 (3)
P+GA	0.8 (0.01)	145 (1)	15.1 (0.2)	547 (5)	43.7 (0.1)	41 (1)	71 (1)	391 (5)
P+PGA	7.4 (0.1)	136 (1)	15.6 (0.2)	529 (3)	40.3 (0.2)	37 (0)	70 (2)	378 (1)
P+MU	36.8 (0.3)	150 (2)	16.8 (0.0)	630 (7)	37.4 (0.2)	42 (1)	79 (1)	448 (5)
GA+P	2.1 (0.0)	146 (1)	14.8 (0.1)	542 (3)	43.4 (0.2)	39 (1)	70 (1)	396 (2)
PGA+P	5.5 (0.0)	140 (0)	15.4 (0.1)	538 (2)	40.3 (0.5)	39 (1)	71 (1)	394 (4)
MU+P	23.3 (1.3)	142 (1)	16.3 (0.3)	577 (14)	35.4 (0.4)	39 (2)	74 (1)	401 (5)

[†] Carbon contents of organic matter-treated goethites were corrected for the C in pure goethite (0.9 mg g^{-1}).
[‡] Specific surface area.
[§] Average pore diameter.

5.4.2 Porosity changes

Sorption of phosphate to pure goethite decreased the average micropore diameter from 0.85 to 0.78 nm and the volume of 2-5-nm pores (Table 5.2), indicating that phosphate penetrated into pores <5 nm. The diffusion of phosphate into micropores of goethite and drinking-water treatment residuals has been reported before (Strauss et al., 1997; Makris et al., 2004; Mikutta et al., 2006c). The decrease in volume of small mesopores after phosphate addition might also be explained by an aggregation of goethite crystallites by phosphate (Anderson et al., 1985).

Addition of all organics to pure goethite reduced the pore volume of <5-nm pores (Table 5.2). Microporosity decreased up to 16% in the order PGA < GA << MU, while the mesoporosity of <5-nm pores decreased up to 21% in the order MU < GA = PGA (Table 5.2). These results indicate that all organics partially clogged the pores <5 nm of goethite, i.e., decreased the accessibility of pores to N_2 at 77 K. Decreased micro- and mesopore volumes are in line with studies showing that OM penetrates into mineral pores (Kaiser and Guggenberger, 2003; Mayer et al., 2004; Mikutta et al., 2004; Zimmerman et al., 2004a).

In the presence of phosphate, organic substances decreased the micropore volume up to 22% and <5-nm mesopore volume up to 12% compared with pure phosphated goethite (Table 5.2). Mucigel addition to pure and phosphated goethite increased the volume of mesopores >10 nm and hence, the average pore diameter in these treatments was significantly larger than in the GA and PGA treatments (Table 5.2). Both PGA and MU did not prevent the diffusion of phosphate into micropores, as shown by decreasing micropore volumes after phosphate addition when compared to the treatments without phosphate (Table 5.2).

5.4.3 Effects of GA and PGA on the phosphate desorption kinetics

Treatments 'P+OM'. Figure 5.3 shows the phosphate desorption kinetics of pure and OM-treated goethites. In all cases except from the 'PGA+P' treatment, desorption continued and did not reach an equilibrium within two weeks (Fig. 5.3). While 36% of phosphate sorbed to pure goethite was mobilized within two weeks, 31% and 29% were desorbed from phosphated goethite to which GA or PGA had been added (Fig. 5.3a). Kinetic modeling indicated that a similar fraction of phosphate was rapidly desorbed from GA- and PGA-coated samples compared to pure goethite (Table 5.3, a_0). In contrast, the apparent diffusion constants, $(D/r^2)_{app}$, of GA- and PGA-coated goethites were significantly smaller than that of pure goethite (Table 5.3). This may indicate a successful entrapment of phosphate in goethite pores <5 nm by GA and PGA as suggested by porosity measurements (Table 5.2). However, the volumes of micropores and <5-nm mesopores in PGA-treated samples were much smaller than in the GA treatment and hence, a larger diffusion inhibition would be expected in the PGA treatment. But contrary to this reasoning, the phosphate desorption kinetics were almost identical in both treatments (Fig. 5.3a). Also, a micropore clogging of GA with a subsequent inhibition of phosphate diffusion out of pores <5 nm is unlikely given the low competitiveness of GA with respect to pre-sorbed phosphate (Table 5.2). Therefore, on the basis of small differences in apparent diffusion constants, with unknown radii of diffusion *r* that are probably different in the GA and PGA treatments, an entrapment of phosphate in pores by GA and PGA cannot be concluded without ambiguity.

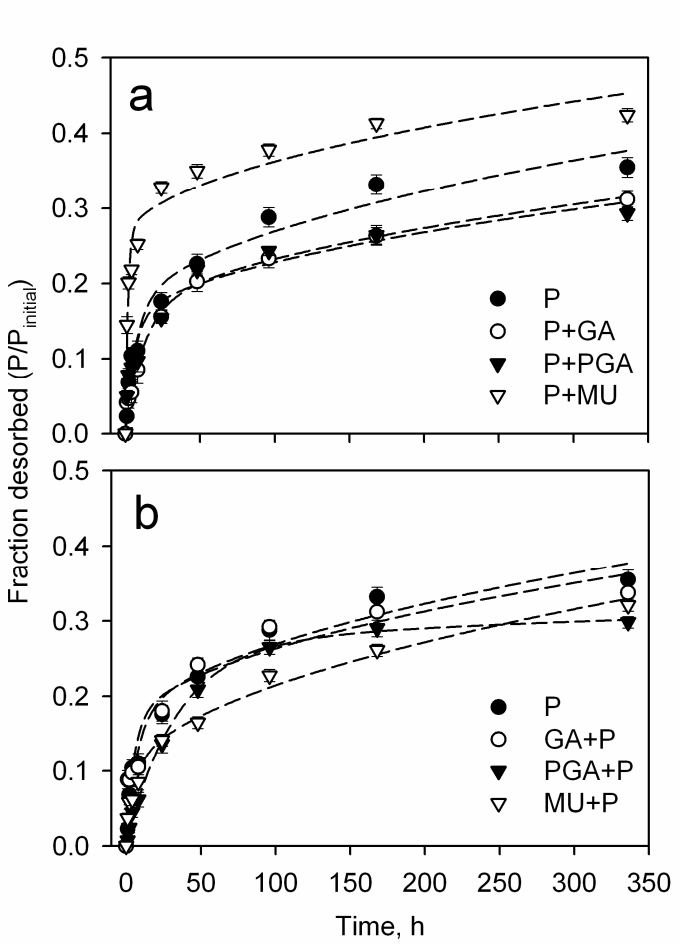

Fig. 5.3. Fractional desorption of phosphate in 0.01 M KNO_3 background electrolyte at pH 5 with a solid concentration of 2 g L^{-1}: (a) OM sorbed to phosphated goethite and (b) phosphate sorbed to OM-treated goethite. Abbreviations used: P, phosphate; GA, galacturonate; PGA, polygalacturonate; MU, mucigel. Sequence of abbreviations indicates the sequence of sorbate addition. Dashed lines are the model fits using Eq.[5.1]. Error bars are given as standard errors of three replicate measurements.

Treatments 'OM+P'. When OM was sorbed to goethite prior to phosphate, the fractional amount of phosphate desorbed after two weeks varied only between 30% and 34% for PGA- and GA-treated goethite, respectively (Fig. 5.3b). The kinetics of phosphate release in the GA treatment was similar to that of pure goethite (Table 5.3).

The desorption of phosphate from PGA-coated goethite showed a near two-fold increase in the fraction of phosphate rapidly desorbed in comparison with the 'P+PGA' treatment (Table 5.3). Although about 86% of the total phosphate desorbed was desorbed by the fast desorption reaction (Table 5.3, 'PGA+P'), the rate constant of the fast desorption *k* was only one-forth of that of the C-free control (Table 5.3). The decreased rate constant *k* might be explained by a collapse of externally sorbed PGA molecules upon drying (Mikutta et al., 2004), leading to a subsequent burial of phosphate by PGA. The increase in the fraction of phosphate rapidly desorbed was coupled with a strong decrease in the rate constant of the slow phosphate desorption and the apparent diffusion constant (Table 5.3), showing that the diffusion resistance for phosphate increased (Table 5.3).

Table 5.3. Amount of phosphate initially present ($P_{initial}$) in the samples, phosphate desorbed after two weeks ($P_{desorbed}$), and parameter estimates obtained by fitting Eq.[5.1] to the phosphate desorption data. Also given is the apparent diffusion constant $(D/r^2)_{app}$ according Eq.[5.2]. Abbreviations used: P, phosphate; GA, galacturonate; PGA, polygalacturonate; MU, mucigel. The sequence of abbreviations indicates the sequence of sorbate addition. Values in parentheses denote standard error.

Treatment	$P_{initial}$ †	$P_{desorbed}$ †	a_0 ‡	k §	b #	$(D/r^2)_{app}$	r^2
	µmol g^{-1}			h^{-1}	x 10^{-3} $h^{-0.5}$	x 10^{-5} h^{-1}	
P-Goethite	312 (3)	111 (4)	0.14 (0.03)	0.13 (0.05)	12.9 (2.2)	4.4 (1.0)	0.98
P+GA	301 (3)	94 (3)	0.13 (0.02)	0.08 (0.02)	9.9 (1.2)	2.6 (0.4)	0.99
P+PGA	291 (3)	85 (3)	0.13 (0.03)	0.16 (0.06)	9.6 (2.1)	2.4 (0.7)	0.96
P+MU	344 (2)	146 (3)	0.25 (0.02)	0.61 (0.15)	10.9 (2.0)	4.2 (1.1)	0.97
GA+P	296 (0)	100 (2)	0.14 (0.04)	0.19 (0.10)	11.9 (3.1)	3.8 (1.4)	0.94
PGA+P	272 (1)	81 (2)	0.26 (0.02)	0.03 (0.00)	2.5 (1.0)	0.22 (0.12)	1.00
MU+P	280 (2)	90 (2)	0.08 (0.01)	0.18 (0.06)	13.8 (1.1)	4.4 (0.5)	0.99

† Corrected for the gravimetric water content (12 ± 1 wt%) as determined with a Quantachrome Autosorb-1 gas sorption system.
‡ Fractional amount of phosphate rapidly desorbed.
§ Rate constant of the fast phosphate desorption.
# Rate constant of the slow phosphate desorption.

This result does not comply with Lang and Kaupenjohann (2003) who reported increased $(D/r^2)_{app}$ values for molybdate desorption from goethites that were pre-incubated with dissolved OM. This inconsistency may be caused by higher C loadings (0.12 and 0.77 mg C m^{-2}) in the study of Lang and Kaupenjohann (2003), and OM differing in structure and reactivity. A decreased $(D/r^2)_{app}$ value in the 'PGA+P' treatment suggests that phosphate diffusion out of goethite pores was impeded by PGA.

Pore clogging by PGA and aggregation of goethite particles may account for differences in the phosphate desorption kinetics of both PGA treatments. However, the volume of micro- and small mesopores were nearly equal in both PGA treatments (Table 5.2). Additionally, the average micropore diameter of the 'PGA+P' and 'P+PGA' treatments decreased similarly from 0.92 nm (PGA-coated goethite) to 0.83 nm, showing that in both treatments phosphate penetrated into micropores. Therefore, our porosity data did not definitely corroborate that pore clogging is the process controlling the phosphate desorption kinetics. This inconsistency might be due to the fact that N_2 porosity data do not reflect the accessibility of pores to phosphate. Additionally, aggregation of goethite crystallites by PGA in the 'PGA+P' treatment might have caused a partial occlusion of sorption sites, thus limiting or preventing the transfer of phosphate and water into aggregates during phosphate sorption prior to in the desorption experiment (Linquist et al., 1997; Gaume et al., 2000). Polygalacturonate is capable of increasing the cohesion of soil particles (Traoré

et al., 2000) and decreasing the wetting rate of soil (Czarnes et al., 2000). Willet et al. (1988) observed the migration of phosphate into aggregates of ferrihydrite with time. Aggregation of ferrihydrite particles by PGA at a similar C loading compared to our 'PGA+P' treatment (~0.03 mg C m^{-2}) decreased the transfer rate of ^{33}P from solution to phosphated ferrihydrite surfaces within aggregates (Gaume et al., 2000). In accordance with these studies, our results suggest that in the 'PGA+P' treatment phosphate was enriched on outer aggregate surfaces, and thus a decreased $(D/r^2)_{app}$ value rather reflects a decreased supply of phosphate from intra-aggregate pores. Following this line of argumentation, the slightly decreased $(D/r^2)_{app}$ values in the 'P+GA' or 'P+PGA' treatments might also be explained by a reduced diffusion of phosphate out of aggregate pores.

5.4.4 Effect of MU on the phosphate desorption kinetics

A significantly larger fraction of phosphate was desorbed in the 'P+MU' treatment compared with pure goethite (42%, Fig. 5.3a). Table 5.3 states the initial P content of the solids used. About 30 µmoles P per gram adsorbent were more present in the 'P+MU' treatment compared with the pure goethite (Table 5.3). The MU contained a large amount of phosphate (Table 5.1, P_{inorg}), which matched the surplus of P present in the MU treatment compared with pure goethite (Table 5.3, $P_{initial}$). Consequently, the MU-bound phosphate likely contributed to the phosphate desorption kinetics and explains the offset of 0.1 in the fraction of phosphate desorbed from MU-treated goethite in relation to pure goethite (Fig. 5.3a). Organic C measurements indicated no net release of C after two weeks of phosphate desorption in this treatment. Therefore, it seems unlikely that organically bound P contributed significantly to the increase in the rate constant and the fraction of the fast desorbing phosphate, respectively (Table 5.3, k, a_0).

In contrast, the rate constant of the slow phosphate desorption, and the apparent diffusion constant of the 'P+MU' treatment did not statistically differ from the C-free control, indicating a similar diffusion resistance for phosphate (Table 5.3, b, $(D/r^2)_{app}$). This result contrasts our N_2 adsorption measurements in that the micropore volume of phosphated goethite was effectively reduced by MU (-17%, Table 5.2).

Also in the 'MU+P' treatment, the slow phosphate desorption kinetics was similar to the C-free control (Table 5.3, b, $(D/r^2)_{app}$). This result again strongly contrasts our N_2 adsorption measurements, showing that in the 'MU+P' treatment the micropore volume was reduced by 22% compared to phosphated goethite (Table 5.2). Therefore, our findings suggest that the slow phosphate mobilization from OM-treated goethite is either not pri-

marily controlled by micropore diffusion, or that reduced micropore volumes measured with N_2 adsorption are only confined to dry samples due to occlusion of mineral surfaces by OM, which is reversible after rehydration.

Comparison of MU with PGA. Figure 5.4 shows SEM images of PGA- and MU-treated goethites with representative EDX spectra. Microaggregates of both treatments differed in their surface morphology, being more 'frayed' in the case of MU. EDX-spectra of MU-treated goethite also supported the presence of layered silicates as indicated by the Al and Si peaks (Fig. 5.4). On a C basis, MU reduced the micro- and small mesopore volume of pure and phosphated goethite far less effectively than PGA (Table 5.2). In accordance, MU affected the kinetics of the slow phosphate desorption less effective than PGA (Table 5.3). Mucigel and PGA showed opposite effects on the phosphate desorption kinetics (Table 5.3). No effects of MU on the slow desorption kinetics of phosphate imply that MU was not as strongly associated with goethite than PGA, and probably existed primarily as a second solid phase.

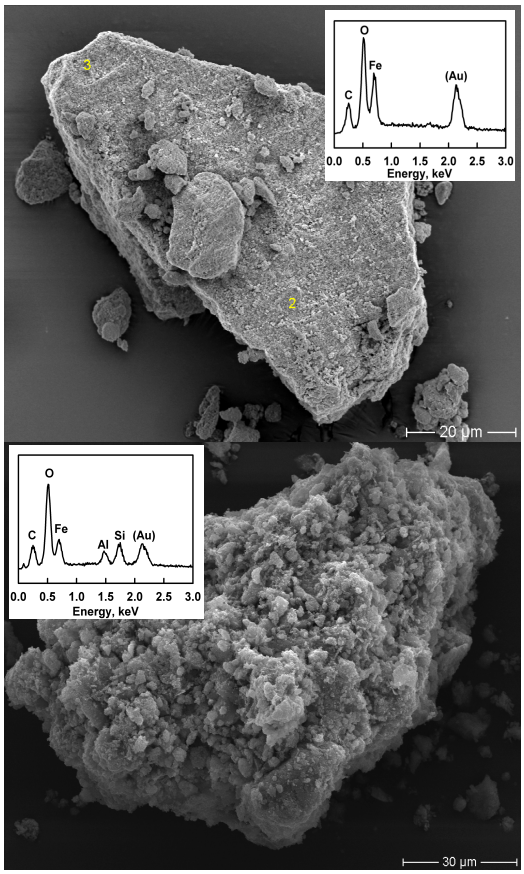

Fig. 5.4. Scanning electron microscopy images of microaggregates of freeze-dried PGA-treated goethite (top) and mucigel-treated goethite (bottom). Insets show representative EDX-spectra of PGA- and MU-treated goethites.

This reasoning is supported by lower affinity of maize mucilage to goethite at pH 5.5 compared with PGA (Grimal et al., 2001) – a circumstance that might have been amplified

in our experiment because of contamination of MU with mineral matter (Fig. 5.2). In addition, the uronic acid content of the MU used was small compared with maize mucilage (Table 5.1). For example, Morel et al. (1986) reported uronic acid contents of 219 mg g^{-1} (dry weight) for maize mucilage from aerial nodal roots of soil-grown maize plants (non-axenic) and 340 mg g^{-1} (dry weight) uronic acid for maize mucilage collected from hydroponic cultures under axenic conditions. Assuming a C content of nodal root mucilage of approx. 39% (Morel et al., 1986), our MU would have an uronic acid content of about 21 mg g^{-1}, which is close to the 30 mg g^{-1} of axenically secreted maize mucilage given by Bacic et al. (1986). Our findings imply (i) that PGA is inappropriate as a model substance for maize mucigel, and (ii) that maize mucilage collected from axenically grown maize seedlings (Watt et al., 1993; Read et al., 1999) or from aerial nodal roots (Morel et al., 1986) may differ by its chemical composition and hence its reactivity from maize mucigel.

5.4.5 Ecological implications

In order to prepare organic coatings on phosphated goethite, we used initial C concentrations of about 125 mg C per gram adsorbent, corresponding to about 71 µmol C m^{-2}. Despite these high C concentrations in solution, both GA and PGA displaced only up to 7% of pre-sorbed phosphate within 12 hours of equilibration, showing the low competitiveness of both compounds (Table 5.2). When organic sorbates were added before phosphate, they inhibited phosphate sorption by only up to 13% (Table 5.3). Compared with low-molecular-weight organic acid anions, the ability of the organics used to impair the sorption of phosphate to goethite at pH 5 was small (Geelhoed et al., 1998; Mikutta et al., 2006c). It is particularly noteworthy that MU was capable of storing large amounts of organic and inorganic P, the latter likely complexed by polyvalent cations (Table 5.1) or molecules possessing anion exchange sites like protonated amino groups. This ‘trapping’ of P by MU might be of environmental importance when phosphate becomes bioavailable due to its rapid desorption (Fig. 5.3a) and organically-bound P is released upon mineralization of MU in the rhizosphere. The ability of complexes between P and Fe or Al bound to OM to contribute to P retention in soils has been documented by several researchers (Appelt et al., 1975; Bloom, 1981; Borie and Zunino, 1983; Gerke and Hermann, 1992; Gerke et al., 1995). In Figure 5.5 we plotted the difference (ΔP, µmol g^{-1}) in the amount of phosphate sorbed (desorbed) between pure and each OM-treated goethite. A comparison of ΔP of phosphate sorption with ΔP of phosphate desorption indicates the net bioavailability of phosphate after one sorption (15 days) and desorption run (14 days). In four out of six

treatments Δ*P* of phosphate sorption and desorption were equal, indicating a zero net effect on the bioavailability of phosphate. Contrary, in the 'PGA+P' and 'MU+P' treatments Δ*P* of phosphate sorption was larger than Δ*P* of phosphate desorption, showing a slightly positive net effect on the bioavailability of phosphate.

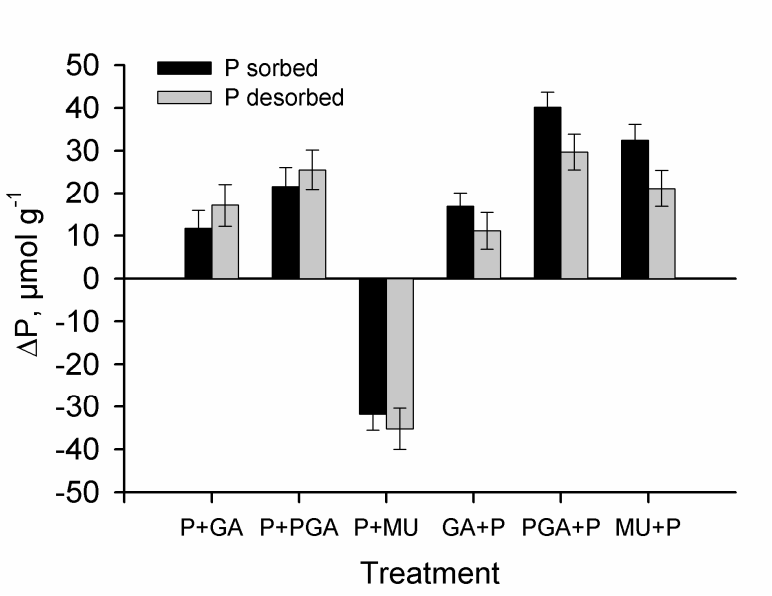

Fig. 5.5. Difference in the amount of phosphate sorbed (15 days) and desorbed (14 days) between pure goethite and OM-treated goethites (Δ*P*). Abbreviations used: P, phosphate; GA, galacturonate; PGA, polygalacturonate; MU, mucigel. Sequence of abbreviations indicates the sequence of sorbate addition. Error bars denote standard error.

5.5 Conclusions

The order of PGA and phosphate addition significantly affected the fraction of phosphate that was desorbed by the fast and slow desorption reaction. This phenomenon can be explained by pore clogging and aggregation. The release kinetics of phosphate in MU-treated goethite samples was contrary to that of PGA, which is ascribed to its differing chemical composition. Our results indicate that in contrast to PGA, MU has to be treated as a separate phase rather than a coating of the mineral. Accordingly, PGA seems inappropriate as a model substance for maize MU collected from sand cultures under non-axenic conditions. An entrapment of phosphate in <5-nm pores of goethite could not be verified without ambiguity, when organic matter was added to goethite after phosphate. We conclude that due to the high competitiveness of phosphate under the experimental conditions chosen (I = 0.01 M, pH 5, C loadings ≤21 µmol m^{-2}), the net effects of root exudates on the bioavailability of phosphate are small.

6 Restructuring of polygalacturonate on alumina upon hydration – Effect on phosphate sorption kinetics

Christian Mikutta[1], Jaane Krüger[1], Gabriele Schaumann[2], Friederike Lang[1]

Accepted for publication in Geochimica et Cosmochimica Acta

[1] Department of Soil Science, Institute of Ecology, Berlin University of Technology, Salzufer 12, D-10587 Berlin, Germany

[2] Department of Environmental Chemistry, Institute of Environmental Technology, Berlin University of Technology, Straße des 17. Juni 135, D-10623 Berlin, Germany

6.1 Abstract

Hydration of organic coatings in soils is expected to affect the immobilization of oxyanions by Fe and Al oxides. We hypothesized that the hydration of polygalacturonate (PGA) coatings on alumina (Al_2O_3) increases their permeability for phosphate. Pure and PGA-coated alumina were equilibrated in deionized water for two and 170 hours at pH 5 and 20°C before studying (i) their porosity with N_2 gas adsorption and ^{1}H-NMR relaxometry, (ii) structural changes of PGA-coatings with differential scanning calorimetry (DSC), and (iii) the kinetics of phosphate sorption and PGA desorption in batch experiments. Scanning electron micrographs revealed that PGA molecules formed three-dimensional networks with pores ranging in size from <10 to several hundred nanometers. Our NMR results showed that the water content of intraparticle alumina pores decreased upon PGA sorption, indicating a displacement of pore water by PGA. The amount of water in interparticle alumina pores increased strongly after PGA addition, however, and was attributed to water in pores of PGA and/or in pores at the PGA-alumina interface. The flexibility of PGA molecules and the fraction of a PGA gel phase increased within one week of hydration, implying restructuring of PGA. Hydration of PGA coatings increased the amount of instantaneously sorbed phosphate by 84%, showing that restructuring of PGA enhanced the accessibility of phosphate to external alumina surfaces. Despite the fact that the efficacy of phosphate to displace PGA was higher after 170 hours than after two hours, a higher phosphate surface loading was required after 170 hours to set off PGA desorption. Our findings imply that the number of PGA chain segments directly attached to the alumina surface decreased with time. We conclude that hydration/dehydration of polymeric surface coatings affects the sorption kinetics of oxyanions, and may thus control the sorption and transport of solutes in soils.

6.2 Introduction

In soils and sediments, minerals are partially covered with organic matter (Heil and Sposito, 1995; Ransom et al., 1997; Mayer and Xing, 2001; Kaiser and Guggenberger, 2003; Gerin et al., 2003). Under field and laboratory conditions, organic matter is subjected to moisture fluctuations that may change its physico-chemical properties due to interaction with water molecules (LeBoeuf and Weber, 2000; Schaumann 2005; Schaumann et al., 2000; Schaumann and LeBoeuf, 2005). Hydration-induced changes in the macromolecules' mobility (Schaumann and LeBoeuf, 2005) may affect the retention of nutrients and pollutants by minerals coated with organic matter. The ability of soils and soil organic matter to sorb or release organic pollutants has been shown to depend on the state of hydration, hydration time, wetting and drying cycles and the water content of the samples (Gaillardon, 1996; Johnson et al., 1999; Altfelder et al., 1999; Schaumann et al., 2004). In addition, the structure of organic matter can be affected by the dehydration technique applied in the laboratory, e.g., prior to sorption experiments (Altfelder et al., 1999). For example, structural changes of organic matter upon freeze-drying have been reported (Wedlock et al., 1983; Jouppila and Roos, 1997; Allison et al., 1998; Souillac et al., 2002). The hydration/dehydration-induced change of molecular structures of organic matter is therefore expected to affect the transport of solutes like hydrophobic pollutants through organic matter of soils and sediments (Brusseau and Rao, 1989; Pignatello and Xing, 1996; Cornelissen et al., 1998).

It has been suggested that soil organic matter (SOM) consists of rubbery (more flexible) and glassy (less flexible) domains (LeBoeuf and Weber, 1997) as known for synthetic polymers. The glass transition temperature, T_g, marks the temperature at which a glassy matrix becomes rubbery (Young and Lovell, 1991), and is a function of the side chain mobility in macromolecules. Usually, the incorporation of water molecules into the polymeric framework of isolated humic substances, soil and peat samples upon hydration reduces T_g, i.e., plasticizes polymer matrices (LeBoeuf and Weber, 1997; Schaumann and Antelmann, 2000; Schaumann and LeBoeuf, 2005).

It has been found by differential scanning calorimetry (DSC) and ^{1}H-NMR-relaxometry analyses that peat or humus-rich soil samples exhibit first-order swelling kinetics upon hydration with time constants of up to six days (Schaumann et al. 2004, 2005; Schaumann and LeBoeuf, 2005). Changes in proton relaxation times upon swelling of organic matter depend on the pore size distribution initially present in organic samples and on the quality of the organic material studied (Schaumann et al., 2004): While swelling of

starch led to an increase in proton relaxation times, swelling of semolina or organic matter in peat and soil samples generally reduced the relaxation times (Schaumann et al., 2004, 2005). These effects were interpreted as an increase in intraparticle pore size and a decrease in interparticle pore size of organic matter upon water absorption (Schaumann et al., 2004, 2005).

Swelling of mineral-associated polymers through the incorporation of water molecules into the polymer structure might affect the sorption of oxyanions like phosphate or arsenate to Fe and Al oxides. An increase in intraparticle pore size of organic matter voids upon swelling of organic matter in conjunction with an increased mobility of polymer chains upon hydration might facilitate the Brownian motion and Fickian diffusion through more flexible (rubbery) polymer domains and hence favor the fast sorption of oxyanions. Contrary, a decrease in interparticle pore size of sorbed organic matter upon swelling might reduce the accessibility of mineral surfaces to oxyanions.

The objective of this study was therefore to test whether the slow swelling of polymers sorbed to Fe and Al oxides affects phosphate sorption kinetics. Specifically, we hypothesized that the hydration of polygalacturonate (PGA) coatings on alumina (Al_2O_3) increases their permeability for phosphate. We used PGA as a well-defined model substance for the gelatinous mucilage covering the root apices of many plant species (Knee et al., 2001). Mucilage exuded by plant's root caps is confined to the soil-root interface because mucilage components diffuse very slowly into the soil (Rovira, 1969; Sealey et al., 1995). Mucilage of maize plants consists of 90-95% polysaccharides with about 20-35% of uronic acids (Cortez and Billes, 1982; Morel et al., 1986), and is susceptible to swelling due to water absorption (e.g. Guinel and McCully, 1986). At the soil-root interface the cycling of nutrients is therefore likely to be influenced by the state of hydration of organic coatings made up of macromolecular root exudates.

6.3 Materials and Methods

We used alumina as a non-paramagnetic high-surface-area model adsorbent that could be used for ^{1}H-NMR measurements. Pure and PGA-coated alumina samples were saturated in doubly deionized water at pH 5 for two and 170 hours. After each equilibration time, phosphate sorption experiments were performed. Similarly, changes in pore size distribution were then monitored with ^{1}H-NMR relaxometry and N_2 gas adsorption at 77 K. Differential scanning calorimetry (DSC) was used to identify changes in the molecular structure of sorbed PGA molecules upon hydration for two and 170 hours, respectively.

6.3.1 Preparation of organic coatings

The activated, weakly acid alumina (type 506-C-I) was purchased from Aldrich (Sigma-Aldrich Chemie GmbH). The mesoporous alumina had a particle size of 150 mesh (<105 µm) and an average pore size of 5.8 nm (Aldrich). Polygalacturonic acid (P81325, $(C_6H_8O_6)_n$, >95%, M = 25-50 kDa) was purchased from Fluka (Sigma-Aldrich Chemie GmbH) and comprised 37.2 % C and 0.05% N (Elementar Vario EIII C/N/S Analyzer). The PGA contained negligible amounts of polyvalent cations with Ca being the most dominant with 5.7 mmol kg^{-1}. The content of paramagnetic Mn and Fe species was below 0.3 mmol kg^{-1}. Polygalacturonate solutions were prepared by dissolving polygalacturonic acid in 0.01 M KNO_3 solutions with the addition of 10 µL 1 M KOH mg^{-1} PGA. Afterwards, the pH of the solutions was adjusted to pH 5 using 0.01 M HNO_3 without any visible flocculation occurring.

We followed a standardized procedure in order to prepare PGA coatings on alumina prior to our ^{1}H-NMR, DSC and phosphate sorption experiments. This procedure ensured comparability between experimental results of different methodologies.

To disperse alumina and hydrate adsorption sites, 7.5 g alumina were weighed into a 1-L PE bottle and shaken in 10 mL 0.01 M KNO_3 background electrolyte (pH 5) for 24 hours on a reciprocating shaker (85 rev min^{-1}). Subsequently, either 990 mL of 0.01 M KNO_3 solution containing 1515 mg PGA-C L^{-1} (pH 5) or 990 mL of background electrolyte solution (pH 5) were added. The PGA solution also contained 5 µM $AgNO_3$ to impair microbial activity. The pH was maintained at 5 ± 0.02 using dilute HNO_3. After 24 hours the suspension was repetitively centrifuged at 5,500 x g for 20 min and washed with 500 mL doubly deionized water until the total organic C (TOC) concentration in the supernatant solution of PGA-treated alumina was negligible (<5 mg C L^{-1}, Shimadzu TOC-5050A Autoanalyzer). After determination of the gravimetric water content, the samples were instantaneously used for subsequent analyses (^{1}H-NMR, DSC, phosphate sorption). In all experiments, the gravimetric water content of pure and PGA-coated alumina was 42 ± 1% and 60 ± 1%, respectively. Because the water content is a crucial parameter in the DSC analysis and highly variable at small scale, we additionally determined the water content of the individual samples used for DSC analysis (see section 6.3.4). A part of the pure and PGA-coated alumina was freeze-dried for total organic C determinations and N_2 adsorption measurements. Freeze-drying was accomplished after freezing the samples at -80°C in an Christ alpha 2-4 freeze drier (Osterode, Germany). In addition, the freeze-dried

samples were examined by scanning electron microscopy (Hitachi S-4000) after the samples had been surface sputtered with Au (~5 nm Au layer thickness).

To test the influence of hydration time on porosity, organic matter quality, and phosphate sorption, samples were stored (non-agitated) in the dark at 20°C at pH 5 for two and 170 hours, respectively.

6.3.2 Nitrogen adsorption

Specific surface area (*SSA*) and porosity were determined with a Quantachrome Autosorb-1 automated gas sorption system (Quantachrome, Syosset, NY). Approximately 100 mg pure and PGA-coated alumina were degassed until the increase of pressure rate by vapor evolution was below about 1.3 Pa min^{-1} within a 0.5-min test interval. Helium was used as a backfill gas. We used 79-point N_2 adsorption and desorption isotherms from 1.0×10^{-5} to 0.995 P/P_0. Specific surface area was calculated from the BET equation (Brunauer et al., 1938). Micropore (<2 nm) volume and average micropore diameter were determined according to the Dubinin-Radushkevic method (Gregg and Sing, 1982). The mesopore (2-50 nm) size distribution was calculated from the adsorption leg using the BJH method (Barrett et al., 1951). Total pore volume was taken at 0.995 P/P_0 and the average pore diameter was calculated as $D_p = 4V_{liq}/SSA$, where V_{liq} is the volume of liquid N_2 contained in pores at 0.995 P/P_0, and *SSA* is the BET surface area. All isotherms were recorded in triplicate.

6.3.3 ^{1}H-NMR Relaxometry

We used ^{1}H-NMR relaxometry to determine changes in pore size distribution of water-saturated pure and PGA-coated alumina samples. The principle of ^{1}H-NMR relaxometry has been described elsewhere (Kenyon, 1992, 1997; Schaumann et al., 2004, 2005). Triplicate samples of moist pure and PGA-coated alumina (~20 g) were weighed into 50-mL centrifuge tubes (Nalgene, polypropylene). The gravimetric water content of pure and PGA-coated alumina was 42 ± 1% and 60 ± 1%, respectively. The samples were allowed to equilibrate in a climate-controlled room at 20°C. The ^{1}H-NMR relaxation experiments were performed two and 170 hours after PGA sorption. The measurements were conducted on a 2 MHz relaxometer at a magnetic flux density of 0.047 T (Maran 2, Resonance Instruments, U.K.). We used the Carr-Purcell-Meiboom-Gill (CPMG, 90°-τ-180°) pulse sequence with 4096 recorded echoes, a 150-µs echo spacing τ and a 1.2-s delay time. The scans were stacked 512 times. Provided that (i) water protons in porous media are in the

fast diffusion limit (Brownstein and Tarr, 1979) and (ii) relaxation coming from the presence of paramagnetic materials is negligible, the transversal relaxation time constant T_2 is related to the relaxation time constant of the bulk water, the transversal surface relaxivity, and the pore size (Kenyon, 1992, 1997; Hinedi et al., 1997; Straley et al., 1997):

$$1/T_2 = 1/T_{2b} + \rho_2 SA/V = 1/T_{2b} + \rho_2 m/D_p, \quad [6.1]$$

where T_2 is the measured transversal relaxation time constant of water in a porous medium (s), T_{2b} is the bulk relaxation time constant of water at infinite distance from the pore walls (s), m is a shape factor, which is 4 assuming cylindrical pore geometry (Hinedi et al., 1997), D_p is the pore size (m), ρ_2 is the transversal surface relaxivity that parameterizes the strength of the surface relaxation (m s^{-1}), SA is the internal surface area (m^2), V is the volume of water contained in pores of the sample (m^3).

Using the inverse algorithm implemented in the WinDXP software package (Resonance Instruments Ltd., UK), we fitted the magnetization decay curves with a sum of exponential decay curves using 128 time constants between 0.1 and 6000 ms to calculate robust T_2 distributions. To ensure comparability between pure and PGA-coated alumina, the T_2 time constant distributions of each adsorbent were normalized to the mass of alumina present in the sample. This was done because in the PGA-coated alumina samples 31% less water-filled alumina pores were present compared to the pure alumina samples. Additionally, the relaxation decays, $M(t)$, monitored during application of the CPMG pulse sequence were normalized to their amplitude and fitted to a sum of three exponential decay functions:

$$M(t) = F_1 \exp(-t/T_{2-1}) + F_2 \exp(-t/T_{2-2}) + F_3 \exp(-t/T_{2-3}), \quad [6.2]$$

where F_i is the fraction of water held in the i-th pore domain, and T_{2-i} are the respective transversal relaxation time constants (s) of water relaxing in the i-th pore water domain, and t is time (s). Coefficients of determination of the fits were always ≥0.99. The transversal surface relaxivity ρ_2 was calculated from Eq.[6.1] for adsorbents that were equilibrated in water for two hours. We used ρ_2 to scale T_2 time constants to pore size assuming a cylindrical pore geometry. We calculated T_2 in Eq.[6.1] as the mean time constant of the three-exponential fit (Eq.[6.2]) obtained after weighing each time constant by its fraction

F_i. The bulk relaxation time T_{2b} of water is usually around 2.5 s and can thus be neglected to calculate ρ_2 from Eq.[6.1].

6.3.4 Differential scanning calorimetry

In order to characterize the state of water in PGA-coated alumina samples, we studied the freezing and melting of water using DSC analysis. Triplicate or quadruplicate samples of PGA-coated alumina (5-10 mg) that had been equilibrated for two and 170 hours at 20°C were weighed into standard Al pans, which were sealed hermetically prior to the DSC experiment. Differential scanning calorimetry experiments were performed with a DSC Q1000 (TA Instruments, Germany). The samples were abruptly cooled in the DSC instrument to -80°C and then heated with 10 K min^{-1} from -80°C to 110°C, followed by a second abrupt cooling and subsequent heating cycle. In the cooling cycles, the freezing temperature (-20°C) was reached within a maximum of 10 min, and the low temperature limit (-80°C) was reached within 20 min. Nitrogen was employed as a purge gas. Baseline was corrected with the TZero technology® by TA instruments.

DSC data were analyzed using Universal Analysis software Version 4.1 (TA Instruments). The glass transition is indicated by an inflection point in the thermogram. Operationally, three tangent lines were applied for the evaluation, and the glass transition temperature (T_g) is defined as the temperature at the half-width of the central tangent line. The change of heat capacity (ΔC_p, J g^{-1} K^{-1}) was calculated from the height of the central tangent line. The amount of freezable and non-freezable water was determined by analyzing the endothermic melting peak between -11°C and 27°C. The transformation energy E (J g^{-1}) due to melting was calculated by integration of the peak using a linear baseline, and compared with the differential heat of fusion for free water (H_{fus} = 333.5 J g^{-1}, Ping et al., 2001) to estimate the amount of freezable and non-freezable water. Standard errors of freezable and non-freezable water were calculated from the standard error of the transformation energy E and the gravimetric water content of the samples, respectively. In order to determine the gravimetric water content of each individual sample, the Al pans were perforated after DSC analysis and dried at 105°C for six hours. The water content was then calculated from the weight difference before DSC measurement and after drying.

To calculate the means of T_g and ΔC_p, each subsample was analyzed eight times in order to minimize the nonsystematic error of data evaluation. The means of the glass transition temperature T_g, change in heat capacity ΔC_p, freezable and non-freezable water obtained for the two different equilibration times were compared using the unpaired t-test.

6.3.5 Phosphate sorption kinetics

Triplicate water-saturated samples with a mass equivalent to 0.625 g (dry weight) of pure or PGA-coated alumina were weighed into 2-L HD-PE bottles that were coated with Al-foil to exclude light. Subsequently, 250 mL of background electrolyte (0.01 M KNO_3, pH 5) were added before the samples were shaken on a horizontal shaker for one hour at 150 rev min^{-1}. After pre-equilibration of the adsorbents, 1 L of background electrolyte solution was added containing 500 µM phosphate (as KH_2PO_4 p.a., Merck) and 5 µM $AgNO_3$ to impair microbial activity. The final phosphate concentration amounted to 400 µM. The pH was manually maintained at 5 ± 0.05 using dilute HNO_3 or KOH. After 0.5, 1, 2, 4, 8, 24, 48, 120, 144 and 168 hours a 10-mL aliquot was removed from each sample and 0.45-µm membrane filtered (polyethersulfone, Pall Life Science Supor®-450). The desorption of PGA-C was assessed by measuring total organic C in the 0.45-µm filtrates (Shimadzu TOC-5050A Autoanalyzer). A 2.5-mL aliquot of the 0.45-µm filtrate was ultracentrifuged at 440,000 x g for one hour and phosphate was measured photometrically at 710 nm in the supernatant using the ascorbic-molybdenum blue method of Murphy and Riley (1962). The analytical precision of the photometric determination of phosphate was <1%. Subsample variability was generally <1.5%. Preliminary tests showed that matrix interferences of phosphate with polyvalent cations bound in the PGA structure did not occur during ultracentrifugation, i.e., phosphate concentrations in solution did not decrease due to sedimentation of PGA during ultracentrifugation.

The amount of phosphate sorbed was corrected for the water content of the samples (13 ± 1%), which was determined by outgassing the samples in an automated Autosorb-1 gas sorption system (Quantachrome, Syosset, NY) until the rate of pressure increase due to vapor evolution was below about 1.3 Pa min^{-1} within a 0.5-min test interval. Outgassing at elevated temperature was not performed in order to avoid thermal transformation of PGA or the loss of chemisorbed water.

The phosphate sorption data were fitted with a linear combination of a modified first-order rate equation and the parabolic rate law (Crank, 1976) in order to account for the fast sorption to external alumina surfaces and the slow diffusion-controlled sorption of phosphate to alumina (Lang and Kaupenjohann, 2003; Mikutta et al., 2006a-c):

$$q_t = c_m\text{-}a_0\, e^{-kt} + bt^{0.5}, \qquad [6.3]$$

where q_t is the amount of phosphate sorbed at time t (µmol g^{-1}), c_m is the maximum amount of phosphate sorbed by the fast reaction (µmol g^{-1}), (c_m-a_0) is the amount of phosphate

operationally defined as 'sorbed instantaneously' (µmol g^{-1}), i.e., at times <<0.5 hours, k is the rate constant of the fast phosphate sorption (h^{-1}), t is time (h), and b is the apparent rate constant of the slow sorption (µmol g^{-1} $h^{-0.5}$). The parameters c_m, a_0, k and b were determined by minimizing the sum of the squared differences between the observed and predicted values of the phosphate sorption data using the Marquardt-Levenberg algorithm implemented in SigmaPlot 7.0 for Windows (SPSS Inc.).

The rate constant of the slow phosphate sorption, b, is related to the apparent diffusion constant $(D/r^2)_{app}$ (h^{-1}):

$$b = 4q_\infty \pi^{0.5} (D/r^2)_{app}^{0.5}, \qquad [6.4]$$

where q_∞ is the amount of phosphate diffused at infinite time (µmol g^{-1}), D is the apparent diffusion coefficient (m^2 h^{-1}), and r is the radius of diffusion (m). We used the total amount of phosphate present at t = 0 hours (µmol g^{-1}) corrected for the total amount of phosphate sorbed to external surfaces (c_m) as an approximation for q_∞ in Eq.[6.4] to calculate the apparent diffusion constant $(D/r^2)_{app}$.

6.4 Results and Discussion

6.4.1 SEM Analysis

Figure 6.1 depicts SEM images of pure and PGA-coated alumina. Particles of the pure oxide possessed feather-edged structures that, when further resolved, showed a cauliflower-like surface microtopography with pore entrances of about 5 nm (image 5). The cauliflower-like surface structure shown in the high-resolution SEM image 5 (Fig. 6.1) is likely due to Au isles formed during sputtering. Similar structures have been observed on surfaces of layer silicates like pyrophyllite or vermiculite (not shown). Coatings of PGA greatly modified the microtopographical features of alumina. They comprised dense networks on external alumina surfaces that 'smoothed' the sharp edges of particle surfaces. Images 6-8 of Fig. 6.1 reveal that PGA polymers formed three-dimensional networks of interlacing fibrils having a length of up to several hundreds of nanometers. Aggregation of several PGA chains to larger fibrils in aqueous solution has been deduced from molecular dynamics calculations (Manunza et al., 1997). The nesting of PGA fibrils that existed as simple or multiple strands created new pores; the size of which varied considerably, ranging from less than 10 nm to several hundred nanometers (image 7 and 8). Similar structures

have been reported for Ca-polygalacturonate coatings on garlic roots (Gessa and Deiana, 1992).

6.4.2 Porosity changes upon hydration

The C contents of PGA-coated alumina were stable upon equilibration in doubly deionized water for one week, showing that microbial activity was effectively reduced (Table 6.1). Porosity data obtained by N_2 gas adsorption at 77 K are presented in Table 6.1 and Figure 6.2. Data in Table 6.1 indicate that PGA sorption to alumina hardly affected specific surface area, total pore volume, and micropore volume.

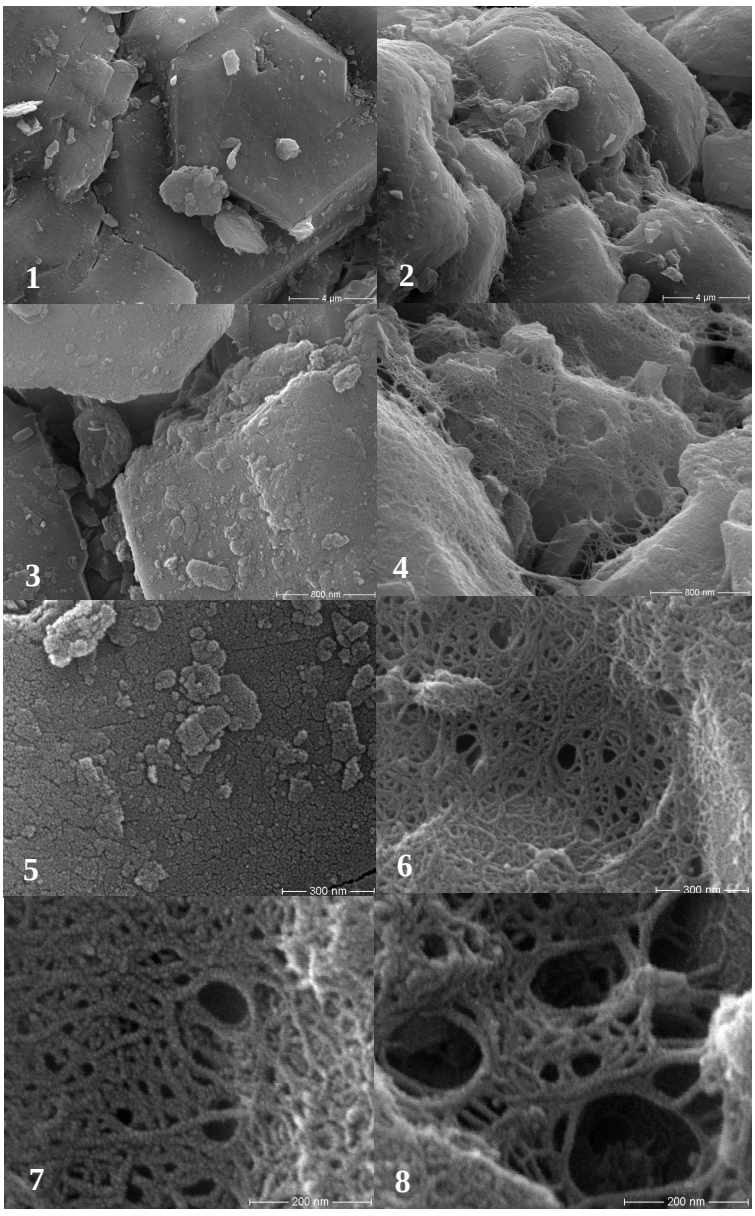

Fig. 6.1. Scanning electron microscopy images of pure (1, 3, 5) and PGA-coated alumina (2, 4, 6-8). The magnification of these images was x 7000 (1+2), x 40,000 (3+4), x 100,000 (5+6), and x 200,000 (7+8). Note that images 1-6 allow a direct comparison between pure and PGA-coated alumina. Images were obtained under ultra-high vacuum.

Table 6.1. Carbon content, specific surface area (*SSA*) and pore characteristics of pure and PGA-coated alumina as determined with N_2 adsorption at 77 K. Carbon contents are given as means obtained from C contents in the samples used for each experiment conducted (NMR, DSC, phosphate sorption). Values in parentheses are given as standard errors.

Treatment	Time elapsed before Analysis	C content	SSA	Total Pore Volume	D_p †	Micropore Volume	Average Micropore Diameter
	h	mg g^{-1}	m^2 g^{-1}	mm^3 g^{-1}	nm	mm^3 g^{-1}	nm
Al_2O_3	2	1.0 (0.1)	212 (2)	290 (5)	5.5 (0.1)	62 (1)	0.97 (0.01)
	170	0.8 (0.1)	215 (2)	293 (3)	5.5 (0.1)	65 (0)	0.97 (0.00)
Al_2O_3+PGA	2	8.3 (0.6)	207 (1)	282 (1)	5.4 (0.1)	60 (1)	0.95 (0.00)
	170	8.4 (0.6)	213 (2)	275 (0)	5.2 (0.0)	63 (0)	0.93 (0.01)

† Avererage pore diameter.

The BJH pore size distributions of both adsorbents obtained after equilibration in water for two and 170 hours showed a monomodal distribution with a large peak at ~3 nm (Fig. 6.2). Judged on the pore size distribution of freeze-dried samples, no obvious difference existed between either pure and PGA-coated alumina and samples that had been equilibrated for two and 170 hours, respectively (Fig. 6.2).

Complementary to the BJH pore size distribution of freeze-dried samples, Fig. 6.3 depicts the time constant distribution of water-saturated samples obtained from NMR relaxometry experiments. Each peak in Fig. 6.3 reflects a pore water domain or state of water binding in pores of varying size. The intensities are proportional to the amount of protons of water molecules relaxing with a defined time constant. The time constants of pure and PGA-coated alumina samples showed a bimodal distribution as identified from the magnetization decay curves using the regularization technique implemented in WinDXP software. Accordingly, one peak belonged to time constants <10 ms. The maximum of the major peak occurred between 55 ms and 100 ms for both adsorbents.

We calculated the mean transversal surface relaxivity ρ_2 for pure and PGA-coated alumina in order to assign peaks in Fig. 6.3 to either intra- or interparticle pores. The mean transversal surface relaxivity ρ_2 was 0.125 ± 0.011 nm ms^{-1} for pure alumina, and 0.169 ± 0.057 nm ms^{-1} for PGA-coated alumina (mean ± standard error). The ρ_2 parameters are at the lower end of published values. For example, D'Orazio et al. (1989) found values between 0.11-1.09 nm ms^{-1} for porous silica glass, and Mikutta et al. (2004) obtained 0.363 nm ms^{-1} for a hydrous Al oxide (γ-AlOOH). Differences in surface relaxivity among different types of minerals are mainly caused by differing physico-chemical properties of the materials (Hinedi et al., 1993). Based on ρ_2, a time constant of 10 ms (approximately middle between both peaks in Fig. 6.3) is equivalent to a pore size of about 5 nm assuming

a cylindrical pore geometry. Therefore, the <10-nm peaks in Fig. 6.3 accord well with the pore size maximum of the BJH pore size distributions (Fig. 6.2), and can be attributed to intraparticle porosity. The 55-100-ms peaks are consequently attributed to water held in interparticle voids.

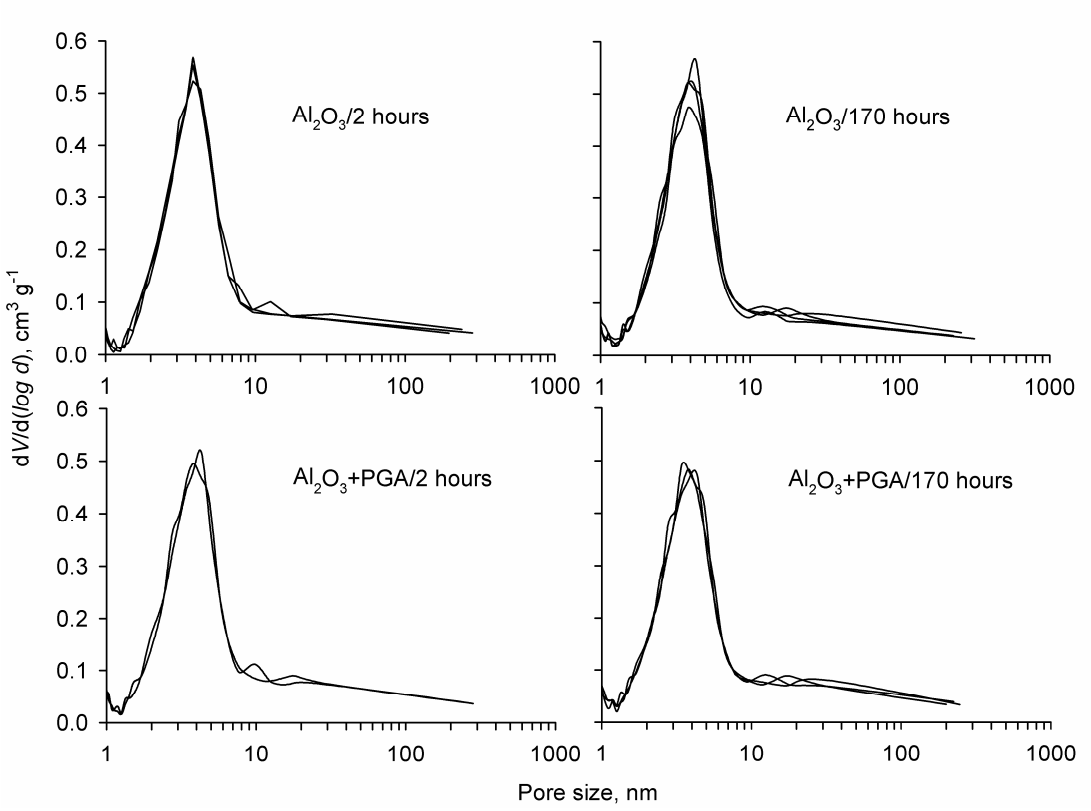

Fig. 6.2. Pore size distribution derived from the N_2 adsorption isotherm according to the BJH model (Barrett et al., 1951) of pure and PGA-coated alumina determined after two and 170 hours of equilibration in doubly deionized water at 20°C and pH 5. Before the N_2 adsorption measurements, the samples were frozen at -80°C and freeze-dried. Note the log-scale of the x-axis.

Figure 6.3 shows that PGA sorption caused a redistribution of water in alumina samples; the amount of water held in intraparticle pores decreased concomitantly with an increase in the intensity of water held in larger pores. The decrease in water held in intraparticle alumina pores due to PGA sorption is shown by a statistically significant decrease in the sum of intensities below the <10-nm peaks of pure alumina after PGA sorption, independent of the equilibration time of the samples in water (Fig. 6.3, unpaired *t*-test, $P < 0.01$). We attribute the decrease in water content held in intraparticle pores to the displacement of pore water by PGA molecules. The incorporation of low- and high-molecular-weight amino acids into mesopores of silica and alumina has been proposed by Zimmerman et al. (2004a, b). However, pore size changes upon sorption of PGA to alumina were hardly detectable when samples were freeze-dried (Fig. 6.2). For PGA-coated samples, the 55-100-ms peaks consist of a mixture of mineral interparticle pores and pores

created by PGA coatings. It should be noted that under moist conditions, PGA does probably not contain pores according to IUPAC nomenclature, i.e., cavities of porous solids that are deeper than wide (Rouquerol et al., 1994). Rather, PGA 'pores' represent interspaces between single PGA strands. The increase in peak amplitude of the 55-100-nm peak upon PGA-sorption (Fig. 6.3) could be solely attributed to PGA pores when a water content of PGA coatings of ≥98 wt% is assumed. In the presence of free water, root-cap mucilage can have water contents of up to 100,000% of its dry weight (Guinel and McCully, 1986).

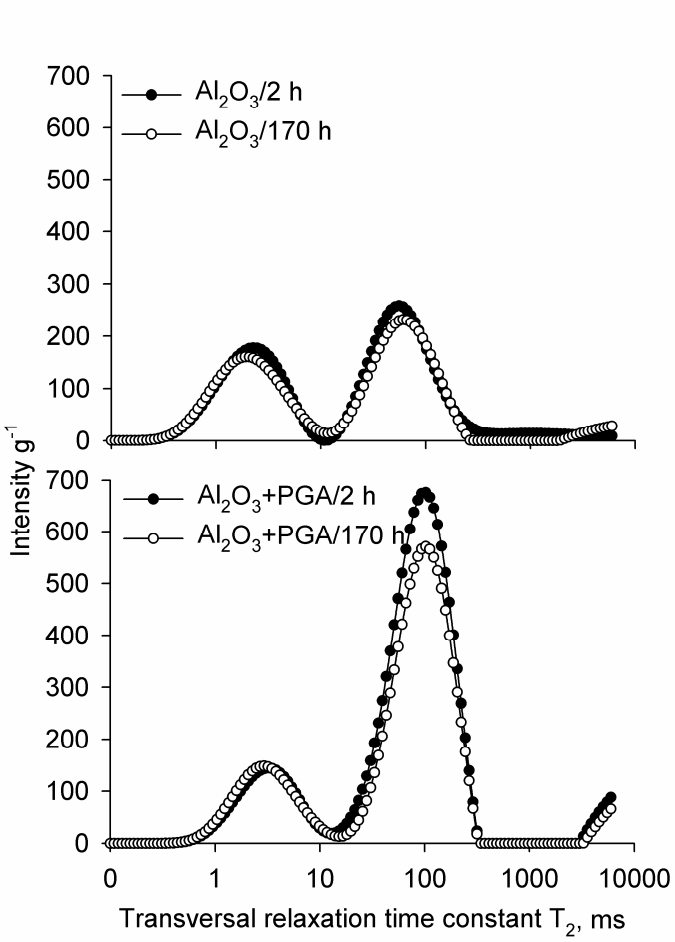

Fig. 6.3. Transversal relaxation time constant (T_2) distributions of pure and PGA-coated alumina obtained after two and 170 hours of equilibration in doubly deionized water at 20°C and pH 5. For the sake of clarity only the results of one replicate sample are presented. Differences in peak amplitudes among replicate samples shown are not statistically significant at $P = 0.05$. Relaxation time constant distributions were highly reproducible in replicate samples of each treatment (not shown). The distributions were normalized to the mass of alumina in the samples. Note the log-scale of the x-axis.

However, the water content reported for pure hydrogels is usually smaller than 98 wt% (Bajpai and Singh, 2006; Léveseque et al., 2005; Ruiz-Cabrera et. al., 2005). Therefore, the difference between the major peak of pure and PGA-coated alumina samples (Fig. 6.3) is attributed to PGA pores and pores located at the PGA-alumina interface.

Our NMR results point at no significant porosity changes with time in moist PGA-coated alumina samples (Fig. 6.3), and thus accord with the N_2 adsorption results (Table 6.1, Fig. 6.2). Pores of PGA with widths of less than 100 nm (Fig. 6.1) were not detectable by N_2 adsorption at 77 K (Fig. 6.2) although they probably contributed significantly to the increase in amplitude of the 55-100-nm peak of PGA-coated alumina (Fig. 6.3). Dehydration of PGA-coatings upon freeze-drying probably led to conditions where the volume between interlacing PGA fibrils adds insignificantly to the total N_2-porosity of alumina particles. Because the distribution of water in a sample is a prerequisite for solute transport from the bulk water phase into intraparticle pores, porosities obtained on dehydrated organic matter-coated specimens using gas adsorption may not adequately reflect the 'effective' pore size distribution.

6.4.3 Differential scanning calorimetry

Figure 6.4 shows representative DSC thermograms of the PGA-coated alumina after two and 170 hours of equilibration in water, respectively. Both thermograms are comparable in shape and show a step transition between -50°C and -20°C followed by an endothermic peak with a maximum between 4°C and 6°C. In accordance to findings for gelatine gels (Nishinari et al., 1997), starch gels (Tananuwong and Reid, 2004) and water-gellan systems (Hatakeyama et al., 1999), we interpret the step transition as glass transition of the solidified amorphous gel matrix, and the endotherm was attributed to melting of frozen water.

The shape of DSC thermograms of hydrogels is generally explained as follows: Various kinds of hydrogels form glassy matrixes by quenching to low temperatures (Nishinari et al., 1997). During cooling of hydrogels, ice crystallization can occur only before the matrix becomes glassy. A part of the water molecules associated closely with the polymers solidifies in an amorphous state (Nishinari et al., 1997). The system is then separated into an ice phase and an unfrozen phase, which results in many small, discrete ice crystals embedded in a continuous, rubbery phase of freeze-concentrated polymer and unfrozen water. At a sufficiently low temperature, this unfrozen phase solidifies into a glassy state, and ice formation ceases because of kinetic restrictions, although a certain amount of water still remains unfrozen. The unfrozen water in the amorphous phase has been proposed to be associated in some way closely with the solute molecules, although it may not totally be immobilized or "bound" (Tananuwong and Reid, 2004).

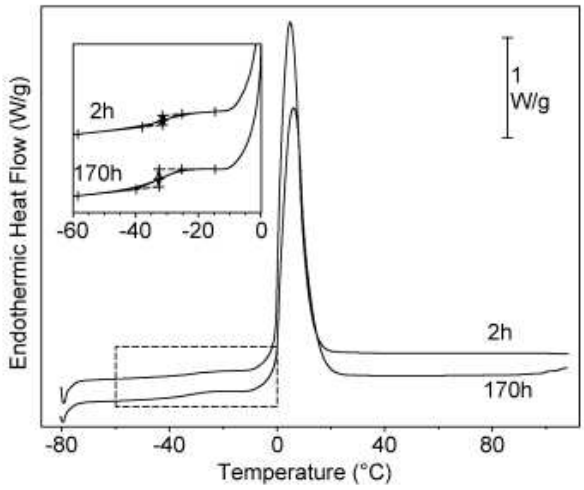

Fig. 6.4. Differential scanning calorimetry thermograms of the PGA-coated alumina after two and 170 hours of equilibration in doubly deionized water at 20°C and pH 5. The inset shows the expanded view of the glass transition region. For better visualization graphs are stacked.

By heating during the DSC experiment, the amorphous ice (which is associated with the matrix) becomes mobile, and the increase in mobility expresses as glass transition at T_g (Nishinari et al., 1997), while melting of the ice crystallites is expressed by the endothermic peak above T_g. The glass transition temperature decreases with increasing content of unfrozen water in the low-water-content region of hydrogels (Nishinari et al., 1997; Hatakeyama et al., 1999). This decrease is explained with the plasticizing effect of water (Hatakeyama et al., 1999). The change of heat capacity, ΔC_p, is a measure for the quantity of the amorphous phase, which is related to the amount of unfrozen water. An increase of ΔC_p is thus connected with a decrease in the glass transition temperature (T_g). T_g re-increases in the higher water-content region due to increasing restrictions of the polymer mobility around ice crystallites (Hatakeyama et al., 1999). The quantity and the restriction of the glassy amorphous phase is in this case directly related to the total surface of the ice crystallites, and thus, both T_g and ΔC_p increase with increasing amount of frozen water.

Table 6.2 summarizes the melting and glass transition characteristics of the PGA-coated alumina for the two equilibration times. The samples revealed water contents of 58% with a standard error of 4% (total mass basis); differences between the equilibration times were not significant. While the glass transition temperature decreased significantly from -31.9°C to -33.4°C with equilibration time, ΔC_p showed a significant increase from 0.26 $J\,g^{-1}\,K^{-1}$ to 0.38 $J\,g^{-1}\,K^{-1}$. This indicates that the system behaves like low-water-content gels, in which water acts as plasticizer, i.e., increases the content of more rubbery gel domains. The change in heat capacity, ΔC_p, is a direct measure for the quantity of amorphous phase. The increase of ΔC_p thus indicates an increase of the amorphous (gel) phase with equilibration time. This conclusion is in accordance with the observation that

ΔC_p is slightly higher in fully gelatinized gels than in partly gelatinized gels (Tananuwong and Reid, 2004). The lower T_g suggests that PGA molecules became more flexible after 170 hours of equilibration.

Table 6.2. Changes in T_g, ΔC_p, the energy of transformation E upon hydration of PGA-coated alumina for two and 170 hours. Also given are estimates of freezable and non-freezable water. Figures in parentheses denote standard error.

Parameter	PGA-coated Al_2O_3 equilibrated for	
	2 hours	170 hours
T_g (°C)	-31.9 (0.4)	-33.4 (0.3)**
ΔC_p (J g^{-1} K^{-1})	0.26 (0.03)	0.38 (0.01)**
Transformation Energy E (J g^{-1})	173 (6)	159 (5)NS
Freezable water (%)	52 (4)	48 (4)NS
Non-freezable water (%)	7 (6)	11 (6)NS

**, significant differences between equilibration times on the P = 0.01 propability level.
NS indicates nonsignificant differences between equilibration times on the P = 0.05 level.
Water contents and transformation energy are related to the total sample mass.

The area of the endotherm peaks indicates transformation energies E of 173 J g^{-1} and 159 J g^{-1} for equilibration times of two and 170 hours, respectively, which suggests a higher amount of unfrozen water after 170 hours of equilibration (11%) than after two hours of equilibration (7%). Although the differences were not significant on the P = 0.05 level, they show the tendency expected from the increase in ΔC_p and thus support the assumption that the amount of a gel phase increased during equilibration. For a final verification of this relation, the water contents of the individual samples need to be determined with higher accuracy. In summary, the DSC investigation suggests an increase in the flexibility of PGA molecules and the amount of a PGA gel phase, and most probably indicates a hydration-induced swelling of the PGA coatings.

6.4.4 Phosphate sorption kinetics

To test our initial hypothesis that restructuring of PGA sorbed to alumina affects the kinetics of phosphate immobilization, we conducted batch experiments after equilibrating both adsorbents in doubly deionized water for two and 170 hours, respectively. The phosphate sorption to pure and PGA-coated alumina comprised a fast and a slow reaction as shown for PGA-coated samples in Fig. 6.5. The fast initial sorption is attributed to sorption of phosphate to external, rapidly accessible sorption sites, while the slow phosphate sorption has been explained by diffusion of phosphate to internal sorption sites (Shin et al.,

2004). The kinetic parameters obtained by fitting Eq.[6.3] to the phosphate sorption data are presented in Table 6.3. PGA-coatings reduced the total amount of phosphate immobilized by the fast sorption reaction and the amount of phosphate that was operationally defined as instantaneously sorbed (Table 6.3, c_m, c_m-a_0 for t = 2 hours). The apparent diffusion constant, $(D/r^2)_{app}$, of pure alumina was 4.7×10^{-4} h^{-1} (Table 6.3). From this value we estimated the apparent diffusion coefficient D_{app}. Because the radius of diffusion is probably much less than one-half of the particle's diameter (<105 µm), we arbitrarily chose a diffusion path length of 10 µm and calculated D_{app} with 1.1×10^{-12} m^2 day^{-1}. The D_{app} was seven orders of magnitude lower than the diffusion coefficient D_0 of $H_2PO_4^-$ in water at 25°C (7.6×10^{-5} m^2 day^{-1}, Edwards and Huffman, 1959), showing that the diffusion of phosphate in intraparticle pores of alumina was considerably slowed down. However, parameters referring to the slow phosphate sorption remained unaffected by the PGA coating, which indicates that the diffusion of phosphate into intraparticle pores was not impaired by PGA (Table 6.3).

.

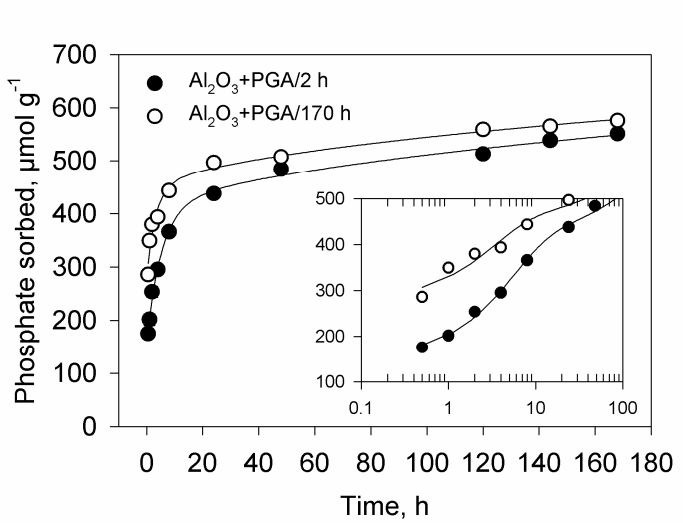

Fig. 6.5. Phosphate sorption kinetics of PGA-coated alumina after two and 170 hours of equilibration in doubly deionized water at 20°C, pH 5, I = 0.01 M, and an initial phosphate concentration of 400 µM. The solid concentration was 0.5 g L^{-1}. The inset shows the phosphate sorption of the first 100 h with a logarithmic x-axis. Error bars are smaller then the symbol size. Solid lines indicate model fits of Eq.[6.3].

The phosphate sorption kinetics of pure alumina remained more or less unaffected by the pre-equilibration time (Table 6.3). In contrast, the phosphate sorption kinetics of PGA-coated alumina strongly depended on the duration of equilibration in water. The amount of phosphate being instantaneously sorbed (c_m-a_0) and the total amount of phosphate sorbed by the fast reaction (c_m) increased by 84% and 12%, respectively (Table 6.3). The result implies that after equilibration of PGA-coated samples for 170 hours, external alumina surfaces became more accessible to phosphate. The phosphate sorption kinetics is in line

with our DSC measurements showing that PGA molecules became more 'flexible' after 170 hours of equilibration in doubly deionized water.

Table 6.3. Kinetic parameters obtained by fitting Eq.[6.3] to the phosphate sorption data of pure and PGA-coated alumina that had been equilibrated at pH 5 in doubly deionized water for two and 170 hours, respectively, prior to phosphate sorption. Parameter meaning: c_m, total amount of phosphate sorbed fast; c_m-a_o, operationally defined amount of phosphate sorbed instantaneously; k, rate constant of the fast phosphate sorption; b, rate constant of the slow phosphate sorption; $(D/r^2)_{app}$, apparent diffusion constant according Eq.[6.4]. Values in parentheses indicate standard error.

Treatment	Time elapsed until P Sorption	c_m	c_m-a_0	k	b	r^2	$(D/r^2)_{app}$
	h	µmol g^{-1}		h^{-1}	µmol g^{-1} $h^{-0.5}$		x 10^{-4} h^{-1}
Al_2O_3	2	506 (22)	296 (31)	0.20 (0.05)	14.3 (2.1)	0.99	4.7 (0.9)
Al_2O_3	170	504 (38)	296 (53)	0.15 (0.06)	8.7 (3.7)	0.98	1.7 (1.0)
Al_2O_3+PGA	2	383 (14)	150 (20)	0.19 (0.03)	12.8 (1.4)	1.00	1.8 (0.3)
Al_2O_3+PGA	170	430 (21)	276 (31)	0.32 (0.12)	11.4 (2.1)	0.98	1.9 (0.5)

Although the swelling kinetics of soil organic matter represents a slow process with time constants varying between one and six days (Schaumann et al., 2004), the slow phosphate sorption to alumina remained unaffected by the state of sorbed organic matter (Table 6.3, b, $(D/r^2)_{app}$). One possible explanation is that structural changes of PGA molecules proceeded too fast to have a significant impact on the slow phosphate sorption. This reasoning accords with the finding that mucilage of maize plants, which comprises about 90-95% polysaccharides with 20-35% uronic acids (Cortez und Billes, 1982; Morel et al., 1986), swells within minutes due to water absorption (Guinel and McCully, 1986; McCully and Sealey, 1996; Sealey et al., 1995). Another explanation for the lacking effect on structural changes of PGA on the slow phosphate sorption kinetics is that after two hours of equilibration in water, PGA desorption was so fast that structural changes of the remaining PGA at the alumina surface did not affect the slow phosphate sorption. Indeed, during the first 0.5 hours after phosphate addition 68% of the total desorbed PGA-C were desorbed (Fig. 6.6).

Another line of evidence indicating a decrease in PGA surface coverage with increasing equilibration time comes from Fig. 6.6, showing the relationship between the quantities of phosphate sorbed and PGA-C desorbed. Phosphate is highly competitive with presorbed PGA (Mikutta et al., 2006a, b). During phosphate sorption to PGA-coated alumina for one week, phosphate displaced 54% and 41% of the initial PGA-C in samples that had been equilibrated for two and 170 hours, respectively. The slopes of the linear regressions presented in Fig. 6.6 show that after a two-hour equilibration period each phosphate dis-

placed on average 0.4 C atoms. The slope increased by a factor of two when the samples were equilibrated for 170 hours before phosphate addition, indicating a higher efficacy of phosphate to desorb PGA-C in samples in which the PGA coating comprised more rubbery domains. In addition, Fig. 6.6 shows that a much larger portion of phosphate was required to achieve a significant C desorption in samples that had been equilibrated for 170 hours. Contrary, although phosphate was less competitive with PGA-C in samples that were equilibrated for two hours only, PGA-C desorption started at a lower phosphate surface loading in these samples (Fig. 6.6).

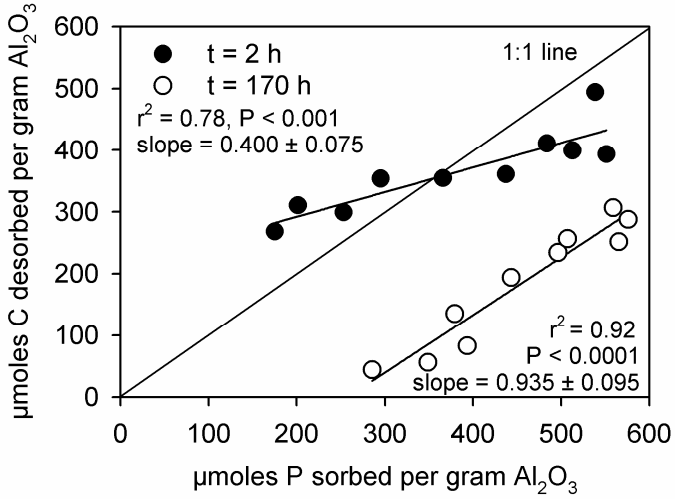

Fig. 6.6. Plot of the amount of phosphate sorbed versus PGA-C desorbed during one week of phosphate sorption to PGA-coated alumina at pH 5 in 0.01 M KNO_3 with an initial phosphate concentration of 400 µM and a solid concentration of 0.5 g L^{-1}.

6.4.5 Conceptual model

In Fig. 6.7 we present a conceptual model for the experimental results of our DSC and phosphate sorption experiments. The picture shows a planar alumina surface coated with linear PGA polymers. The PGA polymers are shown as chains with each link representing a galacturonate monomer. Dark gray chain segments indicate monomers that are directly attached physically or chemically to the alumina surface. White spheres symbolize phosphate ions. Accordingly, after two hours of equilibration in doubly deionized water, a larger fraction of PGA is sorbed in a comparatively flat conformation (poorly hydrated state, less flexible), in which PGA polymers are intimately attached to the mineral surface. Consequently, less sorption sites are rapidly accessible to phosphate (Table 6.3, c_m-a_0) and phosphate is less able to displace a PGA molecule from the surface (‘octopus’ effect, Podoll et al., 1987; see Fig. 6.6). Based on the high competitiveness of phosphate with presorbed PGA (Mikutta et al., 2006a, b), a lower phosphate loading is required after two hours to induce PGA desorption.

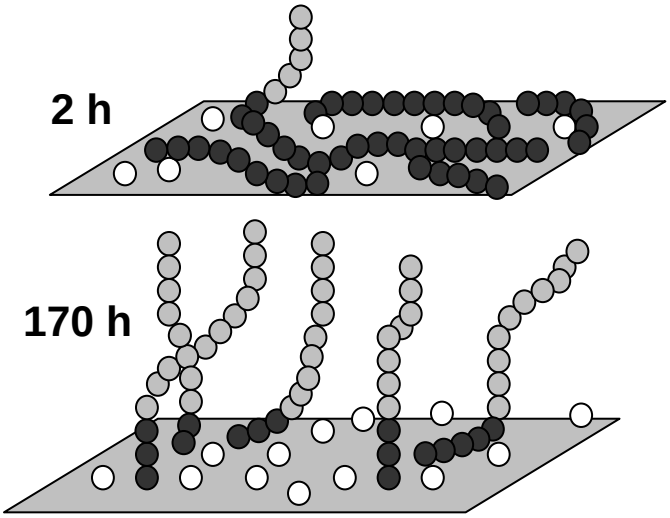

Fig. 6.7. Conceptual model of the dynamics of PGA ions at the alumina surface and its consequences for phosphate sorption and PGA desorption. Gray spheres indicate chain segments of PGA (galacturonic acid monomers): dark gray = monomers linked to the surface; light gray = unbound chain segments with respect to the alumina surface; white spheres symbolize phosphate ions. For explanations refer to section 6.4.5.

After equilibration of PGA-coated alumina for 170 hours in water, PGA molecules rearrange and the mobility of polymer chains increases (swollen state, more flexible). This process decreases the surface coverage of alumina by PGA and facilitates the diffusion of phosphate ions from the bulk water solution to external alumina surfaces (Table 6.3, c_m, c_m-a_0). Upon hydration, PGA polymers become less intimately associated with the mineral surface as indicated by less dark gray chain segments of PGA molecules after 170 hours (Fig. 6.7). When the external surfaces reach saturation with phosphate ions, phosphate increasingly competes with sorbed PGA at higher phosphate surface loading. As the polymers are less intimately attached to the mineral surface, the efficacy of phosphate to displace PGA-C increases (Fig. 6.6).

Noteworthy, at a given s phosphate loading more PGA-C is desorbed in samples that had been equilibrated for two hours than for 170 hours although the PGA-C seems to be less susceptible to desorption by phosphate in the 2-hour treatment (Fig. 6.6). This observation probably results from a greater portion of weakly bound PGA in the 2-h treatment which is readily displaced by phosphate at times <0.5 hours. Factors that may influence the efficacy of phosphate to desorb PGA include (i) the average strength of PGA-oxide interaction which depends on the distribution of weak and strong bindings (e.g., electrostatic vs. specific interaction) of PGA segments to the alumina surface, (ii) the amount of free binding sites (type A-hydroxyls) remaining for specific interaction with phosphate after initial PGA sorption, (iii) the affinity of phosphate to the oxide surface relative to that of presorbed PGA, and (iv) the destabilization of sorbed PGA polymers by locally increased

negative surface charge of alumina imparted by phosphate. It is worth mentioning that the concept developed is oversimplified but following the rule of parsimony (Ockham's razor) it provides a reasonable explanation for our experimental results.

6.5 Conclusions

Porosity studies with ^{1}H-NMR and N_2 gas adsorption of moist and freeze-dried PGA-coated alumina, which had been equilibrated in water for two and 170 hours, respectively, revealed no swelling-induced change in pore size. Our NMR measurements showed that water held in intraparticle pores of alumina was partially displaced by sorbed PGA. Additionally, the hydration of PGA networks on external alumina surfaces increased the amount of water held in interparticle pores of alumina-PGA associations, suggesting the formation of new intra-organic pores between alumina particles.

The analysis of the state of water binding in PGA-coated samples with DSC showed that within 168 hours of equilibration in water the quantity of the PGA gel phase increased, indicating an increase in rubbery domains of the PGA coating. Accordingly, the accessibility of external sorption sites for phosphate was larger after 170 hours than after two hours. The slow phosphate sorption to alumina was independent of equilibration time. The restructuring of sorbed polymers with time changed the efficacy of phosphate to desorb PGA. When PGA coatings became more flexible upon hydration for 170 hours, PGA molecules were less intimately attached to the mineral surface. As a consequence, phosphate was more efficient in displacing PGA-C. However, a higher surface loading of phosphate was required because more free binding sites existed on external alumina surfaces. We finally conclude that structural changes upon hydration/dehydration of plant- or microbe-derived macromolecules sorbed to minerals can be regarded as a crucial factor influencing sorption and transport phenomena of solutes in soils.

7.1 Controls of the phosphate sorption/desorption kinetics of organic matter-goethite associations at pH 5

Based on the findings presented in this work and assuming that precipitation of Fe phosphates (Li and Stanforth, 2000; Ler and Stanforth, 2003) and film diffusion (Boyd et al., 1947) of phosphate were negligible in my experiments, the overall rate of the slow phosphate sorption to C-coated goethites, R_{Slow}, can be conceptualized by

$$R_{Slow} = (F \times R)_{Pore\text{-}Diff} + (F \times R)_{C\text{-}Diff} + (F \times R)_{C\text{-}Desorb} \quad [7.1]$$

where $R_{Pore\text{-}diff}$ is the rate of phosphate diffusion into goethite pores, $R_{C\text{-}Diff}$ is the rate of phosphate diffusion through C coatings, and $R_{C\text{-}Desorb}$ is the rate of the slow phosphate sorption induced by the desorption of C from the goethite surface. As the process with the highest rate in Eq.[7.1] will kinetically control the rate of the slow phosphate sorption only if it dominates all other simultaneously occurring reactions, each rate R in Eq.[7.1] must be weighed by the fraction F_i that the i-th process contributes to the overall slow phosphate reaction. Equation [7.1] thus represents the sum of possible controls of the slow phosphate sorption to organic matter-goethite associations.

Pore clogging by high- and low-molecular-weight root exudates

Thirteen samples of goethite coated with polygalacturonate (PGA) were studied for their phosphate sorption kinetics at pH 5 in 0.01 M KNO_3. Apart from PGA-coated samples with low C loadings, micro- and <5-nm mesopore volumes determined on freeze-dried samples were effectively reduced by PGA (Chapter 2, 3).

Based on a reduced porosity of goethite following the addition of PGA, I expected decreased $(D/r^2)_{app}$ values, i.e., increased diffusion resistances for phosphate in comparison with a C-free control. Only in two freeze-dried PGA-coated goethite samples with low C loadings this expectation was met, implying that the diffusion of phosphate into <5-nm pores of goethite was impaired (Table 2.3, G6; Table 3.2, G1/0.37). However, the higher diffusion resistance for phosphate observed for the freeze-dried G1/0.37 sample diminished when moist samples with a similar C loading were analyzed for their phosphate sorption kinetics (Table 3.2). This result shows that in one sample, the ‘pore clogging effect’ observed probably originated from aggregation.

In 11 out of the 13 PGA-coated goethite samples, $(D/r^2)_{app}$ remained either unchanged (n = 6) or increased with respect to the C-free control (n = 5). Accordingly, the diffusion of phosphate into mineral pores <5 nm of PGA-coated goethite was either hardly affected or superimposed by other processes controlling the slow sorption reaction, so that $(F \times R)_{Pore\text{-}diff}$ in Eq.[7.1] was negligible for samples with increased $(D/r^2)_{app}$ values. This reasoning is supported by a decreasing capability of PGA to inhibit the sorption of phosphate with time (Fig. 7.1).

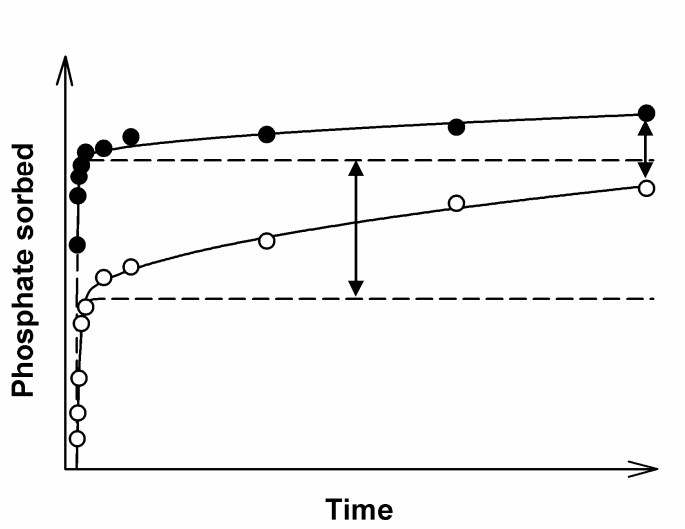

Fig. 7.1. Typical phosphate sorption kinetics of pure (black spheres) and PGA-coated goethite (white spheres). Dashed lines indicate the kinetics of phosphate sorption to external goethite surfaces according to the combined model (Eq.[2.2]). Arrows mark differences in the amount of phosphate sorbed to external goethite surfaces and phosphate sorbed after a prolonged period of time, respectively.

The decreasing ability of PGA to inhibit the sorption of phosphate with time shows that a slow phosphate reaction partially compensated for the strong decrease in the fast phosphate sorption (dashed lines in Fig. 7.1). This observation is incompatible with the hypothesis that the diffusion of phosphate into goethite pores controlled the slow phosphate reaction in PGA-coated samples. Rather, the slow step-by-step desorption of PGA or the diffusion of phosphate through PGA coatings or both explain the increased $(D/r^2)_{app}$ values of five PGA-coated goethite samples (Chapter 3). In samples where the slow phosphate sorption was not affected by PGA despite a reduced micro- and mesoporosity, the C loading might have been too low to induce significant effects on the slow phosphate sorption after C desorption during the initial stage of the phosphate sorption run. Additionally, drying effects cannot be excluded as possible reasons for the lacking sensitivity of the slow phosphate sorption to changes in micro- and mesoporosity by PGA. Drying may have caused a collapse of PGA at the surface, which probably led to a higher surface coverage of PGA and thus to a lower intraparticle porosity than would be present in moist samples. Likewise, reversible aggregation of PGA-coated goethites upon drying may account for no

observable effects of reduced porosities on the slow phosphate sorption kinetics, because drying would reduce the interparticle porosity that might be restored after rewetting the samples. In conclusion, the results indicate that pore clogging by PGA is not rate-limiting for the slow phosphate sorption to PGA-coated goethites.

In contrast to PGA, citrate has been shown to inhibit the slow phosphate sorption to pure and C-coated goethite, thus corroborating my hypothesis that low-molecular-weight root exudates like anions of polycarboxylic low-molecular-weight organic acids (LMWOA) are capable of impeding the diffusion of phosphate into micropores of goethite. Micropore volume and micropore diameter of both pure and C-coated goethite decreased after citrate addition (Table 4.1). In addition, citrate was capable of dissolving pure and C-coated goethite by up to 2.3 mol% within three weeks of phosphate sorption (Fig. 4.4). However, the contribution of micropore clogging is certainly larger than that of the ligand-induced goethite dissolution; for example in the treatment where citrate was added three hours before phosphate to pure goethite, the slow phosphate reaction was totally reduced (Table 4.3), while goethite dissolution accounted for only 1.9 mol% within three weeks (Fig. 4.4). Consequently, $(F \times R)_{Pore\text{-}Diff}$ became the term in Eq.[7.1], which controls the rate of the slow phosphate sorption in the presence of citrate.

Steric arrangement of acid polysaccharides on mineral surfaces

To test effects of hydration-induced swelling of PGA coatings on the phosphate sorption kinetics, I compared the phosphate sorption kinetics of PGA-coated alumina samples that were equilibrated in water at pH 5 for two and 170 hours, respectively (Chapter 6). Results obtained from differential scanning calorimetry analysis implied that with increasing equilibration time in water the flexibility of PGA molecules and the fraction of a PGA gel phase increased, and most probably indicated a hydration-induced swelling of PGA coatings. The kinetics of phosphate sorption and PGA-C desorption implied a weaker binding of PGA to the alumina surface with increasing equilibration time. The restructuring of PGA molecules upon hydration increased the amount of phosphate that was instantaneously sorbed after 170 hours (Table 6.2), supporting my hypothesis that hydration of acid polysaccharide coatings increases their permeability for phosphate.

7.2 Implications for the dynamics of phosphate in the rhizosphere

Coatings of mucilage similar in physico-chemical properties to PGA may successfully impair the slow immobilization of phosphate in pores of Fe and Al oxides. Due to the high

competitiveness of phosphate with pre-sorbed acid polysaccharides, pores located underneath these coatings will become progressively accessible to phosphate when macromolecules are partly or fully displaced by phosphate. In all PGA treatments phosphate desorbed on average 51% C of pre-sorbed PGA within up to three weeks (n = 14, 18% standard deviation). However, an embedding of Fe or Al oxides in mucilaginous matrixes in the root cap zone is likely to occur. The engulfing of clay minerals by humic materials and exocellular polysaccharides has been observed in soils and sediments (Jenny and Grossenbacher, 1963; Fontes et al., 1992; Ransom et al., 1997, 1999). Accordingly, the particle diffusion inhibition for phosphate by exuded polysaccharides can be expected to be much stronger in the rhizosphere than observed in batch experiments, because the C loading and the surface coverage of organic matter would be much higher. In addition, phosphate concentrations in the rhizosphere soil solution are much smaller than 20 µM, which is about two orders of magnitude lower than phosphate concentrations used in my experiments (250-500 µM). Consequently, the desorption of C by phosphate would be less intense in the rhizosphere. The clogging of pores of Fe and Al oxides by polysaccharides exuded by plant roots will furthermore depend on the physico-chemical properties of the exudates. The properties of mucilage may change due to the colonization of mucilage by microbes or the incorporation of mineral particles as shown by Jenny and Grossenbacher (1963). Mary et al. (1993) and Knee et al. (2001) have provided evidence that mucilage can be used as a C source for microbes. In Chapter 5 I showed that the phosphate desorption from goethite treated with mucigel (MU) of maize plants was contrary to that of PGA. Based on the phosphate desorption kinetics, no indications of a clogging of goethite pores by MU were found. This finding was attributed to a suite of minerals present in the MU (Fig. 5.1), and its low content in uronic acid (Table 5.1). The high content of phosphate in the MU (Table 5.1) suggests that MU may act as a phosphate adsorbent in the rhizosphere, which may render MU a diffusion barrier for phosphate.

The micropore clogging of Fe and Al oxides by polycarboxylic LMWOA anions will be confined to a region close to the root because LMWOA anions are rapidly consumed by microorganisms. Jones et al. (1996) predicted that 99% of exuded LMWOA anions remain within a distance of up to 1 mm of the root surface. In Chapter 4 it has been shown that the time scale of both micropore clogging and the degradation of LMWOA anions in soils (Jones, 1998; Jones and Darrah, 1994) are similar. In addition, considering the high efflux rates of polycarboxylic LMWOA anions of P-starved plants (Ryan et al., 2001 and ref. therein) which may cause concentrations in the rhizosphere soil solution similar to those

used in my experiments (Jones, 1998), the clogging of micropores of Fe and Al oxides may be regarded as an important mechanism by which P-starved plants increase the bioavailability of phosphate.

Experiments presented in Chapter 6 revealed that the state of hydration of acid polysaccharide coatings on alumina surfaces affects the sorption kinetics of phosphate. Transferred to rhizosphere conditions, the results might imply that hydrated mucilage may be more permeable for oxyanions than dry mucilage. This reasoning is compatible with observations showing that the water content of fully hydrated maize mucilage can be up to 99.9% on a wet basis (Guinel and McCully, 1986). Consequently, the volume of maize mucilage may drastically decrease upon desiccation, which would lower its surface tension and increase its viscosity (Walker et al., 2003). Therefore, drying of mucilage presumably increases the diffusion resistance for oxyanions in the gel. Guinel and McCully (1986) reported a water potential of root-cap mucilage of only –7 kPa, implying a poor if any water-holding capacity of mucilage under normal field conditions. Likewise, McCully and Boyer (1997) concluded that root-cap mucilage of maize *per se* has almost no capacity to retain water in the rhizosphere. The dehydration-induced shrinkage of the mucilaginous layer on root caps, which can extend several tens of micrometers (Jenny and Grossenbacher, 1963; Vermeer and McCully, 1982), may facilitate the diffusion-controlled transport of phosphate to the root in the soil solution. It might also be hypothesized that the stronger adherence of mucilage to soil particles upon desiccation as proposed by Whalley et al. (2005) intensifies the pore clogging of Fe and Al oxides. The effect of hydration and dehydration of plant mucilage on the diffusion of oxyanions through the polymeric matrix has not yet been studied and warrants future research.

Summing up, my experiments showed that at pH 5 polycarboxylic LMWOA anions exuded by plant roots may increase the bioavailability of phosphate via the clogging of micropores of goethite in addition to sorption competition and the decrease in surface charge. The clogging of goethite pores by acid polysaccharides is much less pronounced compared to polycarboxylic LMWOA anions. In the rhizosphere, the capability of acid polysaccharide coatings to clog pores of sesquioxides and thus to inhibit the pore diffusion of phosphate may also depend on their state of hydration.

8 References

Adu, J.K., and J.M. Oades. 1978. Physical factors influencing decomposition of organic materials in soil aggregates. Soil Biol. Biochem. 10:109-115.

Aharoni, C., and D.L. Sparks. 1991. Rates of soil chemical processes: a theoretical treatment. *In* D.L. Sparks and D.L. Suarez (ed.) Rates of soil chemical processes, SSSA Spec. Publ. 27, Soil Science Society of America, Madison, WI.

Aharoni, C., D.L. Sparks, S. Levinson, and I. Ravina. 1991. Kinetics of soil chemical reactions: relationships between empirical equations and diffusion models. Soil Sci. Soc. Am. J. 55:1307-1312.

Allison, J.D., D.S. Brown, and K.J. Novo-Gradac. 1991. MINTEQA2/PRODEFA2, A geochemical assessment model for environmental systems: Version 3.0 User's Manual. United States Environmental Protection Agency, Office of Research and Development, Washington.

Allison, S.D., T.W. Randolph, M.C. Mannung, K. Middleton, A. Davis, and J.F. Carpenter. 1998. Effect of drying methods and additives on structure and function of actin: mechanisms of dehydration-induced damage and its inhibition. Archives Biochem. Biophys. 358:171-181.

Altfelder, S., T. Streck, and J. Richter. 1999. Effect of air-drying on sorption kinetics of the herbicide chlortoluron in soil. Environ. Qual. 28:1154-1161.

Alvarez-Puebla, R.A., and J.J. Garrido. 2005. Effect of pH on the aggregation of a gray humic acid in colloidal and solid states. Chemosphere 59:659-667.

Amelung, W., K. Kaiser, G. Kammerer, and G. Sauer. 2002. Organic carbon at soil particle surfaces - evidence from X-ray photoelectron spectroscopy and surface abrasion. Soil Sci. Soc. Am. J 66:1526-1530.

Anderson, M.A., M.I. Tejedor-Tejedor, and R.R. Stanforth. 1985. Influence of aggregation on the uptake kinetics of phosphate by goethite. Einviron. Sci. Technol. 19:632-637.

Appelt, H., N.T. Coleman, and P.F. Pratt. 1975. Interactions between organic compounds, minerals, and ions in volcanic ash derived soils: II. Effects of organic compounds on the adsorption of phosphate. Soil Sci. Soc. Am. Proc. 39:628-630.

Asher, C.J., and J.F. Loneragan. 1967. Response of plants to phosphate in solution culture: I. Growth and phosphorus content. Soil Sci. 103:225-233.

Au, K.-K., S. Yang, and C.R. O'Melia. 1998. Adsorption of weak polyelectrolytes on metal oxides surfaces: a hybrid SC/SF approach. Environ. Sci. Technol. 32:2900-2908.

Bacic, A., S.F. Moody, and A.E. Clarke. 1986. Structural analysis of secreted root slimes from maize (*Zea mays* L.). Plant Physiol. 80:771-777.

Bajpai, S.K., and S. Singh. 2006. Analysis of swelling behavior of poy(methacrylamide-co-methacrylic acid) hydrogels and effect of synthesis conditions on water uptake. Reactive and Functional Polymers 66:431-440..

Barber, S.A. 1974. Nutrients in the soil and their flow to plant roots. p. 161-168. *In* J.K. Marshall (ed.) The belowground ecosystem: a synthesis of plant-associated processes. Range Sci. Series 26, Colorado State University, Fort Collins.

Barrett, E.P., L.G. Joyner, and P.P. Halenda. 1951. The determination of pore volume and area distributions in porous substances. I. Computations from nitrogen isotherms. J. Amer. Chem. Soc. 73:373-380.

Barrón, V., N. Gálvez, M.F. Hochella Jr., and J. Torrent. 1997. Epitaxial overgrowth of goethite on hematite synthesized in phosphate media: a scanning force and transmission electron microscopy study. Am. Min. 82:1091-1100.

Barrow, N.J., L. Madrid, and A.M. Posner. 1981. A partial model for the rate of adsorption and desorption of phosphate by goethite. J. Soil. Sci. 32:399-407.

Barrow, N.J., G.W. Brümmer, and R. Strauss. 1993. Effects of surface heterogeneity on ion adsorption by metal oxides and by soils. Langmuir 9:2606-2611.

Bertrand, I., and P. Hinsinger. 2000. Dissolution of iron oxyhydroxide in the rhizosphere of various crop species. J. Plant Nutrition 23:1559-1577.

Bertrand, I., P. Hinsinger, B. Jaillard, and J.C. Arvieu. 1999. Dynamics of phosphorus in the rhizosphere of maize and rape grown on synthetic, phosphated calcite and goethite. Plant Soil 211:111-119.

Bhatti, J.S., N.B. Comerford, and C.T. Johnston. 1998. Influence of oxalate and soil organic matter on sorption and desorption of phosphate onto a spodic horizon. Soil Sci. Soc. Am. J. 62:1089-1095.

Blakemore, L.C., P.L. Searle, and B.K. Daly. 1987. Methods for chemical analysis of soils. NZ Soil Bureau Scientific Report 80, NZ Soil Bureau, Lower Hutt.

Blakeney, A.B., and L.L. Mutton. 1980. A simple colorimetric method for the determination of sugars in fruit and vegetables. Sci. Food Agri. 31:889-897.

Bloom, P.R. 1981. Phosphorus adsorption by an aluminum-peat complex. Soil Sci. Soc. Am. J. 45:267-272.

Blumenkrantz, N., and G. Asboe-Hansen. 1973. New method for quantitative determination of uronic acids. Anal. Biochem. 54:484-489.

Bolan, N.S., R. Naidu, S. Mahimairaja, and S. Baskaran. 1994. Influence of low-molecular-weight organic acids on the solubilization of phosphates. Biol. Fertil. Soils 18:311-319.

Bolan, N.S., J. Elliot, P.E.H. Gregg, and S. Weil. 1997. Enhanced dissolution of phosphate rocks in the rhizosphere. Biol. Fertil. Soils 24:169-174.

Bondietti, G., J. Sinniger, and W. Stumm. 1993. The reactivity of Fe(III) (hydr)oxides: Effects of ligands in inhibiting the dissolution. Colloid Surf. A. 79:157-167.

Borggaard, O.K. 1988. Phase identification by selective dissolution techniques. p. 83-98. *In* J.W. Stucki, B.A. Goodman, and U. Schwertmann (ed.) Iron in soils and clay minerals. Reidel, Dordrecht.

Borggaard, O.K. 1990. Kinetics and mechanism of soil iron oxide dissolution in EDTA, oxalate, and dithionite. Sci. Geol. Mem. 85:139-148.

Borie, F., and H. Zunino. 1983. Organic matter-phosphorus associations as a sink in P fixation processes in allophanic soils of Chile. Soil Biol. Biochem. 15:599-603.

Boyd, G.E., A.W. Adamson, and L.S. Meyers Jr. 1947. The exchange adsorption of ions from aqueous solutions by organic zeolites. II. Kinetics. J. Am. Chem. Soc. 69:2836-2848.

Bradford, M.M. 1976. Rapid and sensitive method for quantification of microgram quantities of protein utilizing principle of protein-dye binding. Anal. Biochem. 72:248-254.

Breeze, V.G., A. Wild, M.J. Hopper, and L.H.P. Jones. 1984. The uptake of phosphate by plants from flowing nutrient solution. II. Growth of *Lolium perenne* L. at constant phosphate concentrations. J. Exp. Bot. 35:1210.1221.

Brewster, J.L., K.K.S. Bhat, and P.H. Nye. 1976. The possibility of predicting solute uptake and plant growth response from independently measured soil and plant characteristics: V. The growth and phosphorus uptake of rape in soil at a range of phosphorus concentrations and a comparison of results with predictions of a simulation model. Plant Soil 44:295-328.

Brownstein, K.R., and C.E. Tarr. 1979. Importance of classical diffusion in NMR studies of water in biological cells. Physics Review A 19:2446-2453.

Brunauer, S., P.H. Emmett, and E. Teller. 1938. Adsorption of gases in multimolecular layers. J. Am. Chem. Soc. 60:309-319.

Brusseau, M. and P.S.C. Rao. 1989. Sorption nonideality during organic contaminant transport in porous media. Crit. Rev. Environ. Control 19:33-99.

Cabrera, F., P. de Arambarri, L. Madrid, and C.G. Toca. 1981. Desorption of phosphate from iron oxides in relation to equilibrium pH and porosity. Geoderma 26:203-216.

Cervini-Silva, J., and G. Sposito. 2002. Steady-state dissolution kinetics of aluminum-goethite in the presence of desferrioxamine-B and oxalate ligands. Environ. Sci. Technol. 36:337-342.

Cheah, S.F., S.M. Kraemer, J. Cervini-Silva, and G. Sposito. 2003. Steady-state dissolution kinetics of goethite in the presence of desferrioxamine B and oxalate ligands: implications for the microbial acquisition of iron. Chem. Geol. 198:63-75.

Chen, Y.S.R., J.N. Butler, and W. Stumm. 1973. Kinetic study of phosphate reaction with aluminum oxide and kaolinite. Environ. Sci. Technol. 7:327-332.

Chenu, C. 1993. Clay- or sand-polysaccharide associations as models for the interface between micro-organisms and soil: water related properties and microstructure. Geoderma 56:143-156.

Chiarizia, R., and E.P. Horwitz. 1991. New formulations for iron oxides dissolution. Hydrometallurgy 27:339-360.

Ciurli, S., C. Marzadori, S. Benini, S. Deinana, and C. Gessa. 1996. Urease from the soil bacterium *Bacillus Pasteurii*: immobilization on Ca-polygalacturonate. Soil Biol. Biochem. 28:811-817.

Cornelissen, G., P.C.M. van Noort, and H.A.J. Govers. 1998. Mechanisms of slow desorption of organic compounds from sediments: A study using model sorbents. Environ. Sci. Technol. 32:3124-3131.

Cornell, R.M., and P.W. Schindler. 1980. Infrared study of the adsorption of hydroxycarboxylic acids on α-FeOOH and amorphous Fe(III)-hydroxide. Colloid Polymer Sci. 258:1171-1175.

Cornell, R.M., and U. Schwertmann. 2003. The iron oxides. Structure, properties, reactions, occurrences and uses. 2nd ed., Wiley-VCH, Weinheim.

Cortez, J., and G. Billes. 1982. Rôle des ions calcium dans la formation du mucigel de Zea mays. Acta Oecol. Plant. 3:67-78.

Courchesne, F., M. Turmel, and P. Beauchemin. 1996. Magnesium and potassium release by weathering in spodosols: grain surface coating effects. Soil Sci. Soc. Am. J. 60:1188-1196.

Crank, J. 1976. The mathematics of diffusion. Oxford Univ. Press, New York.

Czarnes, S., P.D. Hallett, A.G. Bengough, and I.M. Young. 2000. Root- and microbial-derived mucilages affect soil structure and water transport. Eur. J. Soil Sci. 5:435-443.

Dakora, F.D., and D.A. Phillips. 2002. Root exudates as mediators of mineral acquisition in low-nutrient environments. Plant Soil 245:35-47.

Deiana, D., B. Manunza, A. Palma, A. Premoli, and C. Gessa. 2001. Interaction and mobilization of metal ions at the soil-root interface. p. 127-148. *In* G.R. Gobran, W.W. Wenzel, and E. Lombi (ed) Trace elements in the rhizosphere. CRC Press, Boca Raton.

De Jonge, H., and M.C. Mittelmeijer-Hazeleger. 1996. Adsorption of CO_2 and N_2 on soil organic matter: nature of porosity, surface area and diffusion mechanisms. Environ. Sci. Technol. 30:408-413.

Dinkelaker, B., and H. Marschner. 1992. *In vivo* demonstration of acid phosphatase activity in the rhizosphere of soil-grown plants. Plant Soil 144:199-205.

D'Orazio, F., J.C. Tarczon, W.P. Halperin, K. Eguchi, and T. Mizusaki. 1989. Application of nuclear magnetic resonance pore structure analysis to porous silica glass. J. Appl. Phys. 65:742-751.

Duff, S.M.G., G. Sarath, and W.C. Plaxton. 1994. The role of acid phosphatases in plant phosphorus metabolism. Physiol. Plant. 90:791-800.

Edwards, A.P., and J.M. Bremmer. 1967. Microaggregates in soils. The Journal of Soil Science 18:64-73.

Edwards, O.W., and E.O. Huffman. 1959. Diffusion of aqueous solutions of phosphoric acid at 25°. J. Phys. Chem. 63:1830-1833.

Fine, P., and M.J. Singer. 1989. Contribution of ferrimagnetic minerals to oxalate- and dithionite extractable iron. J. Soil Sci. Soc. Am. 53:191-196.

Fischer, L., E. zur Mühlen, G.W. Brümmer, and E. Niehus. 1996. Atomic force microscopy (AFM) investigations of the surface topography of a multidomain porous goethite. Eur. J. Soil Sci. 47:329-334.

Fontes, M.R., S.B. Weed, and L.H. Bowen. 1992. Association of microcrystalline goethite and humic acid in some Oxisols from Brazil. Soil Sci. Soc. Am. J. 56:982-990.

Foth, H.D., and B.G. Ellis. 1997. Soil fertility. 2nd ed., Lewis Publishers, Boca Raton.

Freese, D., W.H. van Riemsdijk, and S.E.A.T.M. van der Zee. 1995. Modeling phosphate-sorption kinetics in acid soils. Eur. J. Soil Sci. 46:239-245.

Fuller, C.C., J.A. Davis, and G.A. Waychunas. 1993. Surface chemistry of ferrihydrite: Part 2. Kinetics of arsenate adsorption and coprecipitation. Geochim. Cosmochim. Acta 57:2271-2282.

Furrer, G., and W. Stumm. 1986. The coordination chemistry of weathering. I. Dissolution kinetics of γ-Al_2O_3 and BeO. Geochim. Cosmochim. Acta 50:1847-1860.

Gaillardon, P. 1996. Influence of soil moisture on long-term sorption of diuron and isoproturon by soil. Pestic. Sci. 47:347-354.

Gardner, W.K., D.A. Barber, and D.G. Parberry. 1983. The acquisition of phosphorus by *Lupinus albus* L. III. The probable mechanism by which phosphorus movement in the soil/root interface is enhanced. Plant Soil 70:107-124.

Gaume, A., P.G. Weidler, and E. Frossard. 2000. Effect of maize root mucilage on phosphate adsorption and exchangeability on a synthetic ferrihydrite. Biol. Fertil. Soils 31:525-532.

Geelhoed, J.S., T. Hiemstra, and W.H. van Riemsdijk. 1998. Competitive interaction between phosphate and citrate on goethite. Environ. Sci. Technol. 32:2119-2123.

Geelhoed, J.S., W.H. van Riemsdijk, and G.R. Findenegg. 1999. Simulation of the effect of citrate exudation from roots on the plant availability of phosphate adsorbed on goethite. Eur. J. Soil Sci. 50:379-390.

Gerin, P.A., M.J. Genet, A.J. Herbillon, and B. Delvaux. 2003. Surface analysis of soil material by X-ray photoelectron spectroscopy. Eur. J. Soil Sci. 54:589-603.

Gerke, J., and R. Hermann. 1992. Adsorption of orthophosphate to humic-Fe-complexes and to amorphous Fe-oxide. Z. Planzenernähr. Bodenk. 155:233-236.

Gerke, J., U. Meyer, and W. Römer. 1995. Phosphate, Fe and Mn uptake by N_2-fixing red clover and ryegrass from an Oxisol as affected by P and model humic substances application. 1. Plant parameters and soil solution composition. Z. Pflanzenernähr. Bodenk. 158:261-268.

Gessa, C., and S. Deiana. 1992. Ca-polygalacturonate as a model for a soil-root interface. II. Fibrillar structure and comparison with natural root mucilage. Plant Soil 140:1-13.

Gessa, C.E., T. Mimmo, S. Deiana, and C. Marzadori. 2005. Effect of aluminium and pH on the mobility of phosphate through a soil-root interface model. Plant Soil 272:301-311.

Goldberg, S., H.S. Forster, and C.L. Godfrey. 1996. Molybdenum adsorption of oxides, clay minerals, and soils. Soil Sci. Soc. Am. J. 60:425-432.

Goldstein, A.H., D.A. Baertlein, and R.G. McDaniel. 1988. Phosphate starvation inducible metabolism in Lycopersicon esculentun. I. Excretion of acid phosphatase by tomato plants and suspension-cultured cells. Plant Physiol. 87:711-715.

Greaves, M.P., and J.F. Darbyshire. 1972. The ultrastructure of the mucilaginous layer on plant roots. Soil Biol. Biochem. 4:443-446.

Gregg, S.J., and K.S.W. Sing. 1982. Adsorption, surface area and porosity. 2nd ed., Academic Press, New York.

Grimal, J.Y., E. Frossard, and J.L. Morel. 2001. Maize root mucilage decreased adsorption of phosphate on goethite. Biol. Fertil. Soils 33:226-230.

Guinel, F.C., and M.E. McCully. 1986. Some water-related physical properties of maize root-cap mucilage. Plant, Cell and Environment 9:657-666.

Guppy, C.N., N.W. Menzies, P.W. Moody, and F.P.C. Blamey. 2005. Competitive sorption reactions between phosphorus and organic matter in soil: a review. Austr. J. Soil Res. 43:189-202.

Harborne, J.B. 1984. Phytochemical methods. 2nd ed., Chapman & Hall, New York.

Hatakeyama, T., K. Nakamura, M. Takahashi, and H. Hatakeyama. 1999. Phase transitions of gellan-water systems. Progress in Colloid and Polymer Science 114:98-101.

Heil, D., and G. Sposito. 1993a. Organic matter role in illitic soil colloids flocculation: II. Surface charge. Soil Sci. Soc. Am. J. 57:1246-1253.

Heil, D., and G. Sposito. 1993b. Organic matter role in illitic soil colloids flocculation: I. Counter ions and pH. Soil Sci. Soc. Am. J. 57:1241-1246.

Heil, D., and G. Sposito. 1995. Organic matter role in illitic soil colloids flocculation: III. Scanning force microscopy. Soil Sci. Soc. Am. J. 59:266-269.

Hendriks, L., N. Claasen, and A. Jungk. 1981. Phosphate depletion at the soil-root interface and the phosphate uptake of maize and rape. Z. Pflanzenernähr. Bodenk. 144:486-499.

Hinedi, Z.R., Z.J. Kabala, T.H. Skaggs, D.B. Borchardt, R.W. Lee, and A.C. Chang. 1993. Probing soil and aquifer material porosity with nuclear magnetic resonance. Water Resources Research 29:3861-3866.

Hinedi, Z.R., A.C. Chang, M.A. Anderson, and D.B. Borchardt. 1997. Quantification of microporosity by NMR relaxation of water imbided in porous media. Water Resources Research 33:2697-2704.

Hinsinger, P. 2001. Bioavailability of soil inorganic P in the rhizosphere as affected by root-induced chemical changes: a review. Plant Soil 237:173-195.

Hiradate, S., and K. Inoue. 1998. Interaction of mugineic acid with iron (hydr)oxides: sulfate and phosphate influences. Soil Sci. Soc. Am. J. 62:159-165.

Hu, H.Q., J.Z. He, X.Y. Li, and F. Liu. 2001. Effect of several organic acids on phosphate adsorption by variable charge soils of Central China. Environmental International 26:353-358.

Hue, N.V. 1991. Effects of organic acids/anions on P sorption and phytoavailability in soils with different mineralogy. Soil Sci. 6:463-471.

Hunter, R.J. 1988. Zeta potential in colloid science. Principles and applications. Academic Press, London.

Hütsch, B.W., J. Augustin, and W. Merbach. 2002. Plant rhizodeposition – an important source for carbon turnover in soils. J. Plant Nutr. Soil Sci. 165:397-407.

Jenny, H., and K. Grossenbacher. 1963. Root-soil boundary zones as seen in the electron microscope. Soil Sci. Soc. Am. Proc. 27:273-277.

Johnson, A.C., R.J. Bettinson, and R.J. Williams. 1999. Differentiating between physical and chemical constraints on pesticide and water movement into and out of soil aggregates. Pestic. Sci. 55:524-530.

Jones, D.L. 1998. Organic acids in the rhizosphere - a critical review. Plant Soil 205:25-44.

Jones, D.L., and P.R. Darrah. 1994. Role of root derived organic acids in the mobilisation of nutrients from the rhizosphere. Plant Soil 166:247-257.

Jones, D.L., P.R. Darrah, and L.V. Kochian. 1996. Critical-evaluation of organic-acid mediated iron dissolution in the rhizosphere and its potential role in root iron uptake. Plant Soil 180:57-66.

Jouppila, K., and Y.H. Roos. 1997. The physical state of amorphous corn starch and its impact on crystallization. Carbohydrate Polymers 32:95-104.

Jungk, A., B. Seeling, and J. Gerke. 1993. Mobilization of different phosphate fractions in the rhizosphere. Plant Soil 155/156:91-94.

Kaiser, K., and G. Guggenberger. 2003. Mineral surface and soil organic matter. Eur. J. Soil Sci. 54:219-236.

Kaiser, K., and W. Zech. 1999. Release of natural organic matter sorbed to oxides and a subsoil. Soil Sci. Soc. Am. J. 63:1157-1166.

Keerthisinghe, G., P.J. Hocking, P.R. Ryan, and E. Delhaize. 1998. Effect of phosphorus supply on the formation and function of proteoid roots of white lupin (*Lupinus albus* L.). Plant Cell Environ. 21:467-478.

Kenyon, W.E. 1992. Nuclear magnetic resonance as a petrophysical measurement tool. Nuclear Geochysics 6:53-171.

Kenyon, W.E. 1997. Petrophysical principles of applications of NMR logging. Log Analyst 38:21-46.

Khare, N., D. Hesterberg, and J.D. Martin. 2005. XANES investigation of phosphate sorption in single and binary systems of iron and aluminum oxide minerals. Environ. Sci. Technol. 39:2152-2160.

Kiem, R., and I. Kögel-Knabner. 2003. Contribution of lignin and polysaccharides to the refractory carbon pool in C-deleted arable soils. Soil Biol. Biochem. 35:101-118.

Kim, T.J., and T.G. Park. 2004. Critical effect of freezing/freeze-drying on sustained release of FITC-dextran encapsulated within PLGA microspheres. Intern. J. Pharmaceutics 271:207-214.

Kim, Y., and R.J. Kirkpatrick. 2004. An investigation of phosphate adsorbed on aluminium oxyhydroxide and oxide phases by nuclear magnetic resonance. Eur. J. Soil Sci. 55: 243-251.

Kirk, G.J.D. 1999. A model of phosphate solubilization by organic anion excretion from plant roots. Eur. J. Soil. Sci. 50:369-378.

Knee, E.M., F.-C. Gong, M. Gao, M. Teplitski, A.R. Jones, A. Foxworthy, A.J. Mort, and W.D. Bauer. 2001. Root mucilage from pea and its utilization by rhizosphere bacteria as a sole carbon source. Mol. Plant Microbe Interact. 14:775-784.

Kosmulski, M., E. Maczka, E. Jartych, and J.B. Rosenholm. 2003. Synthesis and characterization of goethite and goethite-hematite composite: experimental study and literature survey. Advances Colloid Interface Sci. 103:57-76.

Kretzschmar, R., D. Hesterberg, and H. Sticher. 1997. Effects of adsorbed humic acid on surface charge and flocculation of kaolinite. Soil Sci. Soc. Am. J. 61:101-108.

Kuo, S. and E.G. Lotse. 1974. Kinetics of phosphate adsorption and desorption by hematite and gibbsite. Soil Sci. 116:400-406.

Lang, F., and M. Kaupenjohann. 2003. Immobilisation of molybdate by iron oxides: effect of organic coatings. Geoderma 113:31-46.

LeBoeuf, E.J., and W.J. Weber Jr. 1997. A distributed reactivity model for sorption by soils and sediments. 8. Sorbent organic domains: discovery of a humic acid glass transition and an argument for a polymer-based model. Environ. Sci. Technol. 31:1697-1702.

LeBoeuf, E.J., and W.J. Weber Jr. 2000. Macromolecular characteristics of natural organic matter. 2. Sorption and desorption behavior. Environ. Sci. Technol. 34:3623-3631.

Lee, R.B. 1988. Phosphate influx and extracellular phosphatase activity in barley roots and rose cells. New Phytol. 109:141-148.

Ler, A., and R. Stanforth. 2003. Evidence of surface precipitation of phosphate on goethite. Environ. Sci. Technol. 37:2694-2700.

Léveseque, S.G., R.M. Lim, and M.S. Shoichet. 2005. Macroporous interconnected dextran scaffolds controlled porosity for tissue-engineering applications. Biomaterials 26:7436-446.

Li, L., and R. Stanforth. 2000. Distinguishing adsorption and surface precipitation of phosphate on goethite (α-FeOOH). J. Colloid Interface Sci. 230:12-21.

Liang, L., A. Hofmann, and B. Gu. 2000. Ligand-induced dissolution and release of ferrihydrite colloids. Geochim. Cosmochim. Acta 64:2027-2037.

Lima, J.M., S.J. Anderson, and N. Curi. 2000. Phosphate-induced clay dispersion as related to aggregate size and composition in Hapludoxs. Soil Sci. Soc. Am. J. 64:892-897.

Lindsay, W.L. 1979. Chemical equilibria in soils. John Wiley & Sons, New York.

Linquist, B.A., P.W. Singleton, R.S. Jost, and K.G. Cassman. 1997. Aggregate size effects on the sorption and release of phosphorus in an Ultisol. Soil Sci. Soc. Am. J. 61:160-166.

Liu, F., J. He, C. Colombo, and A. J. Violante. 1999. Competitive adsorption of sulfate and oxalate on goethite in the absence or presence of phosphate. Soil Sci. 164:180-189.

Lopez-Hernandez, D., Siegert, G., and J.V. Rodriguez. 1986. Competitive adsorption of phosphate with malate and oxalate by tropical soils. Soil Sci. Soc. Am. J. 50:1460-1462.

Lowell, S., and J.E. Shields. 1984. Powder surface area and porosity. 2nd ed., Chapman & Hall, London.

Madrid, L., and P. J. Arambarri. 1985. Adsorption of phosphate by two iron oxides in relation to their porosity. J. Soil Sci. 36:523-530.

Makris, K.C., W.G. Harris, G.A. O`Connor, and T.A. Obreza. 2004. Phosphorus immobilization in micropores of dinking-water treatment residuals: implications for long-term stability. Environ. Sci. Technol. 38:6590-6596.

Manunza, B., S. Deiana, M. Pintore, and C. Gessa. 1997. Molecular dynamics study of polygalacturonic acid chains in aqueous solution. Carbohydrate Research 300:85-88.

Martin, R.R., R.S.C Smart, and K. Tazaki. 1988. Direct observation of phosphate precipitation in the goethite/phosphate system. Soil Sci. Soc. Am. J. 52:1492-1500.

Mary, B., C. Fresneau, J.L. Morel, and A. Mariotti. 1993. C and N cycling during decomposition of root mucilage, roots and glucose in soil. Soil Biol. Biochem. 25:1005-1014.

Mayer, L.M. 1994. Relationships between mineral surfaces and organic carbon concentrations in soils and sediments. Chem. Geol. 114:347-363.

Mayer, L.M. 1999. Extend of coverage of mineral surfaces by organic matter in marine sediments. Geochim. Cosmochim. Acta 63:207-215.

Mayer, L.M., and B. Xing. 2001. Organic matter-surface area relationships in acid soils. Soil. Sci. Soc. Am. J. 65:250-258.

Mayer, L.M., L.L. Schick, K.R. Hardy, R. Wagai, and J. McCarthy. 2004. Organic matter in small mesopores in sediments and soils. Geochim. Cosmochim. Acta 68:3863-3872.

McCully, M.E., and L.J. Sealey. 1996. The expansion of maize root-cap mucilage during hydration. 2. Observations on soil-grown roots by cryo-scanning electron microscopy. Physiol. Plant. 97:454-462.

McCully, M.E., and J.S. Boyer. 1997. The expansion of root cap mucilage during hydration: III. Changes in water potential and water content. Physiol. Plant. 99:169-177.

McKeague, J.A., J.E. Brydon, and N.M. Miles. 1971. Differentiation of forms of extractable iron and aluminum in soils. Proc. Soil Sci. Soc. Am. 35:33-38.

Mikutta, C., F. Lang, and M. Kaupenjohann. 2004. Soil organic matter clogs mineral pores: evidence from ^{1}H-NMR logging and N_2 adsorption. Soil Sci. Soc. Am. J. 68:1853-1862.

Mikutta, C., J. Krüger, F. Lang, and M. Kaupenjohann. 2006a. Acid polysaccharide coatings on microporous goethites – controls of the slow phosphate sorption. Soil Sci. Soc. Am. J. (in press).

Mikutta, C., F. Lang, and M. Kaupenjohann. 2006b. Kinetics of phosphate sorption to polygalacturonate-coated goethite. Soil Sci. Soc. Am. J. (in press).

Mikutta, C., F. Lang, and M. Kaupenjohann. 2006c. Citrate impairs the micropore diffusion of phosphate into pure and C-coated goethite. Geochim. Cosmochim. Acta (in press).

Miller, W.P., L.W. Zelazny, and D.C. Martens. 1986. Dissolution of synthetic crystalline and noncrystalline iron oxides by organic acids. Geoderma 37:1-13.

Miltner, A., and W. Zech. 1998. Carbohydrate decomposition in beech litter as influenced by aluminum, iron and manganese oxides. Soil Biol. Biochem. 30:1-7.

Mimmo, T., C. Marzadori, O. Francioso, S. Deiana, and C.E. Gessa. 2003. Effects of aluminum sorption on calcium-polygalacturonate network used as soil-root interface model. Biopolymers (Biospectroscopy) 70:655-661.

Mollenhauer, H.H., W.G. Whaley, and J.H. Leech. 1961. A function of the Golgi apparatus in outer root cap cells. J.Ultrastructure Res. 5:193-200.

Möllering, H., and W. Gruber. 1966. Determination of citrate with citrate lyase. Anal. Biochem. 17:369-376.

Moody, S.F., A.E. Clark, and A. Bacic. 1988. Structure analysis of secreted slime from wheat and cowpea roots. Phytochemistry 27:2861-2875.

Morel, J.L., M. Mench, and A. Guckert. 1986. Measurement of Pb^{2+}, Cu^{2+} and Cd^{2+} binding with mucilage exudates from maize (*Zea mays* L.) roots. Biol. Fertil. Soils 2:29-34.

Morel, J.L., Andreux, F., Habbib, L., and A. Guckert. 1987. Comparison of the adsorption of maize root mucilage and polygalacturonic acid on montmorillonite homoionic to divalent lead and cadmium. Biol. Fertil. Soils 5:13-17.

Murphy, J., and J.P. Riley. 1962. A modified single solution method for determination of phosphate in natural waters. Anal. Chim. Acta 26:31-36.

Nagarajah, S., A.M. Posner, and J.P. Quirk. 1970. Competitive adsorption of phosphate with polygalacturonic and other organic anions on kaolinite and oxide surfaces. Nature 228:83-85.

Neumann, G., and V. Römheld. 1999. Root excretion of carboxylic acids and protons in phosphorus-deficient plants. Plant Soil 211:121-130.

Neumann, G., A. Hülster, and V. Römheld. 1999. PCDD/PCDF- mobilizing compounds in root exudates of zucchini. Organohalogen Compounds 41:331-334.

Nishinari, K., M. Watase, and T. Hatakeyama. 1997. Effects of polyols and sugars on the structure of water in concentrated gelatin gels as studied by low temperature differential scanning calorimetry. Colloid Polymer Sci. 275:1078-1082.

Nguyen, C. 2003. Rhizodeposition of organic C by plants: mechanisms and controls. Agronomy 23:375-396.

Nordman, C.E., A.S. Weldon, and A.L. Patterson. 1960. X-ray crystal analysis of the substrates of aconitase. II. Anhydrous citric acid. Acta Crystallogr. 13:418-426.

Olson, R.V., and R. Ellis. 1982. Iron. p. 301-312. *In* A.L. Page (ed.) Methods of soil analysis, part 2, chemical and microbiological properties. Agronomy Monograph No.9, American Society of Agronomy-Soil Science Society of America, Madison, WI.

Osborn, H.M.I., F. Lochey, L. Mosley, and D. Read. 1999. Analysis of polysaccharides and monosaccharides in root mucilage of maize (*Zea mays* L.) by gas chromatography. Journal of Gas Chromatography 831:267-276.

Paull, R.E., and R.L. Jones. 1975. Studies on the secretion of maize root cap slime II. Localization of slime production. Plant Physiol. 56:307-312.

Pignatello, J.J., and B. Xing. 1996. Mechanisms of slow sorption of organic chemicals to natural particles. Environ. Sci. Technol. 30:1-11.

Ping, Z.H., Q.T. Nguyen, S.M. Chen, J.Q. Zhou, and Y.D. Ding. 2001. States of water in different hydrophilic polymers – DSC and FTIR studies. Polymer 42:8461-8467.

Pinheiro-Dick, D., and U. Schwertmann. 1996. Microaggregates from Oxisols and Inceptisols: dispersion through selective dissolutions and physicochemical treatments. Geoderma 74:49-63.

Podoll, R.T., K.C. Irwin, and S. Brendlinger. 1987. Sorption of water-soluble oligomers on sediments. Environ. Sci. Technol. 21:562–568.

Prélot, B., Villiéras, F., Pelletier, M., Gérard, G., Gaboriaud, F. et al. 2003. Morphology and surface heterogeneity in synthetic goethites. J. Colloid Interface Sci. 261:244-254.

Ransom, B., R.H. Bennet, R. Baerwald, and K. Shea. 1997. TEM study of in situ organic matter on continental margins: occurrence of the ‘monolayer’ hypothesis. Marine Geol. 138:1-9.

Ransom, B., R.H. Bennet, R. Baerwald, V.H. Hulbert, and P.J. Burkett. 1999. In situ conditions and interactions between microbes and minerals in fine-grained marine sediments: a TEM microfabric perspective. American Mineralogist 84:183-192.

Read, D.B., P.J. Gregory, and A.E. Bell. 1999. Physical properties of axenic maize root mucilage. Plant Soil 211:87-91.

Reichard, P.U. 2005. Effects of microbial and plant siderophore ligands on the dissolution of iron oxides. PhD thesis. Swiss Federal Institute of Technology, Zurich.

Reisenauer, H. 1964. Mineral nutrients in soil solution. p. 507-508. *In* P.L. Altman, and D.S. Dittmer (ed.) Environmental biology. Fed. Am. Soc. Exp. Biol., Bethesda, Md.

Rougier, M. 1981. Secretory activity of the root cap. p. 542-574. *In* B.W. Tanner and F.A. Loewus (ed.) Extracellular carbohydrates, encyclopedia of plant physiology, new series. Plant Carbohydrates II, Vol. 13, Springer-Verlag, Berlin.

Rouquerol, J., D. Avnir, C.W. Fairbridge, D.H. Everett, J.H. Haynes, N. Pernicone, J.D.F. Ramsay, K.S.W. Sing, and K.K. Unger. 1994. Recommendations for the characterization of porous solids. Pure Appl. Chem. 66:1739-1758.

Rovira, A.D. 1969. Diffusion of carbon compounds away from wheat root. Australian Journal of Biology Science 22:1287-1290.

Ruan, H.D., and R.J. Gilkes. 1995. Dehydroxylation of aluminous goethite: unit cell dimensions, crystal size and surface area. Clays Clay Minerals 43:196-211.

Ruiz-Cabrera, M.A., L. Foucat, J.M. Bonny, J.P. Renou, and J.D. Daudin. 2005. Assessment of water diffusivity in gelatine gel from moisture profiles. II. Data processing adapted to material shrinkage. Journal of Food Engineering 68:221-231.

Ryan, P.R., E. Delhaize, and D.L. Jones. 2001. Function and mechanism of organic anion exudation from plant roots. Annu. Rev. Plant Physiol. Plant Mol. Biol. 52:527-560.

Saito, T., L.K. Koopal, W.H. van Riemsdijk, S. Nagasaki, and S. Tanaka. 2004. Adsorption of humic acid on goethite: isotherms, charge adjustments, and potential profiles. Langmuir 20:689-700.

Sanyal, S.K., S.K. De Datta, and P.Y. Chan. 1993. Phosphate sorption-desorption behavior of some acidic soils of South and Southeast Asia. Soil Sci. Soc. Am. J. 57:937-945.

Schaumann, G.E. 2005. Matrix relaxation and change of water state during hydration of peat. Colloids Surfaces A 265:163-170.

Schaumann, G.E., and E.J. LeBoeuf. 2005. Glass transitions in peat: their relevance and the impact of water. Environ. Sci. Technol. 39:800-806.

Schaumann, G.E., and O. Antelmann. 2000. Thermal characteristics of soil organic matter measured by DSC: A hint on a glass transition. J. Plant Nutr. Soil Sci. 163:179-181.

Schaumann, G.E., C. Sievert, and B. Marschner. 2000. Kinetics of the release of dissolved organic matter (DOM) from air-dried and pre-moistened soil material. J. Plant Nutr. Soil Sci. 163:1-5.

Schaumann, G.E., J. Hurraß, M. Müller, and W. Rotard. 2004. Swelling of organic matter in soil and peat samples: insights from proton relaxation, water absorption and PAH extraction. p. 101-117. *In* E.A. Ghabbour, and G. Davies (ed.) Humic Substances: nature's most versatile materials. Taylor and Francis Inc., New York.

Schaumann, G.E., E. Hobley, J. Hurraß, and W. Rotard. 2005. H-NMR Relaxometry to monitor wetting and swelling kinetics in high-organic matter soils. Plant Soil 275:1-20.

Scheinost, A.C., S. Abend, K.I. Pandya, and D.L. Sparks. 2001. Kinetic controls on Cu and Pb sorption by ferrihydrite. Environ. Sci. Technol. 35:1090-1096.

Schmidt, M., H. Knicker, and I. Koegel-Knabner. 2000. Organic matter accumulation in Aeh and Bh horizons of a podzol – chemical characterization in primary organo-mineral associations. Organic Geochem. 31:727-734.

Schulze, D.G. 1984. The influence of aluminum on iron oxides. VIII. Unit-cell dimensions of Al-substituted goethites and estimation of Al from them. Clays Clay Min. 32:36-44.

Schwertmann, U. 1964. Differenzierung der Eisenoxide des Boden durch Extraktion mit Ammoniumoxalat-Lösung. Z. Pflanzenerähr. Düng. Bodenk. 105:194-202.

Schwertmann, U. 1973. Use of oxalate for Fe extraction from soils. Can. J. Soil Sci. 53:244-246.

Schwertmann, U., and R.M. Cornell. 1991. Iron oxides in the laboratory. VCH, Weinheim.

Schwertmann, U., D.G. Schulze, and E. Murad. 1982. Identification of ferrihydrite in soils by dissolution kinetics, differential C-ray diffraction and Mössbauer spectroscopy. Soil Sci. Soc. Am. J. 46:869-875.

Sealey, I.J., M.E. McCully, and M.J. Canny. 1995. The expansion of maize root-cap mucilage during hydration. 1. Kinetics. Physiologia Plantarum 93:38-46.

Shin, E.W., J.S. Han, M. Jang, S.-H. Min, J.K. Park, and R.M. Rowell. 2004. Phosphate adsorption on aluminum-impregnated mesoporous silicates: surface structure and behaviour of adsorbents. Environ. Sci. Technol. 38:912-917.

Souillac, P.O., C.R. Middaugh, and J.H. Rytting. 2002. Investigation of protein/carbohydrate interactions in the dried state. 2. Diffuse relectance FTIR studies. International Journal of Pharmaceutics 235:207-218.

Stevenson, F.J. 1994. Humus chemistry. Genesis, composition, reactions. 2nd ed., John Wiley & Sons, New York.

Straley, C., D. Rossini, H. Vinegar, P. Tutunjian, and C. Morris. 1997. Core analysis by low field NMR. Log Analyst 38:84-94.

Strauss, R. 1992. Mechanismen der Phosphatbindung an Goethit. Phosphatadsorption und -diffusion in Abhängigkeit von der Goethitkristallinität. Bonner Bodenkundliche Abhandlung 5. Bonn, 284 p.

Strauss, R., G.W. Brümmer, and N.J. Barrow. 1997. Effects of crystallinity of goethite: II. Rates of sorption and desorption of phosphate. Eur. J. Soil Sci. 48:101-114.

Ström, L., A.G. Owen, D.L. Godbold, and D.L. Jones. 2002. Organic acid mediated P mobilisation in the rhizosphere and uptake by maize roots. Soil Biol. Biochem. 34:703-710.

Stumm, W. 1992. Chemistry of the solid-water interface. Wiley & Sons Inc, New York, 428 p.

Stumm, W., and G. Furrer. 1987. The dissolution of oxides and aluminum silicates: examples of surface-coordination-controlled kinetics. p. 197-219. *In* W. Stumm (ed.) Aquatic surface chemistry. Wiley Interscience, New York.

Stumm, W., G. Furrer, E. Wieland, and B. Zinder. 1985. The effects of complex-forming ligands on the dissolution of oxides and aluminosilicates. p. 55-74. *In* J.I. Drever (ed.) The chemistry of weathering. Reidel, Dordrecht.

Su, C., and D.L. Suarez. 2000. Selenate and selenite sorption on iron oxides: a infrared and electrophoretic study. Soil Sci. Soc. Am. J. 64:101-111.

Sulzberger, B., D. Suter, C. Siffert, S. Banwart, and W. Stumm. 1989. Dissolution of Fe(III) (hydr)oxides in natural waters: Laboratory assessment on the kinetics controlled by surface coordination. Mar. Chem. 28:127-144.

Tadano, T., and H. Sakai. 1991. Secretion of acid phosphatase by the roots of several crop species under phosphorus-deficient conditions. Soil Sci. Plant Nutr. 37:129-140.

Tananuwong, K., and D.S. Reid. 2004. Differential scanning calorimetry study of glass transition in frozen starch gels. Journal of Agricultural and Food Chemistry 52:4308-4317.

Temple-Smith, M.G., and R.C. Menary. 1977. Movement of ^{32}P to roots of cabbage and lettuce grown in two soil types. Comm. Soil Sci. Plant Anal. 8:67-79.

Theng, B.K.G. 1979. Formation and properties of clay-polymer complexes. Elsevier, Amsterdam.

Torrent, J. 1987. Rapid and slow phosphate sorption by Mediterranean soils: effect of iron oxides. Soil Sci. Soc. Am. J. 51:78-82.

Torrent, J. 1991. Activation energy of the slow reaction between phosphate and goethites of different morphology. Aust. J. Soil Res. 29:69-74.

Torrent, J., V. Barrón, and U. Schwertmann. 1990. Phosphate adsorption and desorption by goethites differing in crystal morphology. Soil Sci. Soc. Am. J. 54:1007-1012.

Torrent, J., U. Schwertmann, and V. Barrón. 1992. Fast and slow phosphate sorption by goethite-rich natural materials. Clays Clay Min. 40:14-21.

Towe, K.M., and W.F. Bradley. 1967. Mineralogical constitution of colloidal 'hydrous ferric oxides'. J. Colloid Interface Sci. 24:384-392.

Traina, S.J., G. Sposito, G.R. Bradford, and U. Kafkafi. 1987. Kinetic study of citrate effects on othophosphate solubility in an acid, montmorillonitic soil. Soil Sci. Soc. Am. J. 51:1483-1487.

Traoré, O., V. Groleau-Renaud, S. Plantureux, A. Tubeileh, and V. Bœuf-Tremblay. 2000. Effect of root mucilage and modeled root exudates on soil structure. Eur. J. Soil Sci. 51:575-581.

Vermeer, J., and M.E. McCully. 1982. The rhizosphere in *Zea*: new insight into its structure and development. Planta 156:45-61.

Violante, A., C. Colombo, and A. Buondonno. 1991. Competitive adsorption of phosphate and oxalate by aluminum-oxides. Soil Sci. Soc. Am. J. 55:65-70.

Walker, A.L. 1983. The effects of magnetite on oxalate- and dithionite-extractable iron. J. Soil Sci. Soc. Am. 47:1022-1026.

Walker, T.S., H. Pal Bais, E. Grotewold, and J.M. Vivanco. 2003. Root exudation and rhizosphere biology. Plant Physiol. 132:44-51.

Watanabe, S., and S. Matsumoto. 1994. Effect of monosilicate, phosphate, and carbonate on iron dissolution by mugineic acid. Soil Sci. Plant Nutr. 40:9-17.

Watt, M., M.E. McCully, and C.E. Jeffree. 1993. Plant and bacterial mucilages of the maize rhizosphere – comparison of their soil binding-properties and histochemistry in a model system. Plant Soil 151:151-165.

Wattel-Koekkoek, E.J.W., P.P.L. van Genuchten, P. Buurman, and B. van Lagen. 2001. Amount and composition of clay-associated soil organic matter in a range of kaolinitic and smectitic soils. Geoderma 99:27-49.

Wedlock, D.J., G.O. Philips, A. Davies, J. Gormally, and E. Wyn-Jones. 1983. Depolymerization of sodium hyaluronate during freeze drying. Intern. J. Biological Macromol. 5:186-188.

Whalley, W.R., B. Riseley, P.B. Leeds-Harrison, N.R.A. Bird, P.K. Leech, and W.P. Adderley. 2005. Structural differences between bulk and rhizosphere soil. Eur. J. Soil Sci. 56:353-360.

Willet, I.R., C.J. Chartres, and T.T. Nguyen. 1988. Migration of phosphate into aggregated particles of ferrihydrite. J. Soil Sci. 39:275-282.

Young, R.J., and P.A. Lovell. 1991. An Introduction to Polymers. Chapman& Hall, London.

Yuan, G., M. Soma, H. Seyama, B.K.G. Theng, L.M. Lavkulich, and T. Takamatsu. 1998. Assessing the surface composition of soil particles from some podzolic soils by X-ray photoelectron spectroscopy. Geoderma 86:169-181.

Zimmerman, A.R., K.W. Goyne, J. Chorover, S. Komarneni, and S.L. Brantley. 2004a. Mineral mesopore effect on nitrogenous organic matter adsorption. Org. Geochem. 35:355-375.

Zimmerman, A.R., J. Chorover, K.W. Goyne, and S.L. Brantley. 2004b. Protection of mesopore-adsorbed organic matter from enzymatic degradation. Environ. Sci. Technol. 38:4542-4548.

Zinder, B., G. Furrer, and W. Stumm. 1986. The coordination chemistry of weathering. II. Dissolution of Fe(III) oxides. Geochim. Cosmochim. Acta 50:1861-1869.

9 Acknowledgements

I am very grateful to all people who supported me physically and mentally during the last three years. Here, I include a list of people, whom I would like to say thank you! All supporters are listed alphabetically. The order of appearance in this list is not significantly correlated with the extent of support at the $P = 0.001$ level.

Ciglasch, Holger
Dominik, Peter Dr.
Dumke, Sabine
Facklam, Michael
Gernert, Ulrich
Herre, Andrea
Irran, Elisabeth Dr.
Jäger, Fabian
Kaiser, Klaus Dr.
Kaupenjohann, Martin Prof. Dr.
Klatt, Roger-Michael
Klitzke, Sondra
Krüger, Jaane
Kuntz, Claudia
Lang, Friederike Sigrid Dr.
Mikutta, Robert
Müller, Martin Dr.
Neumann, Günter Dr.
Pham, Thi Lam Huong Dr.
Rautenberg, Sabine
Regnery, Jeannette
Schaumann, Gabriele Ellen Dr.
Tesfamariam, Tsehaye
Yildiz, Kotan

Last but not least I would like to thank the German Research Fund for the financial support (DFG, KA 1139/8).

10 Curriculum vitae

since 2003	Staff member of the Institute of Ecology at the Berlin University of Technology, Department of Soil Science
2002	Staff member of the Institute of Interdisciplinary Isotope Research e.V. at the University of Leipzig
	Diploma in Geography, University of Leipzig; Thesis: ‚Andosols in Deutschland – Pedogenese auf tertiären und quartären Vulkaniten'
1997-2002	Study of Geography, Geology and Chemistry at the University of Leipzig
1996-1997	Military Service
1993-1996	Grammar School (Kaiserin-Friedrich) in Bad-Homburg v.d.H.
1990-1993	Grammar School (Oranke Gymnasium) in Berlin
1987-1990	36. Secondary School in Berlin (36. Polytechnische Oberschule)
1983-1987	10. Secondary School in Wolfen
1976	born on September 14 in Leipzig

11 Appendix

List of Tables

Table 1. Raw data of kinetic runs with pure and PGA-coated goethite (Chapter 2). Data are given as mean ± standard deviation.

Sample	Time	PO_4		TOC[†]		Fe		ζ-Potential	
	h	mg L^{-1}				µg L^{-1}		mV	
		µ	σ	µ	σ	µ	σ	µ	σ
G0	0.5	21.5	0.0	0.00	0.07	2	3	-30.7	1.3
	1	20.2	0.0	0.00	0.25	0	3	nd	nd
	2	20.1	0.0	0.00	0.14	3	9	-31.7	0.8
	4	19.8	0.0	0.00	0.12	0	2	-27.6	1.3
	8	19.5	0.0	0.00	0.12	4	5	-28.1	1.6
	16	19.5	0.0	0.00	0.12	2	0	-30.5	1.2
	48	18.6	0.0	0.00	0.32	29	5	-16.0	0.4
	168	18.2	0.0	0.00	0.22	81	36	-8.9	1.0
	336	18.1	0.1	0.08	0.07	148	74	-10.2	1.0
G6	0.5	21.9	0.0	0.00	0.23	7	4	-41.7	1.9
	1	21.7	0.0	0.00	0.52	9	13	nd	nd
	2	21.1	0.0	0.00	0.14	28	22	-41.9	1.4
	4	21.1	0.0	0.00	0.05	6	5	-38.4	1.4
	8	21.1	0.0	0.00	0.11	19	20	-40.0	1.2
	16	19.9	0.1	0.00	0.23	17	9	-40.8	2.5
	48	19.5	0.1	0.00	0.13	41	8	-32.3	1.4
	168	19.2	0.0	0.33	0.12	112	16	-34.4	1.0
	336	19.2	0.0	0.43	0.09	176	52	-30.3	0.9
G7	0.5	22.8	0.0	0.00	0.12	5	0	-41.1	1.1
	1	22.4	0.0	0.00	0.24	8	2	-38.9	0.9
	2	22.4	0.0	0.00	0.18	16	3	-42.4	1.4
	4	21.8	0.0	0.26	0.24	18	11	-41.9	1.5
	8	21.6	0.0	0.15	0.13	17	7	-41.2	1.1
	16	21.4	0.0	0.22	0.17	48	30	-41.1	1.0
	48	20.8	0.0	0.38	0.19	18	4	-39.8	1.5
	168	19.6	0.0	1.01	0.01	38	8	-38.4	0.8
	336	19.4	0.0	1.87	0.01	24	9	-38.9	1.6

[†] Total organic carbon.

nd, not determined.

Table 1 (*continued*)

Sample	Time	PO_4		TOC[†]		Fe		ζ-Potential	
	h	mg L^{-1}				µg L^{-1}		mV	
		µ	σ	µ	σ	µ	σ	µ	σ
G8	0.5	22.6	0.0	0.00	0.13	6	4	-40.2	1.0
	1	22.5	0.0	0.00	0.22	20	12	-41.6	1.9
	2	22.4	0.0	0.00	0.27	19	10	-39.7	0.9
	4	21.9	0.0	0.00	0.12	9	6	-42.4	1.9
	8	21.8	0.0	0.00	0.05	16	10	-41.2	1.5
	16	21.3	0.0	0.24	0.07	48	30	-40.4	1.7
	48	20.9	0.0	0.50	0.09	31	20	-40.0	1.3
	168	20.2	0.0	0.61	0.02	39	15	-39.5	1.4
	336	19.5	0.0	1.92	0.11	47	3	-39.6	1.1
G9	0.5	22.5	0.0	0.00	0.10	12	17	-37.4	1.5
	1	21.8	0.0	0.00	0.07	24	13	-40.6	1.4
	2	21.8	0.0	0.14	1.13	21	5	-40.1	1.4
	4	21.5	0.1	0.97	0.34	22	7	-39.4	1.4
	8	21.5	0.0	0.69	0.07	22	8	-41.5	1.4
	16	21.1	0.0	0.98	0.06	54	11	-40.5	1.5
	48	20.7	0.0	1.40	0.11	75	25	-39.8	1.0
	168	19.7	0.0	1.55	0.14	68	25	-39.0	0.7
	336	19.5	0.0	2.12	0.18	81	25	-39.1	0.8
G10	0.5	22.0	0.0	0.28	0.17	17	14	-38.3	1.0
	1	21.5	0.0	0.53	0.15	12	5	-40.2	0.9
	2	21.4	0.1	0.73	0.16	10	8	-39.6	1.5
	4	21.3	0.1	0.00	0.09	27	5	-39.0	1.5
	8	21.0	0.0	0.00	0.43	26	7	-40.1	1.2
	16	20.8	0.1	1.16	0.11	53	7	-39.6	1.2
	48	20.8	0.0	1.35	0.03	74	9	-38.8	0.7
	168	19.7	0.0	1.27	0.09	165	31	-39.6	1.3
	336	19.7	0.1	1.44	0.76	137	165	-38.5	1.4

[†] Total organic carbon.

nd, not determined.

Table 2. Raw data of kinetic runs with freeze-dried pure and PGA-coated goethites (Chapter 3). Data are given as mean ± standard deviation.

Sample	Time	PO_4		TOC[†]		ζ-Potential	
	h	mg L^{-1}				mV	
		μ	σ	μ	σ	μ	σ
G1/0.0	0.5	26.5	0.2	0.32	0.25	-2.5	0.6
	1	26.4	0.5	0.24	0.14	-2.6	1.0
	2	26.1	0.1	0.42	0.03	-11.3	1.9
	4	25.7	0.4	0.19	0.15	-13.2	3.1
	8	25.7	0.5	0.27	0.18	-13.7	1.8
	24	25.3	0.1	0.11	0.11	-12.1	1.2
	48	24.9	0.4	0.18	0.16	-14.4	0.9
	168	24.5	0.3	0.31	0.18	-9.6	1.3
	336	23.9	0.5	0.56	0.42	-8.5	0.6
	504	23.5	0.1	0.49	0.36	-6.5	2.6
G1/0.37	0.5	29.6	0.1	0.22	0.07	-21.5	1.9
	1	28.9	0.2	0.14	0.17	-21.7	1.7
	2	28.7	0.4	0.41	0.05	-19.0	1.3
	4	28.6	0.2	0.46	0.01	-20.9	1.3
	8	27.3	0.4	0.44	0.17	-23.0	2.1
	24	27.0	0.5	0.13	0.03	-22.6	2.2
	48	26.1	0.0	0.68	0.22	-25.2	1.6
	168	25.7	0.1	0.67	0.19	-26.5	1.3
	336	25.5	0.1	0.96	0.19	-23.7	2.2
	504	25.3	0.3	1.15	0.14	-20.0	1.3
G1/1.76	0.5	33.1	0.4	0.43	0.31	-25.5	2.3
	1	32.4	0.3	0.57	0.13	-24.1	1.6
	2	30.4	0.2	0.92	0.09	-24.8	1.0
	4	30.2	0.5	1.77	0.67	-24.8	0.7
	8	30.1	0.3	2.07	0.71	-23.0	1.9
	24	29.3	0.0	2.48	0.31	-25.8	1.4
	48	28.3	0.2	3.06	0.37	-24.7	1.0
	168	27.3	0.1	4.59	0.53	-25.7	1.6
	336	27.0	0.2	4.54	0.41	-29.4	2.5
	504	26.7	0.3	4.94	0.38	-21.1	4.0

[†] Total organic carbon.

Table 2 (*continued*)

Sample	Time	PO_4		TOC[†]		ζ-Potential	
	h	mg L^{-1}				mV	
		μ	σ	μ	σ	μ	σ
G2/0.0	0.5	31.2	0.5	0.19	0.10	-2.6	0.9
	1	30.2	0.8	0.32	0.27	-2.9	0.8
	2	29.8	0.2	0.35	0.31	-4.4	1.6
	4	29.5	0.4	0.29	0.08	-8.4	1.3
	8	29.3	0.2	0.25	0.07	-14.6	1.6
	24	29.2	0.0	0.14	0.31	-16.8	0.5
	48	29.0	0.1	0.12	0.05	-13.3	0.5
	168	28.9	0.1	0.45	0.19	-11.9	2.9
	336	28.8	0.1	0.28	0.00	-9.7	1.5
	504	28.5	0.2	0.20	0.03	-9.2	1.3
G2/0.30	0.5	32.3	0.2	0.10	0.11	-27.8	1.7
	1	32.1	0.1	0.24	0.09	-28.5	2.2
	2	32.1	0.1	0.47	0.00	-23.7	2.1
	4	31.4	0.1	0.22	0.19	-26.9	2.3
	8	31.3	0.8	0.30	0.12	-23.5	1.4
	24	31.3	0.2	0.44	0.04	-26.8	2.1
	48	31.0	0.1	0.30	0.18	-35.7	2.3
	168	29.7	0.6	0.71	0.06	-29.3	2.6
	336	29.4	0.6	1.60	0.21	-26.2	1.6
	504	29.2	0.7	1.41	0.10	-23.8	1.3
G2/1.43	0.5	35.3	0.6	0.47	0.37	-29.9	2.2
	1	34.7	0.1	0.64	0.29	-27.2	1.5
	2	34.0	0.2	0.97	0.13	-29.0	1.9
	4	32.9	0.3	1.20	0.20	-24.2	4.2
	8	32.5	0.2	1.57	0.58	-29.4	1.7
	24	31.9	0.2	2.46	0.32	-28.3	2.4
	48	31.7	0.1	3.01	0.04	-27.0	3.9
	168	31.2	0.1	3.96	0.38	-28.3	2.0
	336	30.4	0.3	3.99	0.16	-26.4	2.4
	504	30.1	0.2	4.46	0.23	-25.0	2.6

[†] Total organic carbon.

Table 3. Raw data of kinetic runs with non-dried pure and PGA-coated goethites (Chapter 3). Data are given as mean ± standard deviation.

Sample	Time	PO_4		TOC[†]	
	h	mg L^{-1}			
		μ	σ	μ	σ
G1/0.0	0.5	28.0	0.1	0.17	0.12
	1	27.3	0.1	0.09	0.15
	2	26.4	0.0	0.14	0.07
	4	26.3	0.1	0.00	0.12
	8	26.0	0.2	0.02	0.05
	24	25.1	0.5	0.15	0.13
	48	24.7	0.3	0.02	0.11
	168	24.1	0.2	0.23	0.19
	336	23.9	0.3	0.67	0.20
	504	23.9	0.4	0.47	0.09
G1/0.42	0.5	33.1	0.5	0.26	0.00
	1	31.2	0.2	0.54	0.24
	2	28.2	0.3	0.44	0.36
	4	27.6	0.3	0.26	0.39
	8	27.1	0.2	0.33	0.32
	24	26.4	0.3	0.15	0.12
	48	26.2	0.1	0.35	0.23
	168	25.4	0.4	0.70	0.46
	336	25.1	0.1	0.50	0.10
	504	25.2	0.2	0.64	0.04
G1/1.88	0.5	34.4	0.2	0.85	0.69
	1	33.3	0.4	1.04	0.79
	2	32.9	0.4	1.30	0.65
	4	31.9	0.0	1.91	0.39
	8	31.2	0.4	2.68	0.33
	24	29.9	0.3	3.90	0.21
	48	28.4	0.5	5.58	0.22
	168	27.0	0.5	5.60	0.20
	336	26.7	0.4	6.46	0.26
	504	25.9	0.1	6.23	0.18

[†] Total organic carbon.

Table 3 (*continued*)

Sample	Time	PO_4		TOC[†]	
	h	mg L^{-1}			
		μ	σ	μ	σ
G2/0.0	0.5	30.3	0.0	0.06	0.10
	1	30.1	0.0	0.08	0.21
	2	29.4	0.1	0.00	0.11
	4	29.3	0.1	0.00	0.07
	8	29.3	0.1	0.00	0.28
	24	29.1	0.2	0.00	0.05
	48	28.7	0.3	0.05	0.14
	168	28.3	0.1	0.23	0.15
	336	27.9	0.2	0.63	0.05
	504	27.9	0.3	0.38	0.19
G2/0.39	0.5	33.7	0.2	0.26	0.10
	1	31.6	0.2	0.24	0.17
	2	31.0	0.3	0.13	0.23
	4	30.5	0.1	0.10	0.11
	8	30.3	0.1	0.10	0.10
	24	30.0	0.2	0.31	0.36
	48	29.9	0.2	0.23	0.24
	168	29.6	0.3	0.38	0.17
	336	29.2	0.3	0.56	0.10
	504	29.1	0.3	0.88	0.23
G2/1.66	0.5	36.3	0.4	0.39	0.01
	1	36.2	0.2	0.57	0.12
	2	35.2	0.3	1.34	0.69
	4	34.5	0.4	1.62	0.13
	8	34.1	0.2	1.71	0.30
	24	32.7	0.3	3.67	0.35
	48	32.0	0.5	4.08	0.11
	168	29.3	0.5	5.19	0.20
	336	28.0	0.3	5.66	0.51
	504	28.0	0.4	5.89	0.02

[†] Total organic carbon.

Table 4. Raw data of kinetic runs with pure goethite (Chapter 4). Treatments: P, phosphate addition; (C+P), simultaneous addition of citrate and phosphate; C+P, citrate added three hours before phosphate. Data are given as mean ± standard deviation.

Sample	Time	PO_4		Citrate-C[†]		Fe		ζ-Potential	
	h	mg L^{-1}				µg L^{-1}		mV	
		µ	σ	µ	σ	µ	σ	µ	σ
P	0.5	37.3	0.4	nd	nd	108	31	-22.7	0.8
	1	36.7	0.4	nd	nd	53	19	-23.0	1.0
	2	35.9	0.0	nd	nd	58	39	-27.5	2.3
	4	35.9	0.2	nd	nd	19	6	-22.7	0.8
	8	34.5	0.2	nd	nd	32	23	-21.7	0.8
	24	33.8	0.3	nd	nd	11	5	-20.7	1.0
	48	33.4	0.3	nd	nd	45	32	-20.3	0.7
	168	32.7	0.4	nd	nd	29	19	-19.4	0.9
	336	32.4	0.1	nd	nd	54	30	-13.3	1.7
	504	32.0	0.9	nd	nd	111	43	-17.2	1.5
(C+P)	0.5	39.4	0.9	32.2	0.9	290	41	-26.8	1.7
	1	38.9	0.7	32.5	1.1	274	64	-27.7	1.8
	2	38.4	0.6	33.7	0.5	283	28	-27.9	1.6
	4	37.7	0.3	33.0	0.2	341	10	-29.0	1.6
	8	37.6	0.3	33.8	0.1	437	20	-28.4	1.5
	24	36.8	0.2	33.3	0.0	1221	231	-29.1	1.4
	48	36.7	0.2	32.3	0.0	873	144	-30.1	1.2
	168	36.4	0.3	30.8	0.6	2255	75	-29.3	1.2
	336	35.9	0.2	31.2	0.5	3620	55	-28.1	1.4
	504	36.0	0.1	29.0	0.9	5438	290	-28.2	1.2
C+P	0.5	41.1	0.6	30.0	0.0	283	35	-26.2	1.0
	1	40.7	0.6	30.4	0.4	212	17	-25.4	1.6
	2	39.8	0.6	31.1	0.6	266	27	-26.0	1.5
	4	39.0	0.6	31.1	0.1	322	29	-25.6	1.1
	8	38.0	0.3	31.0	0.6	493	35	-26.2	1.2
	24	36.5	0.3	30.8	0.6	1015	183	-27.4	1.3
	48	nd	nd	nd	nd	nd	nd	nd	nd
	168	36.0	0.1	30.8	0.6	2885	80	-27.4	0.6
	336	36.3	0.1	30.2	0.2	4747	216	-29.9	1.5
	504	36.3	0.0	29.3	0.2	5847	19	-30.7	1.0

[†] calculated as water-free citric acid (M = 192.1 g mol^{-1}).

nd, not determined.

Table 5. Raw data of kinetic runs with C-coated goethite (Chapter 4). Treatments: P, phosphate addition; (C+P), simultaneous addition of citrate and phosphate; C+P, citrate added three hours before phosphate. Data are given as mean ± standard deviation.

Sample	Time	PO_4		Citrate-C[†]		Fe		ζ-Potential	
	h	mg L^{-1}				µg L^{-1}		mV	
		µ	σ	µ	σ	µ	σ	µ	σ
P	0.5	39.0	0.5	nd	nd	35	36	-24.6	0.7
	1	38.5	0.3	nd	nd	2	2	-24.3	0.8
	2	37.7	0.4	nd	nd	14	9	-25.9	1.1
	4	37.2	0.4	nd	nd	0	0	-25.0	1.3
	8	36.9	0.3	nd	nd	4	1	-23.5	1.2
	24	36.2	0.3	nd	nd	0	0	-25.8	2.9
	48	35.9	0.2	nd	nd	0	0	-24.4	2.1
	168	34.9	0.3	nd	nd	0	0	-23.0	1.1
	336	34.5	0.4	nd	nd	15	3	-18.3	0.9
	504	34.2	0.5	nd	nd	33	15	-26.3	1.1
(C+P)	0.5	41.6	0.2	33.1	0.0	231	17	-27.0	1.9
	1	41.5	0.2	32.5	0.4	206	5	-26.8	1.5
	2	40.2	0.3	33.1	0.1	266	14	-26.2	1.0
	4	39.9	0.4	33.4	0.1	359	18	-26.6	1.4
	8	39.2	0.3	32.8	0.2	458	14	-27.9	1.9
	24	38.0	0.6	32.7	0.1	876	74	-29.0	1.5
	48	37.7	0.3	32.1	0.0	1237	6	-28.0	1.0
	168	37.1	0.1	31.2	0.0	2590	42	-28.3	1.4
	336	37.2	0.4	31.0	0.9	4268	226	-26.9	0.7
	504	37.2	0.3	29.3	1.0	5923	333	-26.7	1.2
C+P	0.5	41.9	0.2	31.8	0.1	167	93	-24.3	1.2
	1	41.2	0.6	32.0	0.4	124	15	-24.2	1.0
	2	40.9	0.3	31.9	0.2	168	8	-24.8	1.0
	4	38.9	0.5	32.8	0.2	317	20	-25.7	1.0
	8	38.3	0.7	34.0	0.0	576	6	-25.6	0.8
	24	37.4	0.4	32.8	0.2	1101	40	-25.1	1.1
	48	nd	nd	nd	nd	nd	nd	nd	nd
	168	37.2	0.1	31.1	0.1	3194	115	-27.1	1.5
	336	37.1	0.0	30.4	0.4	5777	304	-27.2	0.9
	504	37.0	0.4	29.7	1.1	7072	194	-28.8	1.1

[†] calculated as water-free citric acid (M = 192.1 g mol^{-1}).

nd, not determined.

Table 6. Raw data of kinetic runs in the desorption experiment (Chapter 5). Abbreviations: G, goethite; GA, galacturonate; PGA, polygalacturonate; MU, mucigel. The order of abbreviations indicates order of sorbate addition. Data are given as mean ± standard deviation.

Sample	Time	PO_4		ζ-Potential	
	h	mg g^{-1}		mV	
		μ	σ	μ	σ
G+P	0	26.5	0.5	-18.1	1.3
	1	25.9	0.5	-19.8	1.9
	2	24.7	0.4	-18.6	1.1
	4	23.8	0.2	-18.8	1.7
	8	23.6	0.3	-17.2	1.9
	24	21.8	0.2	-15.9	1.2
	48	20.5	0.3	-15.2	1.2
	96	18.9	0.3	-13.8	1.7
	168	17.7	0.3	0.6	1.5
	336	17.1	0.3	5.0	0.8
G+P+GA	0	25.5	0.4	-17.4	0.4
	1	24.5	0.4	-10.1	1.2
	2	24.3	0.4	-8.9	1.1
	4	24.1	0.5	-6.8	1.6
	8	23.3	0.7	-6.2	1.4
	24	21.5	0.2	-2.2	1.1
	48	20.3	0.5	-1.5	1.1
	96	19.6	0.4	-0.3	0.5
	168	18.8	0.3	1.6	1.9
	336	17.6	0.3	7.7	1.5
G+P+PGA	0	24.7	0.3	-27.6	0.9
	1	23.5	0.2	-27.2	1.3
	2	22.7	0.3	-28.1	1.0
	4	22.5	0.5	-23.1	0.6
	8	22.3	0.4	-24.8	1.4
	24	20.9	0.1	-24.2	1.5
	48	19.3	0.1	-19.4	1.0
	96	18.7	0.0	-16.9	1.2
	168	18.2	0.4	-11.8	2.0
	336	17.4	0.3	1.2	0.7
G+P+MU	0	29.2	0.3	-23.0	1.5
	1	25.0	0.5	-23.7	1.7
	2	23.3	0.3	-21.6	2.3
	4	22.8	0.1	-19.9	1.3
	8	21.8	0.2	-20.1	1.4
	24	19.6	0.3	-19.7	2.2
	48	19.0	0.3	-17.7	2.0
	96	18.2	0.3	-12.5	2.0
	168	17.1	0.1	0.7	1.2
	336	16.8	0.3	4.1	1.8

Table 6 (*continued*)

Sample	Time	PO_4		ζ-Potential	
	h	mg g^{-1}		mV	
		μ	σ	μ	σ
G+GA+P	0	25.1	0.0	-15.4	0.7
	1	22.9	0.5	-13.2	1.5
	2	22.9	0.3	-12.5	1.4
	4	22.6	0.1	-12.0	1.0
	8	22.5	0.1	-11.6	1.0
	24	20.6	0.5	-10.3	1.3
	48	19.0	0.4	-3.5	2.1
	96	17.8	0.4	-7.6	1.9
	168	17.3	0.7	-4.4	2.2
	336	16.6	0.3	12.3	1.5
G+PGA+P	0	23.1	0.2	-29.0	1.6
	1	22.9	0.3	-26.7	1.3
	2	22.6	0.1	-27.1	2.9
	4	22.1	0.1	-23.0	1.7
	8	21.7	0.3	-23.9	1.1
	24	19.9	0.4	-23.4	1.5
	48	18.3	0.3	-19.1	1.0
	96	17.0	0.3	-16.6	1.9
	168	16.4	0.4	-17.5	0.6
	336	16.2	0.2	6.2	0.6
G+MU+P	0	23.8	0.3	-17.1	1.5
	1	22.9	0.1	-17.4	1.3
	2	22.4	0.2	-16.6	1.8
	4	22.3	0.2	-17.5	0.5
	8	21.7	0.3	-16.9	0.8
	24	20.4	0.2	-15.8	0.8
	48	19.8	0.2	-13.0	0.3
	96	18.4	0.2	-11.4	2.3
	168	17.6	0.2	-8.0	1.5
	336	16.1	0.1	-8.3	1.4

Table 7. Raw data of kinetic runs with pure and PGA-coated alumina (Chapter 6). Data are given as mean ± standard deviation.

Sample	Time elapsed before analyis	Time	PO_4		TOC[†]	
	h	h	mg L^{-1}			
			μ	σ	μ	σ
Al_2O_3	2	0.5	25.1	0.9	0.28	0.17
		1	22.7	0.6	0.29	0.10
		2	21.3	0.4	0.23	0.12
		4	20.0	0.4	0.26	0.17
		8	16.9	0.2	0.19	0.05
		24	14.0	0.5	0.27	0.25
		48	12.2	0.5	0.26	0.11
		120	10.2	0.3	0.40	0.02
		144	9.2	0.5	0.36	0.09
		168	9.3	0.3	0.08	0.06
Al_2O_3	170	0.5	26.1	0.4	0.28	0.28
		1	23.1	0.2	0.12	0.05
		2	22.1	0.4	0.13	0.25
		4	20.3	1.1	0.18	0.19
		8	19.6	1.0	0.24	0.26
		24	15.0	0.4	0.29	0.14
		48	14.2	0.2	0.29	0.04
		120	12.7	0.2	0.34	0.28
		144	12.3	0.2	0.40	0.07
		168	12.3	0.3	0.39	0.04
Al_2O_3+PGA	2	0.5	30.6	0.4	1.43	0.60
		1	29.5	0.8	1.65	0.41
		2	27.3	0.8	1.59	0.23
		4	25.6	0.3	1.88	0.15
		8	22.6	0.1	1.88	0.11
		24	19.6	0.3	1.92	0.19
		48	17.7	0.3	2.18	0.37
		120	16.4	0.2	2.12	0.15
		144	15.4	0.4	2.62	0.70
		168	14.8	0.3	2.09	0.31
Al_2O_3+PGA	170	0.5	26.0	0.3	0.23	0.18
		1	23.3	0.2	0.30	0.22
		2	22.1	0.6	0.72	0.14
		4	21.5	0.7	0.44	0.12
		8	19.4	0.3	1.03	0.20
		24	17.1	0.6	1.24	0.28
		48	16.7	0.3	1.36	0.38
		120	14.5	0.4	1.63	0.21
		144	14.2	0.2	1.34	0.43
		168	13.8	0.1	1.53	0.34

[†] Total organic carbon.